UNIVERSITÉ DE STRASBOURG

EDSC
Ecole Doctorale des
Sciences Chimiques

ÉCOLE DOCTORALE DES SCIENCES CHIMIQUES

Institut de Chimie UMR 7177

THÈSE

présentée par

B. Murali KRISHNA

soutenue le : **20 decembre 2012**

pour obtenir le grade de

Docteur de l'université de Strasbourg

Discipline / Spécialité : Chimie / Chimie Théorique

Quantum mechanical investigations of the dynamical and spectroscopic properties of compounds containing heavy elements,

the CuNO case study

THÈSE dirigée par :
  M. MARQUARDT Roberto   Professeur, Université de Strasbourg

RAPPORTEURS :
  M. WERNER Hans-Joachim   Professeur, Universität Stuttgart
  M. GATTI Fabien   Directeur de recherche CNRS, Université Montpellier 2

MEMBRES DU JURY :
  M. MARQUARDT Roberto   Professeur, Université de Strasbourg
  M. WERNER Hans-Joachim   Professeur, Universität Stuttgart
  M. GATTI Fabien   Directeur de recherche CNRS, Université Montpellier 2
  M. BOEGLIN Alex   Chargé de recherche CNRS, Université de Strasbourg

Résumé en Français

Investigation quantique des propriétés dynamiques et spectroscopiques de composées contenant des éléments lourds, étude du cas CuNO

L'interaction d'un monoxyde d'azote avec un atome de métal de transition reçoit une attention croissante de la part d'études tant expérimentales que théoriques car elle est importante dans de nombreux chemins de réaction biochimiques, en chimie atmosphérique, chimie des surfaces et catalyse. Les ions du cuivre jouent un role important dans la chimie rédox des NOx dans la dénitrification biologique. NO étant un sous-produit de la combustion de carburants fossiles mène au brouillard photochimique et sa nature radicalaire en fait un contributeur majeur de la diminution de la couche d'ozone.

L'étude de réactions impliquant NO et des métaux de transition est particulièrement intéressante pour le développement de catalyses efficaces four la réduction de NO. CuNO et ses ions ont été observés par isolement en matrice, et par spectre infrarouge dans l'argon. Afin de sonder la possibilité d'une catalyse homogène impliquant les fragments Cu et NO, une prévision précise de la nature de l'interaction entre ces deux fragments est nécessaire en phase gaz. Une série de questions demande des réponses : Quel est l'état fondamental électronique du système CuNO ? Quelle est l'énergie de dissociation du complexe CuNO ? Quelle est sa géométrie d'équilibre ? Ces quantités ne sont pas connues expérimentalement. Peut-on les prévoir assez précisément ? Peut-on faire un potentiel analytique pour le calcul des transitions de vibration de CuNO ? A quel point ces valeurs sont comparables avec le spectre infra-rouge, même si enregistré en matrice ? Quelle est la dynamique de collision de Cu et NO ? S'attent-on à observer une diffusion réactive ? Quelles sont les étapes élémentaires de la cinétique de réaction induite par la collision de Cu avec NO ? L'atome de Cu peut-il être utilisé pour réduire NO après une telle collision ? Quelle est la barrière d'activation ? Quelle est l'importance des états électroniques excités dans la réduction de NO ?

Pour la plupart de ces questions aucune donnée n'est disponible, tant de l'expérience que de la théorie. Aucun calcul de dynamique quantique a été présenté dans la littérature utilsant un métal de transition tel que Cu en dimensions complètes, principalement à cause de la très haute densité d'états vibrationnels puisqu'il s'agit d'un élément lourd. Pour CuNO, les études théoriques n'ont pas encore été capables d'assigner sans ambigüité l'état fondamental. Les calculs cluster couplé avec excitations simples et doubles (CCSD) donnent un état fondamental triplet de CuNO, alors que l'inclusion d'excitations triples (CCSD(T)) donne un état fondamental singulet de symétrie $^1A'$ avec une structure coudée avec coordination en bout de fragment NO et un énergie de liaison estimée à 18,8 kcal/mol. Dans les calculs utilisant la théorie de la fonctionnelle de la densité (DFT), des fonctionnelles pure densité assignent un état fondamental singulet, alors que des fontionnelles hybrides favorisent un état triplet comme état d'énergie électronique le plus bas.

1

Il est important de noter que les méthodes mentionnées ci-dessus sont essentiellement mono-configurationnelles.

Dans cette thèse, nous répondons à la plupart des questions sus-mentionnées. Dans ce bref résumé de la thèse, nous restreignons le rapport à :

1) Des calculs *ab initio* précis pour obtenir l'énergie de l'état électronique fondamental (et des états excités). Dans la présente étude, une investigation systématique des paramètres de calcul relatives à une prévision précise de la fonction d'onde électronique pour l'état fondamental et les états excités est menée au niveau de théorie champ autocohérent multiconfigurationnel (MCSCF) et interaction de configurations multi-référence internement contractées (MRCI), même si restreintes aux excitations simples et doubles.

2) La nouvelle représentation globale analytique de la surface d'énergie potentielle (SEP) *ab initio*. Un ensemble d'énergies électroniques est ensuite construit à partir des valeurs MRCI (et par une procédure originale de fusion de MRCI et CCSD(T)) pour l'état fondamental $^1A'$. Cet ensemble est ensuite utilisé pour un ajustement d'une surface d'énergie potentielle analytique globale pour le système. Un algorithme de Levenberg-Marquardt modifié a été utilisé pour les ajustements. Du potentiel analytique, on obtient l'énergie de dissociation de l'interaction Cu + NO, et la géométrie d'équilibre de l'état fondamental du complexe.

3) La dynamique quantique du système CuNO à l'état fondamental électronique. Le potentiel analytique global avec le meilleur ajustement des paramètres est finalement utilisé dans des calculs de dynamique quantique à 3 ou 4 dimensions pour la réaction Cu + NO où nous montrons que la collision est bien réactive.

Il est à noter que les trois sections de l'étude représentent un challenge et requièrent une optimisation attentive de nombreux paramètres de réglages de calculs pour obtenir des résultats physiquement sensés.

Pour des raisons de brièveté, n'ont pas été inclues dans ce résumé :

Les réglages détaillés de l'optimisation pour les calculs *ab initio* et de dynamique quantique. Les détails de la procédure d'ajustement de la représentation analytique incluant les valeurs des paramètres d'ajustement. Les calculs détaillés de structures électroniques pour l'état fondamental et les états excités des diatomiques CuO et CuN dont les valeurs ont été utilisées pour l'ajustement des paramètres dans le potentiel analytique. Les calculs CCSD(T) sont complètement révisés et le rôle des corrections relativistes sur l'atome de Cu est également étudié. Nous avons trouvé d'importants effets relativistiques dans l'énergie de dissociation (la profondeur du puit décroît), et les longueurs de liaisons (la

distance Cu-NO diminue). Nous avons également calculé les transitions vibrationnelles du système qui se compare le mieux avec l'expérience. En dynamique quantique, nous étudions l'effet de l'énergie de collision sur la diffusion et aussi l'effet du changement dans le facteur d'impact sur la diffusion. Nous avons aussi créé une nouvelle procédure de fusion pour comparer les données MRCI et CCSD(T) et ajusté ceci avec un potentiel global, qui pourra être utilisé dans des calculs de dynamique à l'avenir.

Dans les sections suivantes, je résume de forme plus détaillé les points 1, 2 et 3 susmentionnés.

Calculs *ab initio*

La configuration tridimentionnelle de l'espace peut être décrite par les coordonnées r_{NO}, r_{Cu} et θ_{Cu} montrées en Figure 1, où r_{Cu} est la distance entre l'atome de cuivre et le milieu de la distance NO.
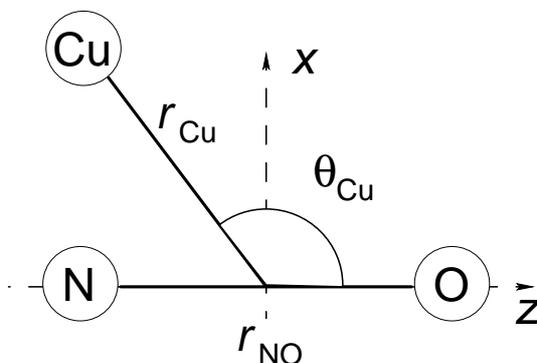
FIG. 1 – Coordonnées générales pour le système {Cu, N, O} ; r_{Cu} est la distance entre l'atome de cuivre et le milieude r_{NO} ; $0 \leq r_{NO} < \infty$, $0 \leq r_{Cu} < \infty$, $0° \leq \theta_{Cu} \leq 180°$.

Les calculs de l'état fondamental et des états excités ont été effectués en utilisant le code de programmes MOLPRO pour les calculs MCSCF, MRCI et CCSD(T). Dans les calculs, nous utilisons la base augmentée consistante avec la corrélation polarisée triple ζ ("aug-cc-pVTZ", mais abréviée ici "AVTZ") de Dunning et collaborateurs, pour N et O, et de Balabanov et Peterson pour des bases convergentes pour les métaux de transition. Une nouvelle base réduite, obtenue depuis la base AVTZ en ommettant la fonction g de Cu et les fonctions f de N et O, appellée ici RVTZ, donne aussi les énergies relatives avec la précision attendue (mE_h).

Dans le présent résumé, nous restreignons la rapport au résultats impliquant les calculs MCSCF/MRCI, pour des raisons de brièveté. Nous choisissons soigneusement le nombre d'états calculés pour chaque symétrie afin de surmonter les défaillances au niveau MCSCF. Un nombre déséquilibré de racines mène à une brisure de symétrie. Aussi, de grâves problèmes d'inversion de racines arrivent quand on arrive pas à inclure tous les états d'un

multiplet électronique dans les calculs MCSCF.

Clairement, les orbitales s et d de Cu sont très proches et on peut anticiper que toutes ces orbitales doivent être inclues dans l'espace actif. Un calcul dans le groupe de symétrie $\mathbf{C_s}$ correspondant à 6 racines $^1A'$ et 6 racines $^1A''$ est vraiment physique et vient naturellement des espèces de symétrie des états asymptotiques de CuNO. Un espace actif qui consiste en 13 orbitales, $9 \times {}^1A'$, $4 \times {}^1A''$ avec 22 électrons, noté CAS $(22, 13)$, donne une convergence propre.

Cependant, les calculs MCSCF avec 12 racines et CAS $(22, 13)$, convergent sur ^2S comme état excité et un ^2D dégénéré comme état fondamental avec une différence d'énergie de plus de 90 mE_h à l'asymptote. Experimentalement, pour Cu, le ^2D se trouve au-dessus du ^2S d'environ 11200 cm^{-1} . Cette inversion articfielle des états dans les calculs MCSCF est aussi observé pour l'atome de Cu seul si nous incluons les orbitales 3d dans l'espace actif.
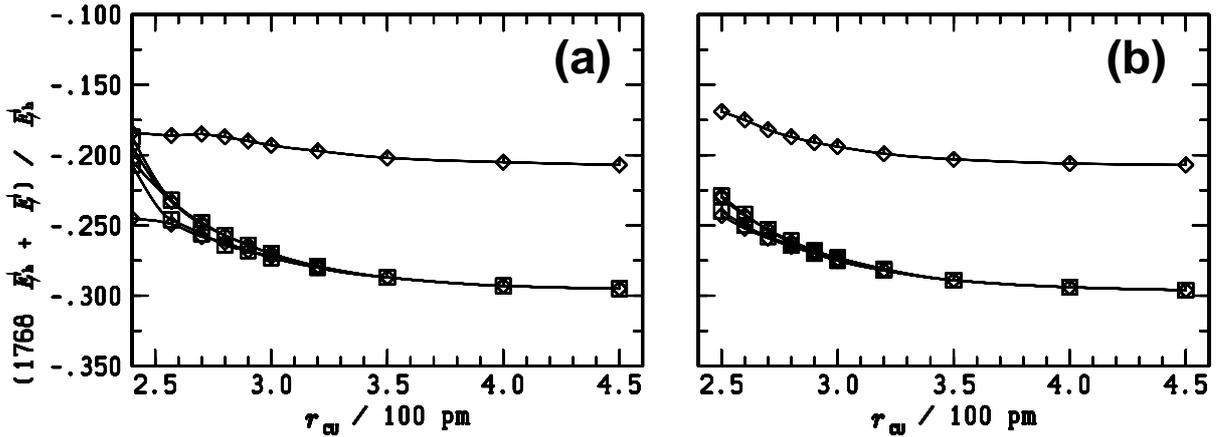
FIG. 2 – Fonctions énergie potnetielle $V(r_{Cu})$ pour l'état singulet linéaire le plus bas de symétrie A' à $r_{NO} = 115$ pm, et $\theta_{Cu} = 180°$ **(a)**, et $\theta_{Cu} = 0°$ **(b)**

Pour palier ceci, nous effectuons des calculs MRCI. Les orbitales naturelles obtenues par les calculs MCSCF sont ensuite utilisées pour effectuer des excitations simples et doubles inclues dans le MRCI de 13 orbitales comme orbitales actives, ainsi corrélant 22 électrons, c.-à-d. un CAS $(22, 13)$. Les calculs MRCI remettent les états dans le bon ordre à l'asymptote. Une composante $^1A'$ non-dégénérée est l'état fondamental. Il est à noter que toutes les configurations menant aux 6 états les plus bas relatifs à chaque espèce de symmétrie est nécessaire pour calculer correctement l'état fondamental du système, rendant le calcul vraiment multi-référence et très multi-configurationnel.

La figure 3 montre l'état lié. Elle montre aussi 5 états excités, qui deviennent dégénérés à
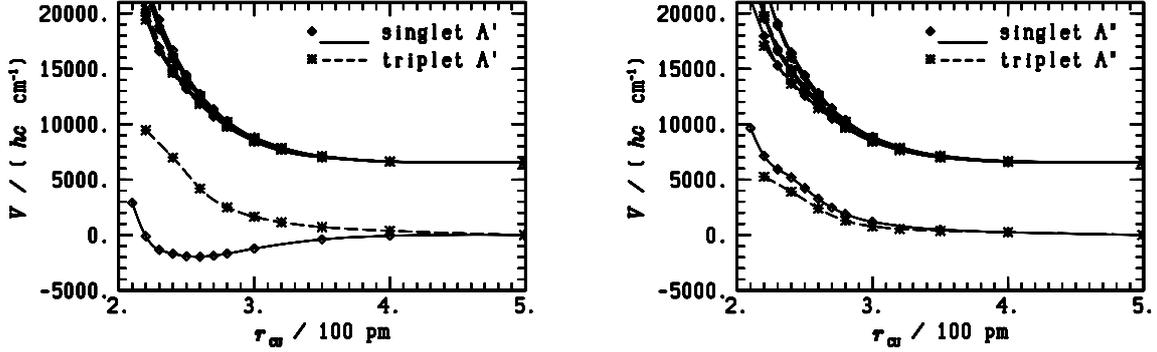
FIG. 3 – Figure 3 : fonction énergie potentielle MRCI $V(r_{Cu})$ pour les plus bas état singulet et triplet de symétrie A$'$ (panneau (**a**)) et A$''$ (panneau (**b**)) à valeurs fixées θ_{Cu} = 130° et r_{NO} = 115 pm. Les énergies ont été obtenues d'après un CAS (22,13) avec la base RVTZ.

l'asymptote (niveau ^{2}D de Cu) avec l'état ^{1}A$'$, alors que les 6 états ^{3}A$'$, les 6 états ^{1}A$''$ et les 6 états ^{3}A$''$ sont essentiellement repulsifs. La structure de l'état lié est aux environs du fond du puit de potentiel du plus bas état ^{1}A$'$ dans la Figure 2 avec une énergie de liaison de 10 mE_h (2188 cm^{-1}), pour le CAS (22,3) avec la base RVTZ. Alors que les présents calculs MRCI confirment l'ordre des états singulets et triplets des résultats précédents, où un ^{3}A$''$ stable est prévu se trouver 11 mE_h plus haut que l'état ^{1}A$'$, ils mènent à une plus large énergie relative triplet-singulet autour du minimum (environ 23 mE_h ici). D'autre part, ils n'indiquent pas que l'état lié triplet existe, contrairement à ce qui a été suggéré dans.

Représentation analytique de la SEP

La surface d'énergie potentielle totale du système CuNO (ou toute triatomique) peut être donné comme une somme

$$\sum_{i=1}^{3} V_{2bi} + V_{3b} \tag{1}$$

où V_{2b} sont les termes à deux corps et V_{3b} est un potentiel de cisaillement.

Nous utilisons un potentiel de Morse modifié pour décrire les fonctions de potentiel d'étirement de liaison. Il y aura un potentiel bien défini et le paramètre r_e peut être interprété comme la longueur de liaison à l'équilibre du potentiel "diatomique". Le terme à trois corps es essentiellement un potentiel de cisaillement. Il peut être vu comme le produit d'une fonction dépendant de θ et deux termes d'ammortissement y_1 et y_2

$$
\begin{aligned}
V_{3b} &= V_b y_1 y_2 \left(y_1 - 2z \right) \tag{2} \\
y_i &= e^{-a_r(r_i - r_e)} \tag{3} \\
z &= -z_1 z_2 z_3 \tag{4}
\end{aligned}
$$

5

$$z_i = b_i - e^{-a_i(\cos\theta - \cos\theta_e)(1 + c_i(\cos\theta - \cos\theta_e)} \tag{5}$$

Les conditions appropriées parmi les paramètres b_i et a_i assurent que V_{3b} prendra la valeur $-V_b$ au minimum global, qui est à l'angle d'équilibre θ_e, et 0, quand r_1 et r_2 tendent vers l'infini.
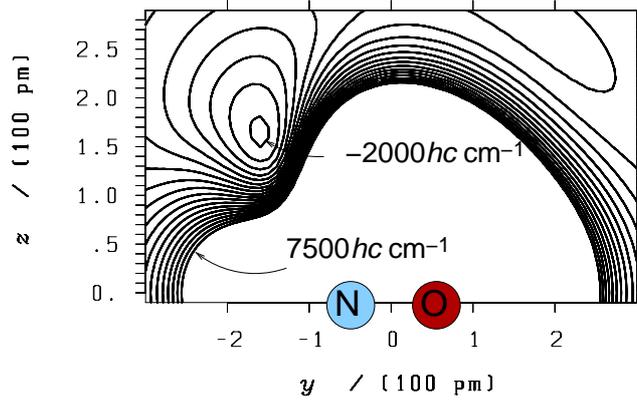
FIG. 4 – SEP analytique à la valeur fixée de $r_{NO} = 115$ pm ; la différence des lignes à niveau est de $500\ hc\,\mathrm{cm}^{-1}$; le zéro d'énergie correspond à l'état Cu + NO.

Cette représentation analytique de la SEP est nouvelle et sera expliquée en détail dans les travaux. Pour la procédure d'ajustemen, un modification de l'algorithme de Levenberg-Marquardt a été utilisée. Nous ajustons 19 paramètres en utilisant 530 points de données *ab initio*. Ici, l'énergie de dissociation est trouvée aux environs de $2000\ hc\,\mathrm{cm}^{-1}$ and la géométrie d'équilibre du système est autour de $r_{Cu} = 2.382$ pm, $r_{NO} = 1.134$ pm et $\theta_{Cu} = 133.495°$.

Dynamique quantique

La représentation analytique du potentiel a par la suite été utilisée dans le code *multiconfiguration time-dependent Hartree* (MCTDH), pour calculer l'évolution du paquet d'onde de la collision de Cu et NO à plusieurs énergies de collision et paramètres d'impact.

Le comportement dynamique de l'état d'un système quantique isolé est décrit par l'équation de Schrödinger,

$$i\hbar\frac{\partial}{\partial t}\Psi(t) = \hat{H}\Psi(t). \tag{6}$$

L'approche MCTDH de la fonction d'onde pour résoudre l'équation de Schrödinger dépendante du temps est écrite comme suit

$$\Psi(Q_1, ..., Q_f, t) = \sum_{j=1}^{n_1} ... \sum_{j_f=1}^{n_f} A_{j_1...j_f}(t) \prod_{k=1}^{f} \phi_{j_k}^{k}(Q_k, t) \tag{7}$$

6

où $Q_1, ...Q_f$ sont les coordonnées nucléaires, les $A_{j_1...j_f}$ représentent les coeffincients d'expansion MCTDH et les $\phi_{j_k}^k$ sont les n_k fonctions d'expansion pour chaque degré de liberté k, connus comme fonction d'une seule particule.

Comme example de résultat de calculs de dynamique quantique , nous montrons ici le flux quantique $\Phi(t)$, ou la quantité de densité de probabilité, à travers une surface divisante S placée à $r_{\text{Cu}} = 800$ pm.

$$\Phi(t) = \int\limits_S j_{r_d}(t) \cdot \mathrm{d}S \tag{8}$$

où

$$j_{r_d}(t) = -\mathrm{i}\frac{\hbar}{2\,\mu_{r_d}} \left(\psi^*(t)\frac{\partial\psi(t)}{\partial r_d} - \psi(t)\frac{\partial\psi^*(t)}{\partial r_d}\right) \tag{9}$$

$(r_d \approx r_{\text{Cu}})$. Dans la Figure 5 nous montrons le flux entrant et le flux sortant le long de la voie de dissociation de Cu-NO avec un temps de propagation total de 600 fs. Ici l'énergie totale du système est conservée. Ici aussi, à $J = 0$, le paquet d'onde s'approche de toutes les directions vers NO dans une situation purement quantique ($\ell = 0$).
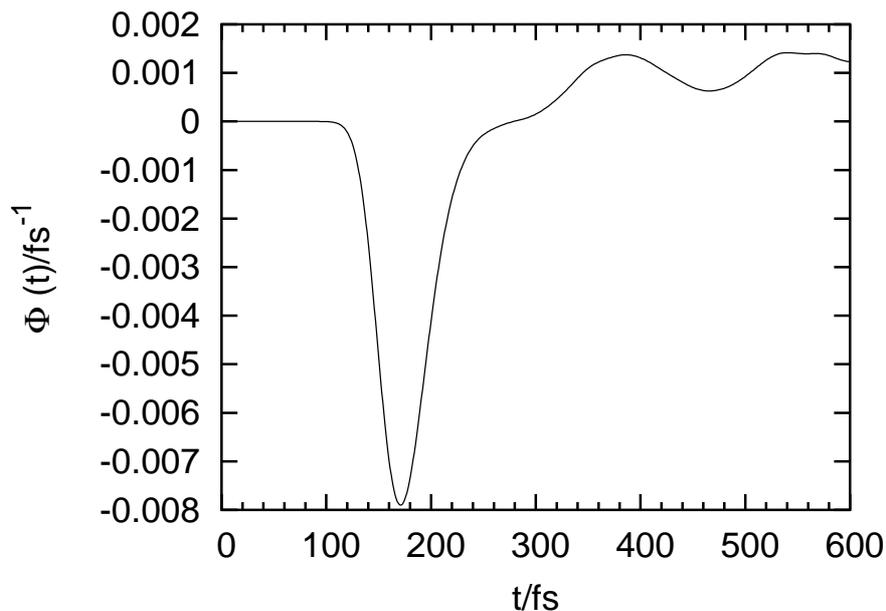
Fig. 5 – Flux à la surface divisante $r_{\text{Cu}} = 800$ pm

Nous calculons la probabilité de réaction au temps t

$$\Delta P(t) = \int\limits_{-\infty}^{t} \Phi(t)\,\mathrm{d}t \tag{10}$$

d'après le flux MCTDH.

Le paquet d'onde entrant bouge à travers la surface divisante entre 145 fs et 240 fs. Le flux sortant arrive 240 fs et 600 fs et montre clairement que c'est une diffusion réactive puisque l'intégrale globale du flux ne s'annule pas, même à une échelle de temps infinie ($\Delta P = -0.003779$).

Nous trouvons aussi que l'énergie de translation va vers un mode de vibration de pliage de CuNO proche des minima. C'est la première fois que les calculs de dynamique quantique ont été effectués avec MCTDH pour des composés métal nitrosyle. La convergence est difficile, à cause de la grande densité d'états vibrationnels, mais elle a été totalement atteinte.

Conclusions

Dans cette thèse, nous avons optimisé avec succès tous les paramètres pour calculer l'état fondamental du système neutre [N,O,Cu].

Il a été montré que les calculs MCSCF incluant 12 racines est nécessaire pour avoir une convergence propre mais donne des états inversés à l'asymptote. Pour décrire proprement l'état fondamental, nous utilisons les calculs coûteux MRCI sur 6 états par espèce de symétrie simultanément. Aussi nous montrons par calculs MRCI, que l'espace actif peut contenir tous les électrons 3d de Cu pour décrire précisément le système. Ici nous utilisons un CAS $(22, 13)$ qui est proche de l'espace de valence complète du système.

Nous avons développé une SEP analytique globale qui peut être utilisée pour modéliser les données *ab initio* obtenues. L'état lié est un état $^1A'$ avec une énergie de $r_{\mathrm{Cu}} = 2.382$ pm, $r_{\mathrm{NO}} = 1.134$ pm et $\theta_{\mathrm{Cu}} = 133.495°$. Les fondamentaux vibrationnels calculés se comparent bien avec les données expérimentales disponibles.

Le potentiel analytique a été utilisé avec succès avec les meilleurs paramètres ajustés pour effectuer des calculs de dynamique quantique sur le complexe, dont les résultats indiquent une diffusion réactive avec un transfer de l'énergie translatoire vers l'énergie vibrationnelle dans le domaine de temps de la femtoseconde.

Des résultats plus avancés non-inclus dans ce résumé impliquent des calculs CCSD(T), incluant des corrections relativistes, et une fusion originale entre les données MRCI et CCSD(T) et modélisées avec la SEP analytique, dont les résultats donnent un puit de potentiel plus profond et réduisent la distance de liaison r_{Cu} (distance Cu-NO). Nous

avons aussi effectué des études de dynamique quantique avec un facteur d'impact variant ($J > 0$) et une diffusion à différentes énergies de collision, toutes deux dans une approche soit isotrope, soit directionnelle du paquet d'onde initial. Nous avons également effectué des calculs précis sur l'état électronique fondamental et sur les états électroniques excités des diatomiques CuO et CuN et obtenu l'énergie de dissociation qui a ensuite été utilisée comme paramètre d'ajustement dans la représentation analytique. Avec ce résumé, nous répondons à plusieur questions posées au début de la thèse. D'autres questions ont également trouvé réponse dans le manuscrit complet de la thèse.

"The first principle is that you must not fool yourself; and you are the easiest person to fool."

Richard Feynman, Cargo Cult Science

Abstract

This thesis aims at validating a theoretical protocol to develop global potential energy surfaces for use in the spectroscopy and dynamics of transition metal nitrosyl complexes. To get an insight into the homogeneous catalysis of NO with Cu and the chemical reaction dynamics, an accurate prediction of the nature of the interaction, as well as of the global potential energy surfaces (PES) is necessary in the gas phase. Experimental data are difficult to obtain, hence the importance of carrying out calculations of the lowest electronic states as accurate as possible to address the structure , spectroscopy and dynamics of this system. All *ab initio* calulations we report here were performed at the multi-reference configuration interaction (MRCI) and at the coupled cluster level of theory. We aslo investigate the importance of relativistic effects in the systems. For CuNO system, it is shown that a complete active space involving 18 valence electrons, 11 molecular orbitals and the prior determination of 12 roots in the MCSCF calculation is needed for overall qualitatively correct results from the MRCI calculations. The present calculations yield a bound singlet A′ ground state for CuNO and comparared with previous results. We have obtained new, complete potential energy functions of the ground electronic states of CuO and CuN systems. The lowest electronic state in the CuO is the $^2\Pi$ state. We also report the barrier to dissociation in the lowest $^2\Sigma^-$ electronic state of which has not been observed before. Again, the active space is chosen carefully so as to be able to describe both the predominantly neutral asymptote and the predominantly ionic equilibrium geometries. Comparison of the term values for the lowest electronic states of CuO and CuN with those previously reported in the literature shows a quite good agreement. We derived a novel analytical representation of the adiabatic potential energy surface in the ground electronic state of the CuNO system as a sum of two-body and three-body terms. This compact and flexible representation enables us to make a physically correct interpolation of the *ab initio* data points at the MRCI level of theory. We use a modified Levenberg-Marquardt algorithm for fitting the potential, which has 19 adjustable parameters and which now enables us to do scattering dynamics of the CuNO system. We perform full dimensional quantum dynamical studies with this new potential. Convergence of the time dependent wavepacket calculation has been achieved. We find that the scattering in CuNO is highly inelastic. Intermediate, excited meta stable reaction products CuNO* live for about 0.5 to 1 ps and maybe more.

Acknowledgements

Contents

List of Figures

List of Tables

Chapter 1

Introduction

The interaction of nitric oxide with transition metal atoms is receiving increasing attention from both experimental and theoretical studies as it is of importance in various biochemical reaction pathways, atmospheric chemistry, surface chemistry and catalysis [1]. Copper ions play an important role in the NOx redox chemistry in the biological de-nitrification [2]. Many life-critical processes require metal ions, including respiration, nitrogen fixation, photosynthesis, nerve transmission and muscle contraction. In biological denitrification pathways, the reduction of nitrite to nitric oxide is carried out by the dissimilatory nitrite reductase, NiR. Two types of NiR are known; those containing Cu as cofactor and those containing heme.

By burning the biomass and fossil fuels, nitrogen, contained in the combustion air and nitrogen as components in the biomass and the fuel, oxidize at higher temperatures to NO, NO_2 and N_2O. NO being a bi-product of the combustion of fossil fuels leads to the photochemical smog and its radical nature makes it a major contributor to the ozone depletion [3]. Different sources of anthropogenic NO_x emissions are known with the most important due to combustion processes in various forms.

The term transition metal is generally restricted to that of an element with at least one ion with an incomplete outer set of d-electrons, and for the first-row transition metals, all valence electrons on the metal are regarded as d-electrons when the metal is in a complex. Transition metal complexes comprise of transition metal ions covalently bonded to other ions or molecules, generally termed ligands. Transition metals like Cu and its ions have a rich chemistry due to close-lying energy bands made up of partly filled d-orbitals, and thus serve as unique agents in a variety of biological processes. In particular, this is

the case for the middle and late first-row transition metal ions, with typically single occupation of at least some of their d-orbitals and the local structure about the metal plays an essential role for catalytic mechanisms. For example, photochemistry of many molecules adsorbed on metal surfaces frequently offers different reaction paths and lower excitation thresholds to those found when they are in the gas phase non interacting with the metal. The reason is the commonly found substrate-mediated mechanism, where incident photons generate hot electrons (holes) in the metal, which in turn attach to an unoccupied (occupied) electronic state of the adsorbate molecule. The threshold is lowered by the energy difference between the occupied adsorbate state and the Fermi level in the surface. This is of great interest in the development of better photocatalysts, which ideally would make efficient use of the solar spectrum.

3d transition-metal oxides, in particular with copper, have shown great promise on a wide range of important applications. They have for a long time challenged our ability to construct a truly many-body theory of the solid state. Copper oxides exhibit interesting properties in bulk which is actually related to the effects of electron correlations, induced through strong Coulomb interactions among the cation 3d electrons, in the narrow d-bands of these oxides. The most famous example of this is that of the Mott-Hubbard insulators. In these oxide insulators, the large on-site Coulomb energy prevails over the kinetic energy and thus suppresses the tendency of electrons to delocalize as driven by their desire to lower the kinetic energy. The transition-metal nitrides are refractory compounds and put forward a technologically important series of materials. Diatomic transition metal nitrides and oxides also serve as simple models for the study of metal-nitrogen and metal-oxygen bonding in inorganic/bioinorganic chemistry.

Investigation of reactions involving NO and transition metals are of particular interest in the development of efficient catalysts for the reduction of NO. It is known that NO dimer formation is one pathway to reduce NO.

Cu surface supports stable NO monomers which forms dimers on the surface; this allows one to investigate the photochemical behavior for both NO monomers and dimers on Cu(110). NO dimer formation is one reason why the noble metal surfaces show high reactivity to NO dissociation and N_2O formation even at liquid nitrogen temperatures. The NO dimer exhibits a highly complex photochemistry in the gas phase. The precise

relationship between the NO monomer and dimer photochemistry and the electronic structure of the substrate Cu is still an open question.

For a fundamental understanding of the nature interaction of the interaction NO molecule with Cu, and to check a possibility for homogeneous catalytic reduction of NO with Cu, we start with the CuNO system in the gas phase. CuNO and its ion has been observed in matrix isolation [5, 9], and infrared spectra in argon [7]. To get an insight into the homogeneous catalysis involving the Cu and NO fragments, an accurate prediction of the nature of the interaction between the two fragments is necessary in the gas phase [10, 11].

There is a series of questions which need to be answered. Starting with : a) What is the ground electronic state of the CuNO system? b) What is the dissociation energy of the CuNO complex? c) What is the equilibrium geometry? As of today, these quantities are not known from experiment. d)Can we predict it accurately enough? e) Can we make an analytical representation of the *ab initio* PES? f) How well do the theoretical vibrational transitions of CuNO values compare with infrared spectra, albeit recorded in matrices? g) What is the dynamics of the collision of Cu and NO? Do we expect to observe inelastic or reactive scattering? h) What are the elementary steps of the reaction kinetics inferred from the collision of Cu with NO? i) Can the Cu atom be used to reduce NO upon such a collision? What is the activation barrier? j) How important are relativistic effects with a heavy atom like Cu? h) What is the importance of electronic excited states in the reduction of NO?

For most of these questions no data is available, neither from experiment nor from theory. No quantum dynamical calculations have ever been reported in the literature using a transition metal like Cu in full dimension, primarily because of the very high density of vibrational states as it is involving a heavy element. For CuNO, the theoretical studies have not yet been able to unambiguously assign the ground state.

The main concern of this thesis is to generate accurate *ab initio* potential energy surface for use in spectroscopy and dynamics of molecules. Computational studies of molecules is nowadays an accurate method for predicting molecular properties such as equilibrium geometric structures, ground and excited electronic states, vibrational frequencies and the energy of dissociation. However, the results obtained from the calculations in this thesis refers to the gas phase and effects such as from solvent environment are neglected.

The motivations for performing calculations of spectral data is in the determination of molecular structure. The way in which a molecule vibrates and undergoes transitions is very dependent on the symmetry and shape of the molecule, and also on the way in which the atoms are connected. By carefully studying the transition frequencies and overall patterns of the spectrum, information about the molecule can be extracted. For example the strength of a bond directly affects the frequency of vibrational transitions along that bond, and the symmetry of the molecule can give certain patterns in the spectrum. In the reverse sense a predicted structure could be tested by performing a calculation and comparing the result with experimental data.

In the thesis, we give answers to most of the questions mentioned above. In Chapter 1, a brief summary of the general theoretical methods for solving the molecular Schrödinger equation is given. This includes the way the Born-Oppenheimer adiabatic approximation can be used to generate potential energy surfaces for molecules. In chemical physics, the limits of the approximations are extended because calculations are becoming so accurate that comparison with experiments show deviations which cannot be attributed to the calculations alone.

In chapter 2 we give a summary of the specific methods to solve the electronic structure and the methods we use in this thesis. We restrict ourselves here to the description of the methods which are termed as 'wave function based'. The other popular method based on Density functional theory is not described here.

In chapter 3 we describe accurate *ab initio* calculations of the ground (and excited states) to obtain electronic energies of the CuNO system. A systematic investigation of all calculation parameters is given in detail. Here we do calculations using Multi-configurational self consistent field (MCSCF), and Multireference configuration interaction (MRCI) methods and coupled cluster methods to obtain the ground electronic state. We also discuss extensively the importance of electron correlation and relativistic effects in the ground electronic state.

In chapter 4 we also describe *ab initio* calculations on the ground and excited states of diatomic fragments CuO and CuN. In particuluar, we are interested in the dissociation channels of CuNO system.

In chapter 5 We derive a novel global analytical representation of the PES and fit it with the MRCi data set with a modified Levenberg-Marquardt algorithm. From the analytical potential, we obtain the dissociation energy of the Cu + NO interaction, and the ground state equilibrium geometry of the complex. The analytical potential with its best fit parameters are good enough to be used in preliminary full dimensional quantum scattering calculations.

In chapter 6 We present the specific methods used here to solve the time-dependent Schrödinger equation for triatomic systems. The quantum dynamics of the CuNO system in the electronic ground state is described. The global analytical potential with the best fit parameters is used in 3 and 4 dimensional quantum dynamical calculations of the Cu + NO reaction where we show that the collisions are indeed highly inelastic.

Chapter 7 is a conclusion

Chapter 2

Theoretical Concepts

In this chapter we will review the general formalism and introduce the basic approximation of molecular physics, the Born-Oppenheimer approximation. We also discuss how relativistic effects can be incorporated in a quantum-mechanical formalism. However, the basic theoretical framework on which the study of atoms and molecules is couched is given by non-relativistic quantum mechanics. The principles of non-relativistic quantum mechanics are discussed in depth in many monographs and we will not discuss them here.

2.1 The Schrödinger equation

The time-dependent schrödinger equation is:

$$\imath\hbar\frac{\partial}{\partial t}\Psi(\boldsymbol{R},\boldsymbol{r},t) = H(\boldsymbol{R},\boldsymbol{r})\Psi(\boldsymbol{R},\boldsymbol{r},t) = [T(\boldsymbol{R}) + T(\boldsymbol{r}) + V(\boldsymbol{R},\boldsymbol{r})]\Psi(\boldsymbol{R},\boldsymbol{r},t) \qquad (2.1)$$

where

H is the Hamiltonian of the molecular system

$$H(\boldsymbol{R},\boldsymbol{r}) \quad = T(\boldsymbol{R}) + T(\boldsymbol{r}) + V(\boldsymbol{R},\boldsymbol{r}) \qquad (2.2)$$

$\Psi(\boldsymbol{R},\boldsymbol{r},t)$ is the wave function, $\boldsymbol{R}$ represents the nuclear Coordinates , $\boldsymbol{r}$ electronic Coordinates, V is the electronic and nuclear Potential, T is the kinetic energy operator

given as

$$T(\boldsymbol{R}) \;=\; \sum_{i=1}^{M} \frac{1}{2M_i} \nabla_i^2 \tag{2.3}$$

$$T(\boldsymbol{r}) \;=\; \sum_{i=1}^{N} \frac{1}{2m_e} \nabla_i^2 \tag{2.4}$$

Stationary states are the solution of the time independent Schrödinger equation (TISE)

$$H(\boldsymbol{R},\boldsymbol{r})\Psi(\boldsymbol{R},\boldsymbol{r},t) \;=\; E\Psi(\boldsymbol{R},\boldsymbol{r},t) \tag{2.5}$$

Separating the space and time variables in the TDSE we obtain,

$$H(\boldsymbol{R},\boldsymbol{r})\Psi(\boldsymbol{R},\boldsymbol{r},t) \;=\; E\Psi(\boldsymbol{R},\boldsymbol{r},t) \tag{2.6}$$

$$\;=\; \imath\hbar\frac{\partial}{\partial t}\Psi(\boldsymbol{R},\boldsymbol{r},t) \tag{2.7}$$

$$\Psi(\boldsymbol{R},\boldsymbol{r},t) \;=\; \Psi(\boldsymbol{R},\boldsymbol{r},0)e^{\imath E t} \tag{2.8}$$

For simplicity, we write $\Psi(\boldsymbol{R},\boldsymbol{r},0) \equiv \Psi(\boldsymbol{R},\boldsymbol{r})$

2.1.1 The Molecular Hamiltonian

Our starting point is the Hamiltonian for the system of electrons and nuclei,

$$
\begin{aligned}
\hat{H} = \;-\; & \sum_{i} \frac{\hbar^2}{2m_e} \nabla_i^2 - \sum_{i,I} \frac{Z_I e^2}{|\boldsymbol{r}_{\mathrm{i}} - \boldsymbol{R}_{\mathrm{I}}|} + \frac{1}{2} \sum_{i \neq j} \frac{e^2}{|\boldsymbol{r}_{\mathrm{i}} - \boldsymbol{r}_{\mathrm{j}}|} \\
-\; & \sum_{I} \frac{\hbar^2}{2M_I} \nabla_I^2 + \frac{1}{2} \sum_{I \neq J} \frac{Z_I Z_J e^2}{|\boldsymbol{R}_{\mathrm{I}} - \boldsymbol{R}_{\mathrm{J}}|},
\end{aligned}
\tag{2.9}
$$

where lower case letters denote the electrons and capital letters, the nuclei of charge Z_I and mass M_I. Eq. (2.9) defines the so-called coloumb Hamiltonian Here we ignore relativistic effects and magnetic fields. The Hamiltonian can be written

$$\hat{H} = \hat{T}_N + \hat{T}_e + \hat{U} \equiv \hat{T}_N + \hat{H}_e, \tag{2.10}$$

where the electron $\hat{H}_e$ contains all the potential terms $\hat{U}$. The nucleus-nucleus interaction is included for convenience; it is just an added energy E_{II} independent of electron coordinates. We will use atomic units where $\hbar, m_e, e$ are unit quantities, so that the equations simplify and the nuclear kinetic energy becomes $\hat{T}_N = \sum_I \frac{m_e}{2M_I} \nabla_I^2$.

A direct solution of the TISE with this Hamiltonian without making any further approximation is an incredibly difficult task which has been pursued only for small atoms and small diatomic molecules. There is one interesting parameter in the problem, the mass ratio $\frac{m_e}{M_I}$. Therefore we start with an analysis which uses only this fact and no other approximations, and which leads to an approximate decoupling of the electronic and nuclear motions, the Born-Oppenheimer approximation.

Strictly speaking, if the charges are not static the Hamiltonian is not fully appropriate as it does not include so-called radiation-reaction effects: a moving charged particle loses kinetic energy as radiation, the main reason why orbits of electrons in atoms are unstable in classical mechanics. A rigorous derivation of the Coulomb Hamiltonian in the presence of a radiation field can be obtained using Quantum Electrodynamics.

2.2   Potential energy surfaces

The Schrödinger equation provides a way of calculating the forces which hold atoms together. The approximate decoupling of nuclear and electronic motions is an important approximation in molecular physics. It greatly simplifies practical computations and also helps to rationalize the fundamental concept of a potential energy surface which is at the basis of modern understanding of molecular dynamics. In the following section, a short overview of this approximation will be presented. In molecules one expects to observe essentially two different timescales for the motions of light particles (electrons) and heavy particles (nuclei), so different that one may assume that, on the one hand, nuclei see only the time-averaged distribution of the electrons while, on the other hand, that the electrons follow instantaneously any movement of the nuclei. If we set the mass of the nuclei to infinity, then the kinetic energy of the nuclei can be ignored, $T_N \equiv 0$, it is the so-called clamped-nuclei Hamiltonian, which corresponds to a system where the nuclei are replaced by infinitely massive ones.

2.2.1   The Born-Oppenheimer approximation

A theoretical justification of this procedure was given by Born and Oppenheimer. In the following we will only provide a general outline of this approach.

In the first step, which depends parametrically on the nuclear geometry, the TISE is solved for one of its 'electronic states'. The eigenvalue becomes then a function of the nuclear geometry, and plays the role of a potential energy for the motion of the nuclei in a second, nuclear-motion Schrödinger equation. This approach leads to division of "low energy scales for nuclear motion" in which the electronic states "follow the nuclei" adiabatically remaining in their instantaneous states, and "high energy scales for electrons" that describe the electronic excitations. Conceptually, the approach goes as follows:

The wave function of the system is approximately given by the product of the electronic and nuclear parts:

$$\Psi(\boldsymbol{R}, \boldsymbol{r}) = \psi_e(\boldsymbol{r}; \boldsymbol{R}) \psi_n(\boldsymbol{R}) \tag{2.11}$$

Solving for the electronic part of Schrödinger equation leads to the concept of potential energy surface

$$\hat{H}_e \psi_e(\boldsymbol{r}; \boldsymbol{R}) = E_e(\boldsymbol{R}) \psi_e(\boldsymbol{r}; \boldsymbol{R}) \tag{2.12}$$

Thus we focus on the Hamiltonian for the electrons, in which the positions of the nuclei are parameters.

This specifies the electronic problem which leads to the electronic states at fixed nuclear positions $\boldsymbol{R}$:

$$\hat{H}_e(\boldsymbol{R}) \Psi_i(\boldsymbol{r}; \boldsymbol{R}) = E_i(\boldsymbol{R}) \Psi_i(\boldsymbol{r}; \boldsymbol{R}). \tag{2.13}$$

This is the many-body equation for interacting electrons in the presence of fixed nuclei.

In a second step, the full solutions for the coupled system of nuclei and electrons

$$\hat{H} \Psi_s(\boldsymbol{r}; \boldsymbol{R}) = E_s \Psi_s(\boldsymbol{r}; \boldsymbol{R}) \tag{2.14}$$

where $s = 1, 2, 3, \dots$, labels the states of the coupled system, can be written in terms of $\Psi_i(\boldsymbol{r}; \boldsymbol{R})$, [19]

$$\Psi_s(\boldsymbol{r}, \boldsymbol{R}) = \sum_i \chi_{is}(\boldsymbol{R}) \Psi_i(\boldsymbol{r}; \boldsymbol{R}), \tag{2.15}$$

if we assume that $\Psi_i(\boldsymbol{r}; \boldsymbol{R})$ define a complete set of states for the electrons at each $\boldsymbol{R}$. This assumption is often a very good one.

The states of the coupled electron–nuclear system are now specified by $\chi_{is}(\boldsymbol{R})$, which are functions of the nuclear coordinates and are the coefficients of the electronic states Ψ_i in state s. In order to find the equations for $\chi_{is}(\boldsymbol{R})$, insert expansion (2.15) into (2.14), multiply the expression on the left by $\Psi_j^*(\boldsymbol{r}, \boldsymbol{R})$, and integrate over electron variables $\boldsymbol{r}$ to find the equation

$$\left[\hat{T}_N + E_i(\boldsymbol{R}) - E_s \right] \chi_{is}(\boldsymbol{R}) = - \sum_{i'} C_{ii'} \chi_{is'}(\boldsymbol{R}), \tag{2.16}$$

where the matrix elements are given by $C_{ii'} = A_{ii'} + B_{ii'}$, with

$$A_{ii'}(\boldsymbol{R}) = \sum_J \frac{1}{M_J} \langle \Psi_i(\boldsymbol{r}; \boldsymbol{R}) | \nabla_J | \Psi_{i'}(\boldsymbol{r}; \boldsymbol{R}) \rangle \nabla_J, \tag{2.17}$$

$$B_{ii'}(\boldsymbol{R}) = \sum_J \frac{1}{2M_J} \langle \Psi_i(\boldsymbol{r}; \boldsymbol{R}) | \nabla_J^2 | \Psi_{i'}(\boldsymbol{r}; \boldsymbol{R}) \rangle. \tag{2.18}$$

Here $\langle \Psi_i(\boldsymbol{r}; \boldsymbol{R}) | \mathcal{O} | \Psi_{i'}(\boldsymbol{r}; \boldsymbol{R}) \rangle$ means integrations over only the electronic variables $\boldsymbol{r}$ for any operator $\mathcal{O}$.

The adiabatic or Born-Oppenheimer approximation is to ignore the off-diagonal $C_{ii'}$ terms, e.g the electrons are assumed to remain in a given state m as the nuclei move. Although the electron wave function $\Psi_i(\boldsymbol{r}; \boldsymbol{R})$ and the energy of state m change, the electrons do not change state and no energy is transferred between the degrees of freedom described by the equation for the nuclear variables $\boldsymbol{R}$ and the degree of freedom of the electrons only adiabatically. The diagonal terms can be treated easily. First, it can be shown that $A_{ii} = 0$ simply from the requirement that Ψ is in $\mathcal{L}^2$. The term $B_{ii}(\boldsymbol{R})$ can be grouped with $E_i(\boldsymbol{R})$ to determine a modified potential function for the nuclei $U_i(\boldsymbol{R}) = E_i(\boldsymbol{R}) + B_{ii}(\boldsymbol{R})$. Thus, in the adiabatic approximation, the nuclear motion is described by a purely nuclear equation for each electronic state i

$$\left[- \sum_J \frac{1}{2M_J} \nabla_J^2 + U_i(\boldsymbol{R}) - E_{in} \right] \chi_{in}(\boldsymbol{R}) = 0, \tag{2.19}$$

where $n = 1, 2, 3, \ldots$, labels the nuclear states within the electronic state i.

So long as we can justify neglecting the off-diagonal terms that couple different electron states, we can solve the nuclear motion problem, Eq. (2.19), given the function $U_i(\boldsymbol{R})$ for the particular electronic state i that evolves adiabatically with nuclear motion.

This is an excellent approximation except for cases where there is degeneracy or near degeneracy of the electronic states. The non-adiabatic terms will become large for configurations where potential energy surfaces cross or come very close to one another.At the same time, while computing the adiabatic approximation is relatively straightforward, the nonadiabatic formalism becomes extremely difficult. Special care must be taken for cases such as transition states in molecules where electronic states become degenerate.

The practice of first solving the clamped-nuclei Hamiltonian and then using the resulting potential surface for the nuclear motion can also be used very far from the potential minumum or, indeed, it can be used for purely repulsive states which have no such minimum at all.

2.2.2 Equilibrium geometry

By 'equilibrium geometry' of a molecule one intends for the set of nuclear coordinate $\boldsymbol{R}_{\mathrm{e}}$ for which the clamped-nuclei energy is a minimum in a given electronic state. It should be remembered, however, that these values do not literally represent the equilibrium position of the nuclei in a reality. Like electrons, nuclei are delocalized over the molecule and the spatial density of a certain nuclear species can be calculated from the squared modulus of the nuclear wave function integrating out the coordinates of all other nuclei. These nuclear density distributions may be strongly peaked at the equilibrium values $\boldsymbol{R}_{\mathrm{e}}$, but need not be in all situations, like for example in the case of highly-excited rotation-vibration states or in that of molecules with only a shallow minimum in the clamped-nuclei Hamiltonian.

The Born-Oppenheimer approximation detailed previously is critical in any vibrational calculation since it separates electron motion from the nuclear motion. This approximation makes it possible to consider a potential energy surface which represents the energy of any configuration of the atoms for a particular electronic state. The vibrational problem can then be solved using a purely nuclear motion Hamiltonian with a potential for

the given electronic state. The potential can be derived from either *ab initio* calculations of the electronic energy of a given nuclear configuration $\boldsymbol{R}$, or by adjusting an analytical function of $\boldsymbol{R}$ to fit experimental data such as the line position of an infrared spectrum. But it should be remembered that problems can arise when the electronic motion is not separable from the nuclear motion and in this case the calculation of vibrational spectra from isolated potential energy surface will likely not suffice. Then a set of coupled vibrational Schrödinger equation must be solved.

2.3 Relativistic effects

2.3.1 The Dirac Hamiltonian

Dirac derived in 1928 a relativistic equation which describes a single particle of mass m with spin $1/2$, e.g. an electron, in an external potential. The wave function of a Dirac particle is a four-component object

$$\boldsymbol{\Psi}(\boldsymbol{r}) = \begin{pmatrix} \psi_1(\vec{r}) \\ \psi_2(\vec{r}) \\ \psi_3(\vec{r}) \\ \psi_4(\vec{r}) \end{pmatrix} \tag{2.20}$$

We are interested in an equation of the form

$$i\hbar \frac{\partial}{\partial t} \boldsymbol{\Psi} = H \boldsymbol{\Psi} \tag{2.21}$$

Because of the first derivative $\frac{\partial}{\partial t}$, we would like to have first derivatives $\frac{\partial}{\partial x}$ etc. as well. Note that the series expansion of the square root in

$$E - V = mc^2 \sqrt{1 + p^2/m^2c^2} \tag{2.22}$$

would contain *all* powers of (p^2/c^2).

Suppose now that the Hamiltonian is linear in all $\frac{\partial}{\partial x_\mu}$ and that the wave function Ψ has N components,

$$\mathbf{\Psi} = \begin{pmatrix} \psi_1 \\ \vdots \\ \psi_N \end{pmatrix} \tag{2.23}$$

Then the most general free-particle wave equation is

$$\imath\hbar\frac{\partial}{\partial t}\Psi_n = \sum_{l=1}^{N}[c\vec{\alpha}_{nl}\cdot\vec{p} + \beta_{nl}mc^2]\Psi_l \tag{2.24}$$

where n runs from $1\ldots N$, and

$$\vec{\alpha}_{nl}\cdot\vec{p} = -\imath\hbar[(\alpha_{nl})_x\frac{\partial}{\partial x} + (\alpha_{nl})_y\frac{\partial}{\partial y} + (\alpha_{nl})_z\frac{\partial}{\partial z} \tag{2.25}$$

In terms of the $N \times N$ matrices $\vec{\boldsymbol{\alpha}}$ and $\boldsymbol{\beta}$,

$$\imath\hbar\frac{\partial}{\partial t}\mathbf{\Psi} = [-\imath\hbar c\vec{\boldsymbol{\alpha}}\cdot\nabla + \boldsymbol{\beta}mc^2]\Psi \equiv h_D\Psi \tag{2.26}$$

with the Dirac Hamiltonian

$$\boldsymbol{h}_D = c\vec{\boldsymbol{\alpha}}\cdot\vec{p} + \boldsymbol{\beta}mc^2 \tag{2.27}$$

The components of α are the $N \times N$ matrices ($N \geq 4$, see below) $\vec{\boldsymbol{\alpha}_x}, \vec{\boldsymbol{\alpha}_y}$ and $\vec{\boldsymbol{\alpha}_z}$. In order for h_D to be hermitian, $\vec{\boldsymbol{\alpha}}$ and $\boldsymbol{\beta}$ must be hermitian:

$$\vec{\boldsymbol{\alpha}}^\dagger = \vec{\boldsymbol{\alpha}}, \quad \boldsymbol{\beta}^\dagger = \boldsymbol{\beta} \tag{2.28}$$

For all points in space-time to be equivalent, $\vec{\boldsymbol{\alpha}}$ and $\boldsymbol{\beta}$ must be constant and dimensionless. Consequently they commute with $\vec{r}$ and $\vec{p}$.

We still want to satisfy

$$E^2 = c^2p^2 + m^2c^4$$

for all components $\psi_1\ldots\psi_N$:

$$-\hbar^2\frac{\partial^2}{\partial t^2}\Psi = [-\hbar^2c^2\nabla^2 + m^2c^4]\Psi \tag{2.29}$$

Then the Dirac equation

$$h_D \mathbf{\Psi} = \imath\hbar \frac{\partial}{\partial t} \mathbf{\Psi}$$

will connect the different components.

From Eq. (2.29), it turns out

$$\boldsymbol{\alpha}_i \boldsymbol{\alpha}_j + \boldsymbol{\alpha}_j \boldsymbol{\alpha}_i \quad = 2\delta_{ij} \boldsymbol{I} \tag{2.30}$$

$$\boldsymbol{\beta}\boldsymbol{\alpha}_i + \boldsymbol{\alpha}_i \boldsymbol{\beta} \quad = 0 \tag{2.31}$$

$$\boldsymbol{\beta}^2 \quad = \boldsymbol{I} \tag{2.32}$$

$\boldsymbol{I}$ being the $N \times N$ unit matrix. Because $\vec{\boldsymbol{\alpha}}$ and $\boldsymbol{\beta}$ were hermitian, their eigenvalues are real. According to Eq. (2.30), the squares of these eigenvalues equal 1. Hence the eigenvalues are ± 1. Dirac showed that Eq. (2.30) is satisfied by

$$\boldsymbol{\beta} = \begin{pmatrix} \boldsymbol{I} & 0 \\ 0 & -\boldsymbol{I} \end{pmatrix} \tag{2.33}$$

$$\vec{\boldsymbol{\alpha}} = \begin{pmatrix} 0 & \vec{\boldsymbol{\sigma}} \\ \vec{\boldsymbol{\sigma}} & 0 \end{pmatrix} \tag{2.34}$$

where

$$\boldsymbol{I} = \begin{pmatrix} 1 & 0 \\ 0 & 1 \end{pmatrix}, \quad \vec{\boldsymbol{\sigma}_1} = \begin{pmatrix} 0 & 1 \\ 1 & 0 \end{pmatrix}, \quad \vec{\boldsymbol{\sigma}_2} = \begin{pmatrix} 0 & -i \\ i & 0 \end{pmatrix}, \quad \vec{\boldsymbol{\sigma}_3} = \begin{pmatrix} 1 & 0 \\ 0 & -1 \end{pmatrix} \tag{2.35}$$

2.3.2   The many-electron Dirac equation

At variance with the Schrödinger equation, the Dirac equation is not rigorously generalisable to systems of many particles and, more generally, a universally-accepted quantum relativistic many-particle theory does not exist. However, applications to atoms and molecules based on generalisations of the Dirac equation have been very successful and the general consensus is that numerical results obtained from the Dirac equation are adequate for chemical purposes.

The Dirac-Coulomb-Breit Hamiltonian applied in a four-component formalism represents the theoretically most rigorous method available today to treat relativistic effects in molecules; unfortunately, it is computationally very intensive and calculations are feasible only on small systems. A two-component quasi-relativistic Hamiltonian for many-electron systems with the inclusion of the Breit term, i.e. the Breit-Pauli Hamiltonian, is gained from the Dirac-Coulomb-Breit Hamiltonian for two-electron systems through the Foldy-Wouthuysen (FW) transformation and a generalisation to N electrons.[60]

2.3.2.1   The Douglas-Kroll-Hess Hamiltonian

The Douglas-Kroll-Hess method [54, 55] belongs to a family of methods where one performs a unitary transformation of the Dirac Hamiltonian with the end of uncoupling the negative energy degrees of freedom. If the transformation is exactly unitary the transformed operator will have exactly the same electronic spectrum of the original Dirac Hamiltonian, but will act on two-component wave functions. The methods, which are sometimes called quasi-relativistic even though they are potentially equivalent to the fully relativistic Dirac Hamiltonian, now available that perform this transformation in a formally exact and computationally efficient way. Here is a very brief summary of the method.

The DK formalism, is an *all electron* method, and is based on a series of unitary transformations $\boldsymbol{U}_0, \boldsymbol{U}_1, \ldots$ of which the lowest is the *free-particle FW-transformation* defined by

$$
\begin{cases}
\boldsymbol{U}_0 = A(1 + \boldsymbol{\beta}R) \\
\boldsymbol{U}_0^{-1} = (R\boldsymbol{\beta} + 1)A
\end{cases}
\tag{2.36}
$$

where we have

$$
A = \sqrt{\frac{E_p + mc^2}{2E_p}}
\tag{2.37}
$$

$$
R = \frac{c\vec{\boldsymbol{\alpha}} \cdot \vec{p}}{E_p + mc^2}
\tag{2.38}
$$

$$
E_p = c\sqrt{p^2 + m^2c^2}
\tag{2.39}
$$

Applying $\boldsymbol{U}_0$ to $\boldsymbol{h}_D = c\vec{\boldsymbol{\alpha}} \cdot \vec{p} + (\boldsymbol{\beta} - 1)mc^2 + V$ gives

$$
\boldsymbol{U}_0 \boldsymbol{h}_D \boldsymbol{U}_0^{-1} = \boldsymbol{\beta}E_p + \boldsymbol{\mathcal{E}_1} + \boldsymbol{\mathcal{O}_1} \equiv H_1
\tag{2.40}
$$

with

$$\boldsymbol{\mathcal{E}_1} = A(V + RVR)A$$

$$\boldsymbol{\mathcal{O}_1} = \boldsymbol{\beta}A(RV - VR)A \tag{2.41}$$

For chemical purposes one more transformation is needed. One uses

$$\boldsymbol{U}_1 = \sqrt{1 + \boldsymbol{W}_1^2} + \boldsymbol{W}_1 \tag{2.42}$$

with $\boldsymbol{W}_1$ anti-hermitian, $\boldsymbol{W}_1^\dagger = -\boldsymbol{W}_1$. Performing the transformation through $\boldsymbol{U}_1$ and expanding the square root in powers of $\boldsymbol{W}_1$,

$$
\begin{aligned}
\boldsymbol{U}_1\boldsymbol{H}_1\boldsymbol{U}_1^{-1} = \;&\beta E_p - [\beta E_p, \boldsymbol{W}_1] + \boldsymbol{\mathcal{E}_1} + \boldsymbol{\mathcal{O}_1} \\
&+ \frac{1}{2}\beta E_p\boldsymbol{W}_1^2 + \frac{1}{2}\boldsymbol{W}_1^2\beta E_p - \boldsymbol{W}_1\beta E_p\boldsymbol{W}_1 \\
&+ [\boldsymbol{W}_1, \boldsymbol{\mathcal{O}_1}] + [\boldsymbol{W}_1, \boldsymbol{\mathcal{E}_1}] + \dots
\end{aligned}
\tag{2.43}
$$

omitting higher order terms. The first-order odd term is eliminated by setting

$$[\beta E_p, \boldsymbol{W}_1] = \boldsymbol{\mathcal{O}_1} \tag{2.44}$$

and solving for $\boldsymbol{W}_1$.

The final result is

$$H^{\text{decoupled}} \cong \beta E_p + \boldsymbol{\mathcal{E}_1} - \beta\Big[\boldsymbol{W}_1 E_p\boldsymbol{W}_1 + \frac{1}{2}[\boldsymbol{W}_1^2, E_p]\Big]. \tag{2.45}$$

The DKH Hamiltonian [56, 57] has now been implemented in a large number of programs, including MOLPRO, which we use in the calculation. Having to deal with an infinite expansion is generally not a serious practical limitation because it has recently been possible to efficiently compute corrections to essentially arbitrary order, and furthermore the convergence in n is usually rapid. These methods can and usually are combined with the neglect of spin-dependent terms; if this is done the methods operate on single-component wave functions as in the non-relativistic case and, as the time required to set up the transformation is essentially negligible, they have the same computational cost as the corresponding non-relativistic method.

For calculating properties, the operator has to be transformed as well, if transformed Hamiltonians are used. This could be quite tedious.

Chapter 3

Solving the Many Body Schrödinger Equation

3.1 Solving the electronic-motion problem

Finding the eigenvalues and the eigenvectors of the Hamiltonian given by the many body Schrödinger equation is difficult and despite numerous studies previously, the task remains challenging.[59, 61] As a general situation, exactly-solvable quantum many-body problems are few.

Because analytical solutions are not obtainable the eigenvalue problem must be solved numerically. This has so far proven to be a difficult task. Generic grid-based or finite element numerical methods developed for partial differential equations scale exponentially with the number of dimensions and thus become essentially impossible to use in systems with more than one or two particles.

A comment on the subject was famously given by Dirac in 1929 [20]

> The underlying physical laws necessary for the mathematical theory of a large part of physics and the whole of chemistry are thus completely known, and the difficulty is only that the exact application of these laws leads to equations much too complicated to be soluble. It is therefore desirable that approximate methods of applying quantum mechanics should be developed,

which can lead to an explanation of the main features of complex systems without too much computation.

3.2   The variational principle

Since exact closed form solutions of the Schrödinger equation are hard to obtain, the search is often restricted to the ground electronic state. In chemistry, the ground electronic state plays a major role. Typical electronic excitations have energies which are significantly higher than thermal energies. As a result the structure of molecules and their thermodynamical properties are determined by the potential surface of the ground electronic state alone.

Obtaining the ground state energy is based on the fact that any guess of a wave function will lead to an energy greater than that of the actual ground state. This fact is called the variational principle.

Consider a Hamiltonian $\hat{H}$ which has eigen functions ϕ_n with energies E_n with $E_1 \leq E_2 \leq ... \leq E_n$ unknown to us. A trial wave function Ψ is examined. Since the set of eigen functions of $\hat{H}$ is complete the function Ψ can be expanded by using the set:

$$\Psi = \sum_n a_n \psi_n \tag{3.1}$$

The expectation of the trial wave function becomes:

$$\langle \Psi | \hat{H} | \Psi \rangle = \langle \sum_n a_n \psi_n | \hat{H} | \sum_m a_m \psi_m \rangle$$
$$= \langle \sum_n a_n \psi_n | \sum_m E_m a_m | \psi_m \rangle$$
$$= \sum_{nm} a_n^* a_m E_m \langle \psi_n | \psi_m \rangle = \sum_n |a_n|^2 E_n \tag{3.2}$$

This result can be used to construct the inequality:

$$\langle \Psi | \hat{H} | \Psi \rangle = \sum_n |a_n|^2 E_n \geq \sum_n |a_n|^2 E_1 = E_1 \sum_n |a_n|^2 \tag{3.3}$$

using the normalization condition $\langle \Psi | \Psi \rangle = \sum_n |a_n|^2 = 1$ and the condition that E_1 is lower than any other energy.

If the trial wave function Ψ is not normalized the theorem can be modified:

$$
\begin{aligned}
\langle\Psi|\hat{H}|\Psi\rangle &= \langle\Psi|\hat{H}|\sum_m a_m\psi_m\rangle \\
&= \langle\Psi|\sum_m E_m a_m|\psi_m\rangle \\
\geq \langle\Psi|\sum_m E_0 a_m|\psi_m\rangle &= E_0\langle\Psi|\sum_m a_m|\psi_m\rangle = E_0\langle\Psi|\Psi\rangle \qquad (3.4)
\end{aligned}
$$

Which can be modified to:

$$
\frac{\langle\Psi|\hat{H}|\Psi\rangle}{\langle\Psi|\Psi\rangle} \geq E_0 \qquad (3.5)
$$

The conclusion: any normalized trial function has an expectation energy value larger than the ground state.

3.3   Hartree-Fock Method

All quantities in this section are dimensionless quantities $Q* = \frac{Q}{[Q]}$, where $[Q]$ is the unit of the quantity. We use atomic units, and for brevity, we omit the asterisk. It is well-known that the difficulty in obtaining the two-electron wave function $\Psi(\vec{r}_1, \vec{r}_2)$ for the helium Hamiltonian originates from the Coulomb interaction term between electrons 1 and 2. D.R. Hartree [21] proposed that the many-electron wave function can still be expressed as a product of two single-particle functions, even in the presence of mutual repulsion. In other words, we will now simply take the functional form $\Psi(\vec{r}_1, \vec{r}_2) = \psi_a(\vec{r}_1)\psi_b(\vec{r}_2)$, but without yet specifying ψ_a or ψ_b.

Given this trial wave function, Hartree's iterative method describes how to determine the single-particle states ψ_a and ψ_b . Again, "iteration" implies that the algorithm analyzes each electron one at a time. Staying with the Helium example, as a starting point, we consider the doubly-charged helium nucleus stripped of both electrons. In assigning a wave function to the first electron around this nucleus, the relevant potential is clearly $V_{\text{nucl}} = -2/r_1$, for which we have available an analytical form of the ground-state eigen function $\psi_a^{(0)}$.

We then move on to electron 2. Recalling that $|\psi_a(\vec{r}_1)|^2$ represents the spatial probability distribution of electron 1, it is plausible to associate a repulsive potential V_{ee} due to the corresponding charge density, $\rho_a = |\psi_a(\vec{r}_1)|^2$. Therefore, the Schrödinger equation (SE)

for electron 2 will involve the electron-electron potential V_{ee} in addition to V_{nucl}. The electrostatic potential energy of the electron-electron interaction can then be obtained as

$$V_{\text{ee}}(\vec{r}_2; \psi_a) = \int d^3r_1 \frac{1}{r_{12}} \rho_a(\vec{r}_1) = \int d^3r_1 \frac{1}{r_{12}} |\psi_a(\vec{r}_1)|^2 \qquad (3.6)$$

where $r_{12} = |\vec{r}_1 - \vec{r}_2|$. The notation for V_{ee} explicitly indicates its dependence on ψ_a.

Returning to electron 1, it is now possible to utilize ψ_b to similarly calculate $V_{\text{ee}}(\vec{r}_1; \psi_b)$. The new SE is solved, yielding $\psi_a^{(1)}(\vec{r}_1)$. The process is repeated, alternating between the two electrons, until the sequences of functions $\left\{ \psi_a^{(i)} \right\}$ and $\left\{ \psi_b^{(i)} \right\}$ converge within some desired precision.

Formally, we are solving the equations

$$\left[-\frac{1}{2}\nabla_1^2 + V_{\text{nucl}}(\vec{r}_1) + V_{\text{ee}}(\vec{r}_1; \psi_b) \right] \psi_a(\vec{r}_1) = E_a \psi_a(\vec{r}_1) \qquad (3.7)$$

$$\left[-\frac{1}{2}\nabla_2^2 + V_{\text{nucl}}(\vec{r}_2) + V_{\text{ee}}(\vec{r}_2; \psi_a) \right] \psi_b(\vec{r}_2) = E_b \psi_b(\vec{r}_2) \qquad (3.8)$$

in an iterative fashion. The essential idea of the Hartree procedure is the reduction of the many-body Hamiltonian to several single-particle Hamiltonians. On the other hand, due to the coupling through V_{ee}, a direct solution to the above set of nonlinear Schrödinger equations is difficult.

The Hartree method ignores the antisymmetry requirement for the many electron wave function. In next section, we will rectify this by introducing the Hartree-Fock (HF) approximation, which takes as its trial wave function Ψ a Slater determinant. The HF approximation is an application of the variational principle described in previous section.

3.4   Slater determinant wave functions

An electron has a spin degree of freedom in addition to its spatial coordinates. In fact, the antisymmetry requirement applies to an exchange of both spatial and spin coordinates, whereas so far we dealt solely with space in our previous discussion of the Hartree iteration. Hence, we must now augment our previous notation to explicitly incorporate spin. The defining property of the Hartree-Fock (HF) approximation, as an improvement on the Hartree method, is that the trial wave function Ψ is chosen

to be a Slater determinant of orthonormal single-particle functions of spin and space coordinates. The motivation arises from the fact that the mathematical properties of a determinant trivially satisfy the antisymmetry requirement.

We use $\vec{x}_i$ to denote the complete set of coordinates associated with the i-th electron, comprised of the spatial $\vec{r}_i$ and spin $w_i = \pm\frac{1}{2}$ components

$$\langle \vec{x}_i | m \rangle = \chi_m(\vec{x}_i) = \chi_m(i) = \psi_m(\vec{r}_i)\lambda_m(w_i) \tag{3.9}$$

The first form is useful when we wish to emphasize the one-electron state, rather than the electron index. The complete one-electron state $\chi_m(\vec{x}_i)$ ("spin orbital"), is separated into its spatial $\psi_m(\vec{r}_i)$ and spin $\lambda_m(w_i)$ components.

With this, the trial determinantal wave function may be written [23]

$$\Phi(\vec{x}_1, \vec{x}_2, ..., \vec{x}_N) = \frac{1}{\sqrt{N!}} \begin{vmatrix} \chi_1(\vec{x}_1) & \chi_2(\vec{x}_1) & \cdots & \chi_N(\vec{x}_1) \\ \chi_1(\vec{x}_2) & \chi_2(\vec{x}_2) & \cdots & \chi_N(\vec{x}_2) \\ \vdots & \vdots & & \vdots \\ \chi_1(\vec{x}_N) & \chi_2(\vec{x}_N) & \cdots & \chi_N(\vec{x}_N) \end{vmatrix} \tag{3.10}$$

$$= \frac{1}{\sqrt{N!}} \sum_{n=1}^{N!} (-1)^{p_n} P_n \{\chi_1(1)\chi_2(2)\ldots\chi_N(N)\} \tag{3.11}$$

In Eq. (3.11), the index n runs over all $N!$ permutations P_n of the N one-electron states. The quantity p_n takes on 0 or 1 depending on whether the permutation P_n is odd or even, respectively. We may regard the action of P_n as permuting the n spin-orbital indices and $(-1)^{p_2} = -1$ by definition.

Our task in computing $\langle \Psi | H | \Psi \rangle$ is made simpler by recognizing the "one- and two-electron" structure of the electronic Hamiltonian, and by using the *indistinguishability* of electrons to take advantage of that structure. Begin by writing:

$$H = \sum_{i=1}^{N} \left(-\frac{1}{2}\nabla_i^2 - \sum_{A=1}^{M} \frac{Z_A}{r_{iA}} \right) + \sum_{i=1}^{N} \sum_{j>i}^{N} \frac{1}{r_{ij}}$$

$$= \sum_{i=1}^{N} h_1(i) + \sum_{i=1}^{N} \sum_{j>i}^{N} h_2(i,j) \tag{3.12}$$

Here, we have identified the *one-electron operator*

$h_1(i) = -\frac{1}{2}\nabla_i^2 - \sum_{A=1}^M Z_A/r_{iA}$ (of the i-th electron)

and the *two-electron operator*

$h_2(i, j) = r_{ij}^{-1}$ (involving electrons i and j).

Only one and two sets of electron coordinates are involved in the matrix elements of $h_1(i)$ and $h_2(i, j)$ respectively. In particular, $h_1(i)$ is also termed the *core-Hamiltonian* of the i-th electron, describing its kinetic and potential energy in the field of the nuclei. $\langle \Psi | h_1(1) | \Psi \rangle$ can be expressed as:

$$
\begin{aligned}
\langle \Psi | h_1(1) | \Psi \rangle &= \frac{(N-1)!}{N!} \sum_{m=1}^N \int d\tau_1 \chi_m^*(\vec{x}_1) h_1(1) \chi_m(\vec{x}_1) \\
&= \frac{1}{N} \sum_{m=1}^N \langle m | h_1(1) | m \rangle
\end{aligned}
\tag{3.13}
$$

where the sum is over the single-particle functions and the integral extends over spatial and spin components. So, we find that the core-energy of electron 1 is an average of the expected core-energy of every single-particle state that comprises the determinant. This is a direct consequence of the indistinguishability of electrons. It is then clear that $h_1(i) = h_1(j)$ for every i, j. We can thus conclude:

$$
\langle \Psi | \sum_{i=1}^N h_1(i) | \Psi \rangle = \sum_{m=1}^N \langle m | h_1(1) | m \rangle
\tag{3.14}
$$

Conventionally, the integration variable of the one-electron integral is taken to be $\vec{x}_1$.

The two electron integrals can be obtained by,

$$
\langle \Psi | \sum_{i=1}^N \sum_{j>i}^N h_2(i, j) | \Psi \rangle = \binom{N}{2} \langle \Psi | h_2(1, 2) | \Psi \rangle = \frac{N(N-1)}{2} \langle \Psi | h_2(1, 2) | \Psi \rangle
\tag{3.15}
$$

This is valid since any pair of electrons will have identical $\langle \Psi | h_2(i, j) | \Psi \rangle$ according to indistinguishability. Furthermore, the double sum accounts for all of the unique pairs among N electrons, of which there are $N(N-1)/2$. Proceeding we obtain:

$$\frac{N(N-1)}{2} \langle\Psi|\, h_2(1,2)\, |\Psi\rangle = \frac{1}{2} \sum_{m=1}^{N} \sum_{n=1}^{N} \left(\langle mn|\, h_2(1,2)\, |mn\rangle - \langle mn|\, h_2(1,2)\, |nm\rangle \right) \quad (3.16)$$

We have then finished computing $\langle\Psi|\, H\, |\Psi\rangle$:

$$
\begin{aligned}
\langle\Psi|\, H\, |\Psi\rangle &= \langle\Psi|\, \sum_{i=1}^{N} h_1\, |\Psi\rangle + \langle\Psi|\, \sum_{i=1}^{N}\sum_{j>i}^{N} h_2\, |\Psi\rangle \\
&= \sum_{m=1}^{N} \langle m|\, h_1\, |m\rangle + \frac{1}{2}\sum_{m=1}^{N}\sum_{n=1}^{N} \left(\langle mn|\, h_2\, |mn\rangle - \langle mn|\, h_2\, |nm\rangle \right) \quad (3.17)
\end{aligned}
$$

In the Hartree-Fock theory, [22] the many-particle wave function Ψ is constrained to remain a Slater determinant formed by mutually orthonormal single-particle functions $\{\chi_m \,|\, m = 1, 2, \ldots, N\}$. However, as in the original Hartree procedure, the single particle states are not yet identified, and therein lies the variational degrees of freedom.

More precisely, we view the energy expectation $\langle\Psi|\, H\, |\Psi\rangle$ as a *functional* on $\{\chi_m\}$. We can then apply the standard techniques of the calculus of variations, seeking an optimal set of single-particle functions that makes $\langle\Psi|\, H\, |\Psi\rangle$ stationary under arbitrary infinitesimal changes, $\chi_m \rightarrow \chi_m + \delta\chi_m$. The variational principle then shows that the resulting set produces the best single-determinant approximation to the ground state using the technique of Lagrange multipliers and minimization. The minimization condition is equivalent to:

$$
\begin{aligned}
f(\vec{x}_1)\chi_m(\vec{x}_1) &= \epsilon_m \chi_m(\vec{x}_1) \quad\quad\quad\quad\quad\quad\quad\quad\quad\quad\quad\quad\quad\quad\quad\quad\quad (3.18) \\
f(\vec{x}_1) &= h_1 + \sum_{n=1}^{N} \int d\tau_2 \frac{1}{r_{12}} |\chi_n(\vec{x}_2)|^2 - \sum_{n=1}^{N} \int d\tau_2 \chi_n^*(\vec{x}_2)\frac{1}{r_{12}} P_2 \chi_n(\vec{x}_2)
\end{aligned}
$$

which holds for $m = 1, 2, \ldots, N$. The action of P_2 on χ_n is to exchange it against χ_m in Eq. (3.18)

These equations, having the form of a single-particle Schrödinger equation, are the *Hartree-Fock equations* that characterize the optimal single-particle states to be used in the Slater determinant. We can also conclude that the corresponding Lagrange multipliers have the important physical interpretation as the single-particle energies. The operator $f(\vec{x}_1)$ is called the *Fock operator*, and the orthogonality of its eigen functions is proved in literature. Unfortunately, the Fock operator couples the N equations, and makes Eq. (3.18) a nonlinear SE; hence the need for iterative methods.

The electronic repulsion term $\sum_{n=1}^{N} \int d\vec{x}_2 \frac{1}{r_{12}} |\chi_n(\vec{x}_2)|^2$ in the HF equations, agrees with the intuition embodied in the original Hartree iteration. However, the additional *exchange term* $\sum_{n=1}^{N} \int d\vec{x}_2 \chi_n^*(\vec{x}_2) \frac{1}{r_{12}} P_2 \chi_n(\vec{x}_2)$ originates from antisymmetrization of the trial wave function.

Recall that to form the many-particle ground state, we seek the N lowest-energy single-particle eigen functions of the Hartree-Fock equation (Eq. (3.18)). When N is even, the Fock operator does not depend on electron spin. It then follows that we can focus on the $\frac{N}{2}$ lowest-energy spatial states $\{\psi_n \mid n = 1, 2, \ldots, N/2\}$, and then doubly occupy each with electrons of opposite spin. Then we just obtain the $\frac{N}{2}$ lowest-energy single-particle eigen functions of the spatial Hartree-Fock equation:

$$f(\vec{r}_1)\psi_n(\vec{r}_1) = \epsilon_n \psi_n(\vec{r}_1) \tag{3.19}$$

3.4.1 Introduction of a basis and Roothan-Hall Equations

In 1951 C.C.J. Roothaan [24] demonstrated that, by introducing a set of known spatial *basis functions*, the differential Hartree-Fock equations could be reformulated as an algebraic equation to be solved by standard matrix techniques. This technique is explained here for a potentially closed shell system.(even number of electrons)

Suppose that $\{\phi_\mu\}$ represents a set of basis functions for the space of square integrable functions. In practice, we must choose some K-element subset of this basis for a computer implementation. We can then approximate the i-th spatial wave function by a linear combination

$$\psi_i = \sum_{\mu=1}^{K} C_{i\mu} \phi_\mu \qquad i = 1, 2, \ldots, (K \geq \frac{N}{2}) \tag{3.20}$$

The above expression would be exact if the truncated basis set $\{\phi_\mu \mid \mu = 1, 2, \ldots, K\}$ correspond in fact to a complete set.[1] However, in practice, the basis functions typically have no claim on rigorous completeness.

To obtain the HF equations in matrix form, consider again the spatial Hartree-Fock equation (Eq. 3.19). Begin by expanding $\psi_m(\vec{r}_1)$ in the chosen basis,

$$f(\vec{r}_1) \sum_\nu C_{\nu m} \phi_\nu(\vec{r}_1) = \epsilon_m \sum_\nu C_{\nu m} \phi_\nu(\vec{r}_1) \tag{3.21}$$

We then multiply by $\phi_\mu^*(\vec{r}_1)$ on the left and integrate, to obtain:

$$\sum_\nu \left\{ \int d\vec{r}_1 \phi_\mu^*(\vec{r}_1) f(\vec{r}_1) \phi_\nu(\vec{r}_1) \right\} C_{\nu m} = \epsilon_m \sum_\nu \left\{ \int d\vec{r}_1 \phi_\mu^*(\vec{r}_1) \phi_\nu(\vec{r}_1) \right\} C_{\nu m} \tag{3.22}$$

This motivates the definition of two matrices. The first is the *Fock matrix* $F_{\mu\nu} = \int d\vec{r}_1 \phi_\mu^*(\vec{r}_1) f(\vec{r}_1) \phi_\nu(\vec{r}_1)$. The second is the *overlap matrix* $S_{\mu\nu} = \int d\vec{r}_1 \phi_\mu^*(\vec{r}_1) \phi_\nu(\vec{r}_1)$. With these definitions Eq. 3.22 becomes,

$$\sum_\nu F_{\mu\nu} C_{\nu m} = \epsilon_m \sum_\nu S_{\mu\nu} C_{\nu m} \tag{3.23}$$

This result may more succinctly written as a single matrix equation, known as the *Roothaan equation*:

$$\mathbf{F}\mathbf{C} = \mathbf{S}\mathbf{C}\epsilon \tag{3.24}$$

Here, the matrix ϵ is diagonal and contains the single-particle energy ϵ_m as the m-th element. Furthermore, $\mathbf{C}$ is the $K \times K$ *coefficient matrix* whose n-th column denotes the expansion coefficients of ψ_n in the basis set $\{\phi_\mu\}$. Hence, solving for the optimal single-particle states in the Hartree-Fock approximation is equivalent to solving for the coefficient matrix $\mathbf{C}$ that solves the Roothaan equation.

$\mathbf{F}$ depends on the coefficient matrix. It then follows that the Roothaan equation is nonlinear, and cannot be directly solved by standard linear techniques.

Instead, we use an iterative approach in which we first compute $\mathbf{F}^{(i-1)}$ based on the previous set of coefficients $\mathbf{C}^{(i-1)}$ (or by an initial guess). The Fock matrix thus generated

---

[1] In order to obtain square matrices, we will seek $K \geq N/2$ spatial orbitals. As long as we have at least $N/2$ one-electron states, we're fine.

is then considered to be fixed, which allows us to solve for the next set of coefficients $\mathbf{C}^{(i)}$ via the Roothaan-Hall [25] equation, which may now be notated as:

$$\mathbf{F}^{(i-1)}\mathbf{C}^{(i)} = \mathbf{S}\mathbf{C}^{(i)}\epsilon \tag{3.25}$$

As in the section on the Hartree ansatz, such iteration is tantamount to holding the wave functions of the other electrons ($j \neq i$) fixed as we generate the new wave function for the i-th electron. The limit of the sequence of matrices $\mathbf{C}^{(i)} \to \mathbf{C}$ is then taken to be the solution of the Roothaan equations. The columns of the coefficient matrix can then be used to express the single-particle wave functions (in the chosen basis) of the Slater-determinant, thus completing our implementation.

There are several matrix techniques for solving Eq. (3.25), which differs from standard eigenvalue equations by the presence of the overlap matrix. We use methods implemented in MOLPRO. The Fock operator determined at the end of a Hartree-Fock calculation is a Hermitian operator and its eigen functions and eigenvalues are given by the canonical molecular orbitals and orbital energies. The $N/2$ molecular orbitals which enter in the definition of $\mathbf{F}$ constitute the occupied orbitals, while all the others are called unoccupied or virtual orbitals. The single-particle picture of molecules which arises from the method is still deeply engrained in modern chemical thinking.

The exact wave function $\boldsymbol{\Psi}$ is an eigen function of $\boldsymbol{S^2}$ and $\boldsymbol{S_z}$. Many stable molecules have an even num

The correlation energy E_{corr} is defined as the difference between the true eigenvalue of the Schrödinger equation and the Hartree-Fock energy E_{HF}:

$E_{\mathrm{corr}} = E_{\mathrm{exact}} - E_{\mathrm{HF}}$

In other words E_{corr} is the residual energy not accounted for by the Hartree-Fock solution, generally intended in its restricted Hartree-Fock variant. For systems where the RHF is not applicable, e.g. systems with an odd number of electrons, the ROHF or the UHF energy are usually taken as reference.

The term correlation has a precise meaning in probability theory which is much more specific and not equivalent to the use of the word in quantum chemistry. In probability theory, a bimodal probability distribution $P(x_1, x_2)$ is said to be composed of two

independent monomodal probability distributions, if $P(x_1, x_2) = P(x_1) \cdot P(x_2)$; both distributions can be correlated, however!

But in quantum chemistry the probability distributions of electrons are said to be un-correlated, when the many-electron wave function is written as a Slater determinant of one-electron spin orbitals. In quantum chemistry terminology, the Hartree-Fock solution is said to be uncorrelated in this sense.

3.5.1 Dynamic and static correlation

The concept of electron correlation gravitates around the concept of electrons mutually influencing each other's motion, not only because they repel one another by Coulomb's law but also because of the anti-symmetry requirement on the wave function of the system. The correlation energy contribution due to inadequacies of the Hartree-Fock method has been called non-dynamic or static correlation, while the remaining part constitutes the dynamical correlation. The correlation energy arising from overestimation of short-range electron repulsions in Hartree-Fock wave functions is usually referred to as dynamical correlation. The static correlation is correlation mandated by degeneracies inforced permutation symmetry.[62, 68, 69]

Where dynamical correlation effects are important, Hartree-Fock will therefore generally overestimate bond lengths and underestimate binding. An extreme example is that of rare-gas dimers, which are unbound at the Hartree-Fock level, but in reality are hold together by dispersion, which can be thought of as a manifestation of dynamic correlation. One useful visualization of non-dynamical correlation is that which is recovered with the minimum CI expansion describing properly all correlation effects due to degeneracies of the wave function; in contrast, convergence of the dynamical correlation energy with increasing size of CI expansion is very slow.

When non-dynamical correlation is weak, Hartree-Fock theory already provides a qualitatively correct description of the wave function. Under such circumstances, which apply generally for molecules in their ground state near equilibrium geometry, one may use single-reference methods to recover the dynamical correlation effect. These methods build on the HF reference determinant, typically using perturbative arguments to define classes of configurations or excitations deemed to be of most importance in constructing

an approximate correlated wave function. For many excited states, for molecules that are close to dissociation, and for situations in which there is near electronic degeneracy, Hartree-Fock is a poor approximation. When static correlation effects are important, Hartree-Fock tends to artificially overbind molecules underestimating bond lengths and overestimating vibrational frequencies. Thus the effects of dynamic and non-dynamic correlation could be in opposition, and the partial cancellation of correlation errors could obscure the value at the SCF level. Static correlation effects often mean that there is no single Slater determinant that dominates the wave function, and perturbative or other approaches that assume a good single-reference starting point are doomed to failure. Under such circumstances, a viable way forward is to first deal with the static correlation problem using a CI expansion that covers all of the important effects. One may then go further using this many-determinant reference as a starting point for further recovery of the dynamic correlation. Such approaches are termed multi-reference methods.

3.6   Configuration Interaction

Methods that improve the Hartree-Fock results by accounting for the correlation energy are known as **post Hartree-Fock methods**. Configuration interaction (CI) [71] is discussed in all major quantum chemistry textbooks. The general idea behind CI is very simple. Express the wave function as a linear combination of Slater determinants with the coefficients obtained variationally

$$|\Psi\rangle = \sum_I c_I |\Phi_I\rangle \tag{3.26}$$

The exact wave function in a finite basis set is the full CI (FCI), which means include all same-spin excitations up to n-tuple ones for n electrons:

$$\Psi_{FCI} = C_0\Phi_0 + \sum_{a,i} C_a^i \Phi_a^i + \sum_{ik,ab} C_{ij}^{ab}\Phi_{ij}^{ab} + \dots \tag{3.27}$$

$$\tag{3.28}$$

where the coefficients, for example $C_{ij\dots}^{ab\dots}$, are normally determined variationally.

One Slater determinant may be chosen as the HF reference wave function ; others might be obtained by exchanging orbitals in the HF reference state by virtual orbitals ("excited determinants") $\{\Phi_a^i\}$, $\{\Phi_{ij}^{ab}\}$ and so on. The full CI is an unambiguous reference model for the correlation problem as it is the best possible solution in any finite basis set. It is variational, invariant to all orbital rotations, and is size extensive. In a complete basis, the full CI, gives the exact solution to the Schrödinger equation. The full CI, however becomes an impossibility for any but quite small molecules in small basis sets.

Assuming that the Hartree-Fock solution is a good approximation one may presume that, in an expansion of the exact wave function in the basis of the single particle functions of the Fock operator, contributions coming from basis functions which differ from the Hartree-Fock ground state by multiple excitations should be smaller and smaller. This assumption leads to a hierarchy of methods where the Hamiltonian is diagonalised in a basis which includes configurations Φ_I obtained from "excited" single particle functions up to a certain level of excitation. Inclusion of excitation orders up to single, double, triple, quadruple, pentuple, hextuple, etc. gives origin to truncated-CI methods referred to by the acronyms CIS, CISD, CISDT, CISDTQ etc [68, 69, 70].

Despite its logical simplicity, configuration interaction has several shortcomings. On the one hand, the scaling in computer time with respect to the number of excitations included rises very quickly; for a basis set containing N functions in the large-N limit CISD scales as N^6, CISDT as N^8 and CISDTQ as N^{10}. The consequence of this very steep scaling is that CISD is for most systems the only computationally-feasible CI level of treatment. Unfortunately CISD energies, even when the reference Hartree-Fock wave function is a good approximation, are not particularly accurate, and higher-order excitations (in particular, quadruple excitations) still give a significant contributions to the correlation energy.

Another very relevant deficiency in the CI approach is that when the Hartree-Fock solution is not a good approximation, for all molecular geometries. It often happens when covalent bonds are broken, the approximate ordering of energy contributions with respect to the level of excitation breaks down and CISD energies will in general be very poor. This limitation, common to all methods which assume the Hartree-Fock solution to be a reasonably good starting point, essentially rules out truncated CI as a method to obtain reliable global potential energy surfaces. Finally, there is another significant

problem with truncated CI which indicates that the strategy of selecting configurations only on the basis of the level of excitation is intrinsically flawed. This problem is the lack of the properties of size-consistency and of size-extensivity of truncated CI, which we will discuss in the following section.

3.7 Size extensivity and size consistency

A precise definition of the concepts was given by Bartlett.[75].

A method is size consistent if the energy calculated for an ensemble of isolated atoms or molecules (e.g., at infinite distance from one another) is equal to the sum of the energies of the individual atoms or molecules calculated with the same method one-by-one. Exact size consistency guarantees that when a bond M-A is stretched to infinity (M represents the fragment molecule and A, the dissociating atom) the energy will asymptotically go to $E(M) + E(A)$ (where the energy of the fragments are computed by the same method). This clearly looks a very desirable property for any method to be used for calculating global potential energy surfaces. The energy of a system made up of two non-interacting subsystems A and B far apart is equal to the sum of the energies A and B computed separately by the same method. For closed-shell systems dissociating to closed-shell fragments, a RHF (restricted Hartree-Fock) reference function is size-consistent e.g He-He dimer.

The term size-extensivity is borrowed from thermodynamics, where an extensive property is one that is proportional to the size of a homogeneous system of non-interacting partcles. A method is size extensive if the energy becomes proportional to the number of non-interacting electrons N in the limit $N \rightarrow \infty$. Size-extensivity is then a sufficient condition for size-consistency of a correlated model of the perturbation-theory or coupled-cluster type based upon that reference function. The RHF method when applied to closed-shell systems is size extensive, as are RHF-based perturbation theory and coupled cluster methods. On the other hand, all forms of truncated CI a part from full-CI are not size extensive.

The lack of exact size consistency in a quantum chemical method may not be a severe drawback if the size-consistency violation is smaller than other sources of error present in the calculation such as basis set incompleteness or higher level electron correlation

effects and if the error induced by size consistency is cancelled in relative energies such as the dissociation energy.

One way to view the lack of size-consistency in variational CI is by considering the Rayleigh quotient correlation energy functional itself:

3.7.1 Size-consistency corrections

$$\epsilon = \frac{\langle \Psi | \, \hat{H} - E^{REF} \, | \Psi \rangle}{\langle \Psi | \, | \Psi \rangle} \tag{3.29}$$

If Ψ is restricted to contain double excitation configurations only, and that the coefficient of the reference wave function is kept fixed. $\langle \Psi | \Psi^{REF} \rangle = 1$, then the numerator of this expression can be shown to grow linearly with system size $\mathbf{N}$; however, the denominator also grows, but as $1 + \lambda N$, where $lambda$ is a constant. This spoils the proper linear scaling of the correlation energy. This analysis gives rise to a number of approximate ways to correct for the effect of lack of extensivity. The simplest, the Davidson or '+Q' correction [31], involves a straightforward rescaling of the correlation energy by $\langle \Psi | \Psi \rangle$, i.e. by replacing the denominator of the above equation by 1 once the wave function has been determined. More explicitly,

$$\epsilon^{CI+Q} = \frac{1 - c_0^2}{c_0^2} \epsilon^{CI} \tag{3.30}$$

where c_0^2 is the weight of the reference wave function Ψ^{REF} in the final normalized CI wave function.Alternative approaches like ACPF [65] introduce at the outset a denominator in the energy functional that does not increase with system size. This modified approximate functional is then minimized to determine the wave function and energy.

3.8 Multi-configurational SCF Method

The main goal of the multi-configurational self consistent field (MCSCF) method is to give a balanced description of the potential energy surface of a molecule even in regions far away from equilibrium, where the Hartree-Fock solution is known to be poor. The complete active space self consistent field method (CASSCF) is a particular version of a class MCSCF of methods. This method is a CI method, in which the coefficients of the Slater determinants in a linear combination are variationally optimized, simultaneously

with the molecular orbitals included in these determinants. This variational optimization is performed iteratively as in the single determinant SCF method. At the starting point of the MCSCF method one considers the Hartree-Fock orbitals both occupied and virtual. In the universally-adopted Hartree-Fock-Roothaan approach the orbitals are expressed as a sum of one-electron basis functions. In the CI approach at this point one would limit the number of configurations included in the expansion on the basis of the level of excitation with respect to the Hartree-Fock reference, and then obtain the linear C_I coefficients by diagonalisation of the Hamiltonian matrix.

The static correlation can be accounted by inclusion of the quasi-degenerated configurations in the MCSCF wave function [26].

$$|\Psi_{MC}\rangle = \sum_I c_I |\Phi_I\rangle \tag{3.31}$$

The energy is then minimized with respect to not only the c_I (as in the CI method) but also but also to changes in the common set of orbitals ϕ_t which are used to construct the Φ_I. These orbitals are called 'active' and the sub-space they define is called the Active Space. In the MCSCF method then a full-CI calculation within the active space is performed. Also, to partially account for excited configurations excluded from the expansion , the coefficients defining the active orbitals are permitted to change. This means that the optimised MCSCF active orbitals will differ from the original Hartree-Fock occupied and virtual orbitals.

In the MCSCF method the selection of the configuration functions (CF) included is different. In the MCSCF method [27], the spaces of the molecular orbitals are divided into three sub-spaces (inactive, active, and external) according to the occupation numbers of electrons in the molecular orbitals. The orbitals in the inactive space are doubly occupied in all the configurations and correspond to the core orbitals. The active space consists of the orbitals which can take the occupation number among $0, 1$, and 2. The definition of the active space is essential in the MCSCF method. The orbitals in the external space are empty in the MCSCF wave function. The multi-configurational character of the wave function due to these partially occupied molecular orbitals allows us to recover a large part of the electronic correlation. Note that orbitals also not included in the active space (inactive orbitals) are modified in the MCSCF method; this happens

because inactive orbitals are defined as the eigen functions of the Fock operator, and the Fock operator depends in turn on the occupied orbitals. This fact also guarantees that all MCSCF orbitals, active and inactive, stay orthogonal between themselves.

If we disregard the change in the orbitals, a CASSCF calculation is equivalent to a regular full CI calculation performed in the (generally small) basis set formed by the active orbitals. If the orbital space is big enough MCSCF energies will thus be qualitatively correct over the whole set of possible molecular geometries. On the other hand, as the active space is necessarily small because of the computational cost, MCSCF energies will not in general be quantitatively very accurate. This is usually expressed by saying that MCSCF recovers the 'static' part of the correlation energy, but is very inefficient in treating the dynamical part.

As mentioned above, a MCSCF calculation involves optimising both the CI coefficients C_I and the active orbital coefficients. The energy depends linearly upon the C_I but highly nonlinearly upon the active orbital coefficients. The overall procedure is iterative, each iteration consisting of the construction of the energy, gradient and hessian, followed by solution of the linear Newton-Raphson equations. The Newton-Raphson equations can be very large in dimension, particularly for a large CASSCF full CI expansion; therefore, usually, they have to be solved iteratively as well, using relaxation or expansion vector techniques similar to the Davidson diagonalization algorithm. These iterations are usually referred to as *microiterations* to distinguish them from the enclosing *macroiterations* in each of which a new expansion point is defined.

Finally, we would like to make a remark on the convergence pattern of the MCSCF correlation energy with respect to basis set size. As we have discussed above the MCSCF method is approximately equivalent to a FCI calculation performed in a chosen active space. When the basis set is enlarged the orbitals defining the active space will change but the size of the active space will always stay the same regardless of the basis set size. As a consequence the MCSCF correlation energy is only very weakly dependent on basis set size.

3.9   Multi-reference configuration interaction

The multi-reference configuration interaction (MRCI) [28, 62] method is also a CI method. Contrary to the single determinant expansion formula in Eq. (3.26), it uses several determinants simultaneously to fill the space of single and double, and potentially higher order excited determinants. The reference determinants can be those obtained from a prior MCSCF calculation, or the linear combination thereof. The MCSCF method is able to recover the static part of the correlation energy, but is very inefficient in recovering the dynamical part. An interesting strategy to remedy this problem is to perform a CI computation on top of a MCSCF one counting the level of excitations from the MCSCF wave function. In general, the optimized MCSCF wave function is taken as reference. For example, we can perform a multi reference configuration interaction singles and doubles (MRCISD) calculation including single and double excitations from all the MCSCF references into the virtuals. The MRCI method can thus account for the interactions between the determinants with the single and double excitations from the reference determinants.

The MRCI method can account for the interactions between the determinants corresponding to the single and double excitations from a reference determinant which is already an excited configuration with respect to the HF wave function. MRCI includes hence configurations which from the point of view of single-reference CI are much more than two times excited.

As the single reference CI methods, we write the MRCI wave function as a linear combination of the CSFs Φ_I taking the MCSCF function as reference.

$$\Psi = \sum_I C_I \Phi_I + \sum_{Sa} C_a^S \Phi_S^a + \sum_{Pab} C_{ab}^P \Phi_P^{ab} \tag{3.32}$$

where I indicates the sum over the CSFs participating at the MCSCF calculations.

We call "internal space" the set of orbitals which construct the reference configurations and "external space" the set of orbitals occupied by the single or double excitations hereof. The orbitals in the external space are symbolized by a and b. The S and P correspond to the single and double excitations from the reference configurations, respectively. The main bottleneck of the MRCISD method is the fact that the size of

the configurations expansion and the computational effort rapidly increases with the number of reference configurations. This handicap becomes dramatic when studying potential energy surfaces, where an reasonable number of configurations is needed to describe the complete configuration space in a balanced way. Various approximations have been proposed to reduce it. Practically, as a division of orbitals in the MCSCF method, we can define the "closed-shells" which are used to correlate electrons occupying the internal space, and, the "core" orbitals, which are always doubly occupied and do not lead to an increase of electron correlation energy in a strict sense. This technique can significantly reduce the size of calculations. We here refer to a scheme known as internal contraction, which is implemented in the MOLPRO program.

In this scheme, whole classes of configurations are summed together with fixed coefficients (i.e. "contracted") and only the resulting sum is employed as a basis for the CI expansion. Single and double excitations of these configurations are done in a connected way. This reduces the number of free variational parameters and hence introduces an important simplification. In the internal contraction scheme the contraction coefficients are determined from the expansion coefficients of the reference wave function. In the implementation of Werner and Knowles used in MOLPRO, [30], only configurations involving two orbitals not belonging to the active space (so called doubly-external configurations) are contracted as these are the most numerous in the calculations.

Internally contracted MRCI wave functions can be rewritten as follows [28, 30]

$$\Psi = \sum_I C_I \Phi_I + \sum_{Sa} C_a^S \Phi_S^a + \sum_D \sum_{Sab} \sum_p C_{Dp}^{ab} \Phi_{Dp}^{ab} \tag{3.33}$$

where I indicates the sum over the CSFs. The configurations of the single excitations to the external space are not contracted. If these configurations of the single excitations were also internally contracted, the number of variational parameters would not depend on the size of the reference space. The Hamiltonian matrix can be diagonalized by using the popular procedure of Davidson, which relies upon the formation of residual vectors that can then be used to generate an updated vector of CI expansion coefficients. Werner and Knowles showed that the error introduced by the internal-contraction is only about 0.3 times the error of fully-uncontracted MRCISD to FCI and is hence negligible.

An unfortunate feature of an MRCI calculation is that, just as in the single reference CISD case, the energy is not an extensive function of the number of non-interacting electrons as it should be. This undesirable feature of any truncated variational CI calculation can to some extent be avoided in MRCI by error cancellation across a potential energy surface; provided, for example, that dissociation asymptotes are computed as super-molecules rather than by adding fragment energies, reasonable results can be obtained for dissociation energies. It is also true that the size-consistency errors for MRCI are usually smaller than for single-reference CISD, since MRCI already contains some of the important quadruple configurations. However, the effects can never be completely avoided.

3.10   Perturbative methods

Alternatively, correlation energy can be recovered by perturbation theory. There are perturbative methods which are size consistent by definition. The starting point for most *ab initio* calculations of molecular energies is the Hartree-Fock (HF) approximation. Therefore, a central problem of quantum chemistry is the construction of an extrapolation from the HF energy to the true energy eigenvalue of the Schrödinger equation. A particularly straightforward approach, at least in principle, is a perturbation theory proposed by Møller and Plesset in which the HF wave function is taken as the zeroth-order approximation for the eigen function. The theory can be formulated by partitioning the Hamiltonian according to

$$H_z = H_0 + (H - H_0)\,z, \tag{3.34}$$

where H_0 is the sum of one-electron Fock operators, H is the Schrödinger Hamiltonian, and z is a perturbation parameter. The energy is then obtained as a power series $E(z) = E_0 + E_1 z + E_2 z^2 + \cdots$. Thus, in Møller-Plesset (MP) theory [40] the energy is a function of z, in the complex z-plane, such that $E(0)$ is equal to the sum of HF orbital energies and $E(1)$ is the extrapolation to the physical energy.

Traditionally, $E(z)$ is calculated by partial summation, that is, the power series is truncated at some given order and then evaluated at $z = 1$. Truncation at order n yields the "MPn" approximation to the energy. Thus, $E(z)$ is evaluated as a polynomial. The

power series is an asymptotic series, which is a rigorously correct solution only in the $z \to 0$ limit. The true functional form of E is much more complicated than a polynomial.

3.10.1   Coupled cluster methods

We begin with the concept of the cluster function which may be used to include the effects of electron correlation in the wave function. Using a formalism in which the cluster functions are constructed by cluster operators acting on a reference determinant, we justify the use of the "exponential ansatz" of coupled cluster theory.

Formally, the coupled-cluster method begins by postulating that the correlated many-body wave function is given by [42, 67, 72]

$$| \Psi \rangle = \exp \left(\hat{T} \right) | \Psi_0 \rangle , \tag{3.35}$$

where we define the correlation operator as

$$\hat{T} = \hat{T}_1 + \hat{T}_2 + \hat{T}_3 + \cdots + \hat{T}_A . \tag{3.36}$$

The correlation operators are defined in a second quantization scheme in terms of n-particle n-hole (np-nh) excitation amplitudes as

$$\hat{T}_1 = \sum_{i<\varepsilon_f, a>\varepsilon_f} t_i^a \hat{a}_a^+ \hat{a}_i , \tag{3.37}$$

$$\hat{T}_2 = \sum_{i,j<\varepsilon_f; ab>\varepsilon_f} t_{ij}^{ab} \hat{a}_a^+ \hat{a}_b^+ \hat{a}_j \hat{a}_i , \tag{3.38}$$

and higher order terms for $\hat{T}_3$ to $\hat{T}_A$. we use the notation that p, q, r, s refers to all orbitals and i, j, k, l index sums the occupied and a, b, c, d index sums virtuals. The total number of single-particle states in therefore is $N_s = N_p + N_h$ where N_p refers to the number of particle states, and N_h is the number of hole states. The creation $\hat{a}_a^+$ and annihilation $\hat{a}_i$ operators create or remove an electron from a spin orbital.

Coupled-cluster theory may thus be hierarchically improved upon by increasing the number of T_i operators one computes. We will call the theory in which only T_1 and T_2 operators are present, CCSD, or coupled-clusters at the single and double excitation level. CCSDT means that T_3 is retained in the correlation operator, while CCSDTQ

refers to keeping both T_3 and T_4 correlation operators. [75] In this uncoupled representation, the correlation amplitudes must obey the fermion-symmetry relations which for the T_2 correlation operators yield $t_{ij}^{ab} = -t_{ji}^{ab} = -t_{ij}^{ba} = t_{ji}^{ba}$. We will use the short-hand notation t_1 and t_2 to represent the array of all $1p$-$1h$ and $2p$-$2h$ amplitude.

We compute the expectation value of the energy from

$$E = \langle \Psi_0 \mid \exp\left(-\hat{T}\right) \hat{H} \exp\left(\hat{T}\right) \mid \Psi_0 \rangle . \tag{3.39}$$

Because the energy is computed using projective, asymmetric techniques, an important question concerns the physical reality of the coupled-cluster energy. Quantum mechanics requires that physical observables should be expectation values of hermitian operators. The coupled-cluster energy expression contains the non-Hermitian operator $\left[\exp(-\hat{T})\hat{H}\exp(\hat{T})\right]$. However, if $\hat{T}$ is not truncated, it can be shown that the similarity-transformed operator exhibits an energy-eigenvalue spectrum that is identical to the original hermitian operator, $\hat{H}$, thus justifying its formal use. From a practical point of view, the coupled-cluster energy tends to follow the expectation value result even when $\hat{T}$ is truncated.

The correlation energy is given by

$$E_{\text{corr}} = E_{exact} - E_{HF} = \sum_{ia} f_{ia} t_i^a + \frac{1}{4} \sum_{aibj} \langle ij \mid\mid ab \rangle t_{ij}^{ab} + \frac{1}{2} \sum_{aibj} \langle ij \mid\mid ab \rangle t_i^a t_j^b . \tag{3.40}$$

For Hamiltonians having maximal two-body interaction terms, this equation is general and is not restricted to the CCSD approximation since higher-order cluster operators such as $\hat{T}_3$ and $\hat{T}_4$ cannot produce fully contracted terms with the Hamiltonian and therefore contribute zero to the energy. Higher-order operators can contribute to the energy indirectly through the equations used to determine these amplitudes. The three terms in Eq.(3.40) are usually referred to as the $\hat{T}_1$, $\hat{T}_2$, and $\hat{T}_1^2$ contributions to the correlation energy.

The equations for amplitudes are found by left projection of excited Slater determinants so that

$$0 = \langle \Psi_i^a \mid \exp\left(-\hat{T}\right) \hat{H} \left(\hat{T}\right) \mid \Psi_0 \rangle , \tag{3.41}$$

$$0 = \langle \Psi_{ij}^{ab} \mid \exp\left(-\hat{T}\right) \hat{H} \left(\hat{T}\right) \mid \Psi_0 \rangle . \tag{3.42}$$

The Baker-Hausdorf relation may be used to rewrite the similarity transformation as

$$\exp\left(-\hat{T}\right)\hat{H}\left(\hat{T}\right) = H_N + \left[\hat{H},\hat{T}_1\right] + \left[\hat{H},\hat{T}_2\right]$$
$$+\frac{1}{2}\left[\left[\hat{H},\hat{T}_1\right],\hat{T}_1\right] + \frac{1}{2}\left[\left[\hat{H},\hat{T}_2\right],\hat{T}_2\right]$$
$$+\left[\left[\hat{H},\hat{T}_1\right],\hat{T}_2\right] + \cdots . \tag{3.43}$$

The expansion terminates exactly at quadruply nested commutators when the Hamiltonian contains at most two-body terms, and at six nested commutators when three-body terms are present. We stress that this termination is exact, thus allowing for a derivation of exact expressions for the t_1 and t_2 amplitudes. To derive these equations is straightforward but tedious work[72].

In order to calculate expectation values of operators we may use the Hellmann-Feynman theorem which states that if we perturb our Hamiltonian such that $\hat{H}' = \hat{H} + \lambda\hat{\Omega}$ where λ is a small quantity and $\hat{\Omega}$ is the operator (either bare or effective) of interest, then the energy changes only by a small amount from its original value of $E(\lambda = 0)$. As a function of λ, the energy becomes $E' = E(\lambda = 0) + \lambda dE/d\lambda$, and the expectation value of the operator is given by

$$\langle\hat{\Omega}\rangle = \frac{dE(\lambda = 0)}{d\lambda} . \tag{3.44}$$

One deficiency of the conventional coupled cluster methods is that they apply only to ground electronic states (or, more accurately, to the lowest-energy states of a given spin and spatial symmetry). Alternatively to that, the equation-of-motion coupled cluster (EOM-CC) method [33] has been devised such that higher-lying electronic states may be studied. These methods have proven to provide reliable accuracy (on the order of 0.2 eV) in the prediction of electronic excitation spectra for states which are well-described by promotion of a single electron from the ground state. Perhaps the most important work in excited-state coupled cluster theory in the next several years will be the development of methods for treating "doubly excited" states and the improvement of the accuracy of EOM-CC to better than 0.1 eV.

All coupled cluster methods depend implicitly upon a reference wave function (usually

the single-configuration Hartree-Fock determinant). However, for cases where this reference fails dramatically, even the CCSD(T) method cannot be expected to provide reliable results. Bond-breaking provides an excellent example of this behavior; as a σ bond is separated, for instance, a single determinant fails to properly include both electronic configurations $[(\sigma)^2$ and $(\sigma^*)^2]$ needed to describe the dissociation process with even qualitatively accuracy. In CuNO, the fragments can dissociate as open-shell singlet and triplet. Here we expect to see the failure of CCSD(T) method far way from equilibrium geometries and at dissociation unless a spin unrestricted method is used to calculate the reference state. In our calculations, we use the CCSD(T) method implemented in MOLPRO [52] where expressions give a perturbative correction for the effects of triple excitations which is consistent to fifth order.

Since a complete potential energy surface is vital to research efforts in reaction dynamics, for instance, much effort has been devoted to the construction of multi-reference coupled cluster (MRCC) schemes based primarily on multi-configurational SCF (MCSCF) reference wave functions. Of particular interest is the work by Piecuch, Adamowicz, and co-workers, in which a MRCCSD wave function, for example, is obtained via selected triple and quadruple excitations from a full CCSDTQ wave function constructed from a single electronic configuration. This approach is similar to that used earlier in multi-reference configuration interaction methods. By retaining a single-determinant reference formalism, one avoids many of the difficulties of a "true" MCSCF-based approach and automated techniques for the construction of higher excitation levels (i.e., beyond quadruples) are promising.

The state selective MRCC by Kállay [76, 78] follows the idea mentioned above. We use Kllay's code as it is interfaced with MOLPRO to calculate CCSDT and also MRCC calculations. This state selective MRCC procedure are closely related to the equation-of-motion (EOM) or linear response CC theory. A complete reference space is assumed, i.e., the active electrons are distributed in all possible ways among the active orbitals and $0-, 1-, ...N_i$-fold excitations from the resulting determinants are considered. One of the reference determinants, practically the most dominant one is selected ($|0\rangle$). This further divides the virtual and occupied orbital space into active and inactive part. The active orbitals could be denoted by bold capital letters and bold lower case letters will stand for inactive ones. Thus **I, J, K,...** indices label active holes;**A, B, C** are active particles;**i, j, k,...** are inactive holes and **a, b, c,...** designate inactive virtual

orbitals. Suppose that we have N_h active holes and N_p active particles, then the maximal excitation level in the active space is $N_a = minN_h, N_p$. The reference space is spanned by the $0-, 1-, ..., N_a$-fold excitations among active orbitals

$$|0\rangle, \left|\Psi_{\mathbf{I_1}}^{\mathbf{A_1}}\right\rangle, \left|\Psi_{\mathbf{I_1 I_2}}^{\mathbf{A_1 A_2}}\right\rangle, ..., \left|\Psi_{\mathbf{I_1...I_{Na}}}^{\mathbf{A_1...A_{Na}}}\right\rangle$$

To account for N_i-fold and lower excitations from these functions, at most $n = N_i + N_a$-fold excitations which carry no more than N_i inactive particle or hole labels, are included in the wave function. This consideration results in the following restricted cluster operator:

$$\hat{T} = \sum_{k=1}^{N_i+N_a} \hat{T}_k \tag{3.45}$$

with this excitation manifold corresponding to the configurations employed in a conventional MRCI calculation provided that allowed excitations out of the symmetry forbidden reference functions are also included in the excitation manifold with the cluster amplitudes grouped according to the number of active/inactive labels.The main advantage of the formalism is that it retains the simplicity and the size-extensive nature of the single-reference CC methods.

Since coupled cluster theory is size consistent by construction, for properties such as dissociation and fragmentation energies, coupled cluster theory used in conjunction with large basis sets is often expected to provide "chemical accuracy," i.e., ± 1 kcal/mol. In recent years, many researchers have asked what would be required to obtain "spectroscopic accuracy", i.e., ± 1 cm^{-1}. The convergence of the coupled cluster (as well as CI and perturbation theory) energies towards a "basis set limit" is much slower than that possible with Hartree-Fock. That is, for a given level of electron correlation (e.g., CCSD), one must use much more complete basis sets (perhaps including high levels of orbital angular momentum, s, p, d, f, etc.) relative to Hartree-Fock if additional improvements to the basis are to make significant contributions to the computed energy.

3.11 Basis Sets

Historically,[34] the quantum calculations for molecules were performed as LCAO MO, i.e. Linear Combination of Atomic Orbitals - Molecular Orbitals. This means that molecular orbitals are formed as a linear combination of atomic orbitals:

$$\psi_i = \sum_{\mu=1}^{n} c_{\mu i} \phi_\mu$$

where ψ_i is the i-th molecular orbital, $c_{\mu i}$ are the coefficients of linear combination, ϕ_μ is the μ-th atomic orbital, and n is the number of atomic orbitals.

Strictly speaking, atomic orbitals (AO) are solutions of the Hartree-Fock equations for the atom, i.e. a wave functions for a single electron in the atom. Anything else is not really an atomic orbital.

There is a lot of confusion in the terminology used. Later on, the term atomic orbital was replaced by "basis function" or "contraction," when appropriate. Early, the Slater type orbitals (STO's) were used as basis functions due to their similarity to atomic orbitals of the hydrogen atom. They are described by the function depending on spherical coordinates:

$$\phi_i(\zeta, n, l, m; r, \theta, \phi) = N r^{n-1} e^{-\zeta r} Y_{lm}(\theta, \phi)$$

where N is a normalization constant, ζ is called "exponent". The r, θ, and ϕ are spherical coordinates, and Y_{lm} is the angular momentum part ("shape" describing function). The n, l, and m are quantum numbers: principal, angular momentum, and magnetic; respectively.

3.11.1   Gaussian basis sets

Unfortunately, functions of this kind are not suitable for fast calculations of necessary two-electron integrals. That is why, the Gaussian type orbitals (GTOs) were introduced. One can approximate the shape of the STO function by summing up a number of GTOs with different exponents and coefficients. Even if one uses 4 or 5 GTO's to represent STO, one will still calculate integrals much faster than if original STOs are used. The GTO (called also cartesian gaussian) is expressed as:

$$g(\alpha, l, m, n; x, y, z) = N e^{-\alpha r^2} x^l y^m z^n$$

where N is a normalization constant, α is called "exponent". The x, y, and z are cartesian coordinates. The l, m, and n are not quantum numbers but simply integral exponents at cartesian coordinates, $r^2 = x^2 + y^2 + z^2$.

Calling gaussians GTOs is probably a misnomer, since they are not really orbitals. They are simpler functions. In recent literature, they are frequently called gaussian primitives. The main difference is that r^{n-1}, the preexponential factor, is dropped, the r in the exponential function is squared, and angular momentum part is a simple function of cartesian coordinates. The absence of r^{n-1} factor restricts single gaussian primitive to approximating only 1s, 2p, 3d, 4f ... orbitals. Examples of gaussian functions are include:

$$1s = Ne^{-\alpha r^2}$$

$$2p_z = Ne^{-\alpha r^2}z$$

$$3d_{xx} = Ne^{-\alpha r^2}x^2$$

$$3d_{xy} = Ne^{-\alpha r^2}xy$$

$$4f_{xyz} = Ne^{-\alpha r^2}xyz$$

etc.

Sometimes, the so-called scale factor, f, is used to scale all exponents in the related gaussians. In this case, the gaussian function is written as:

$$g(\alpha, l, m, n, f; x, y, z) = Ne^{-\alpha f^2 r^2}x^l y^m z^n$$

The sum of exponents at cartesian coordinates, $L = l + m + n$, is used analogously to the angular momentum quantum number for atoms, to mark functions as s-type (L=0), p-type (L=1), d-type (L=2), f-type (L=3), etc.

Gaussian primitives are usually obtained from quantum calculations on atoms (i.e. Hartree-Fock or Hartree-Fock plus some correlated calculations, e.g. CI). Typically, the exponents are varied until the lowest total energy of the atom is achieved. Basis

sets for molecular calculations are therefore frequently augmented with other functions which will be discussed later.

3.11.2   Contractions, diffuse and polarization functions

For efficient molecular calculations, the gaussian primitives have to be contracted, i.e., certain linear combinations of them will be used as basis functions. The coefficients and exponents of Gaussian expansion which minimizes the energy of the hydrogen atom were derived by Huzinaga in 1965. In this case, 4 primitives were contracted to 2 basis functions. It is frequently denoted as (4s) $\rightarrow$ [2s] contraction (some use the (4s)/[2s] notation). The coefficients in function ϕ_2 are then fixed in subsequent molecular calculations.

Some basis sets are good for geometry and energies, some are aimed at properties (e.g. polarizability), some are optimized only with Hartree-Fock in mind, and some are tailored for correlated calculations. Finally, some are good for anions and other for cations and neutral molecules. For some calculations, a good representation of the inner (core) orbitals is necessary (e.g. for properties required to analyze the NMR spectrum), while other require best possible representation of valence electrons.

There are two basic forms of contractions, namely "segmented" and "general". The segmented contractions are disjointed, i.e., given primitive appears only in one contraction. The example given above (4s) $\rightarrow$ [2s] is a segmented contraction. Occasionally, one or two primitives may appear in more than one contraction, but this is an exception to the rule. The general contractions, on the contrary, allow each of the primitives to appear in each basis function (contraction). The segmented contractions are far more popular and will be described first. The reason for their popularity is not that they are better, but simply, that the most popular ab initio packages do not implement efficient integral calculations with general contractions. The computer code to perform integral calculations with general contractions is much more complex than that for the segmented case.

Frequently, the core orbitals are long contractions consisting of many primitive gaussians to represent well the "cusp" of s type function at the position of the nucleus. The "zeta" terminology is often augmented with a number of polarization functions which will be

described later. So, DZP means double-zeta plus polarization, TZP stands for triple-zeta plus polarization, etc.

The original contractions derived from atomic Hartree-Fock calculations are frequently augmented with other functions. The most popular are the polarization and diffuse functions. The polarization functions are simply functions having higher values of L than those present in occupied atomic orbitals for the corresponding atom. The exponents for polarization functions cannot be derived from Hartree-Fock calculations for the atom, since they are not populated.

The basis sets are also frequently augmented with the so-called diffuse functions. These gaussians have very small exponents and decay slowly with distance from the nucleus. Diffuse gaussians are usually of s and p type, however sometimes diffuse polarization functions are also used. Diffuse functions are necessary for correct description of anions and weak bonds (e.g. hydrogen bonds) and are frequently used for calculations of properties (e.g. dipole moments, polarizabilities, etc.). In our *ab initio* calculations we use the basis sets from Dunning and coworkers and those from Kirk A Peterson [37, 51].

3.11.3   Effective core potentials

A significant reduction of the computational effort in quantum chemical investigations can be achieved by restriction of the actual calculations to the valence electron system and the implicit inclusion of the influence of the chemically inert atomic cores by means of suitable parametrized effective (core) potentials. This approach is in line with the chemists view that mainly the valence electrons of an element determine its chemical behavior, cf., e.g., the periodic table of elements. From a quantum mechanical point of view the partitioning of a many-electron system into subsystems is not possible, since electrons as elementary particles are indistinguishable.

The development of Effective Core Potential (ECP) [32] approaches allow treatment of inner shell electrons as if they were some averaged potential rather than actual particles. It is reasonable to replace the core electrons by effective potentials including all informations about them and to treat explicitly the valence electrons. This procedure has advantages specially for atoms owning the large atomic numbers. The size of calculations is proportional to n^4 (n is the number of electrons included in the system),

thus inclusion of the inactive core electrons in pseudopotentials allows us to reduce the actual cost of calculations without loss of the physical and chemical informations.

ECP's are not orbitals but modifications to a hamiltonian, and as such are very efficient computationally. The relativistic effects are very important in describing heavier atoms, principally in the inner orbitals. Another advantage of pseudopotentials is the inclusion of relativistic effects of heavy atoms, in the non-relativistic calculations of valence electrons. All-electron relativistic computations are very expensive. ECP's simplify calculations and at the same time make them more accurate with popular non-relativistic ab initio packages.

In effective core potential theory an effective model Hamiltonian approximation for H_np is searched, which only acts on the states formed by the valence electrons

$$H_v = \sum_i^{n_v} h_v(i) + \sum_{i<j}^{g_v} h_v(i,j) + V_{\text{cc}} + V_{\text{ccp}} \tag{3.46}$$

The subscripts c and v denote core and valence, respectively h_v and g_v stand for effective one- and two-electron operators, V_{cc} represents the repulsion between all cores and nuclei of the system, and V_{ccp} is a core polarization potential (CPP). n_v denotes the number of valence electrons treated explicitly in the calculations.

$$n_v = n - \sum_{\lambda}^{N} (Z_\lambda - Q_\lambda) \tag{3.47}$$

Here Q_λ denotes the charge of the core λ. Several choices exist for the formulation of such a valence-only model Hamiltonian, i.e., four-, two- or one-component approaches and explicit or implicit treatment of relativity. Since a reasonable compromise between accuracy and efficiency is desired, the standard effective core potential schemes use the implicit treatment of relativity (i.e., a nonrelativistic kinetic energy operator and inclusion of relativistic effects via parametrization of the effective core potential) and a one-component (scalar-quasirelativistic) or a two-component (quasirelativistic) treatment.

In this study the method of pseudopotentials we use have the electrons in the inner shells represented by the energy-consistent pseudopotentials V_{PP} and the Hamiltonian

of the electrons in valence is given in atomic units by:

$$H_v = -\sum_i \frac{\Delta_i}{2} + \frac{1}{2}\sum_{i,i'} \frac{1}{r_{i,i'}} + \sum_i V_{\mathrm{pp}}(i) \tag{3.48}$$

where the indices i and i denote the valence electrons.

In this study, we employ the pseudopotentials (ECP10MDF) for Cu, recently reported by Figgen et al. The term means the simultaneously adjusted two-component relativistic pseudopotentials (i.e., scalar-relativistic and spin-orbit), based on the numerical all-electron four-component multi-configuration Dirac-Hartree-Fock (MCDHF) calculation. For Cu, using the ECP10MDF, the 1s, 2s, and 2p orbitals are replaced by pseudopotentials and the outer core 3 spd shells, in addition to 4 sp shells are treated explicitly for the valence.

3.11.4   Basis set superposition error

The basis set superposition error (BSSE) is a particular aspect of basis set incompleteness. As an example, consider a model system composed by two non-interacting atoms A and B and suppose that two atom-centred basis sets are defined for the two atoms. A manifestation of the BSSE is that the energy of the composite non-interacting system A-B is not constant as a function of the distance of the atoms. This happens because when the atoms are infinitely far away each of them can make use only of its own basis functions, while when they approach atom A can also use the basis functions coming from atom B, and vice versa. This leads to an artificial lowering of the energy when the atoms approach.

The error arises from the inconsistent treatment of the monomers. They are able to access additional functions from the other monomer at shorter intermolecular distances, but at large intermolecular distances, the other monomer is too far away (the overlap integrals are too small) for its functions to provide stabilization. This inconsistent treatment of the basis set for each monomer as the intermolecular distance is varied is the source of the basis set superposition error. In the limit of a complete basis set,the BSSE would be reduced to zero.

The Boys and Bernardi counterpoise correction (CP) [35]is a prescription for removing BSSE. The typical, uncorrected interaction energy between monomers A and B would be computed as:

$$\Delta E_{int}(AB) = \sum_{AB}^{AB}(AB) - \sum_{A}^{A}(A) - \sum_{B}^{B}(B) \tag{3.49}$$

where the superscripts denote the basis used, the subscripts denote the geometry, and the symbol in parentheses denotes the chemical system considered. One could obtain the energy of the dissociation limit by a computation of the A+B super-molecule at some very large intermolecular separation (where the distance between A and B would be so large that the basis functions of one monomer would not overlap with those of the other); this might be necessary for theoretical methods which are not size-extensive, such as truncated CI. We can attempt to correct Eq. (3.49) by estimating the amount by which monomer A is artificially stabilized by the extra basis functions from monomer B (and vice versa).

The energy of monomer A in the dimer basis must necessarily be lower (more stable) than the energy of monomer A in the monomer basis, $\sum_{BSSE}^{A}(A) = \sum_{A}^{AB}(A) - \sum_{A}^{A}(A)0$ and similarly for monomer B $\sum_{BSSE}^{B}(B) = \sum_{B}^{AB}(B) - \sum_{B}^{B}(B)0$. If we subtract this error from the interaction energy defined in Eq. (3.49), the terms $\sum_{A}^{A}(A)$ and $\sum_{B}^{B}(B)$ cancel, giving

$$\Delta E_{int}^{CP}(AB) = \sum_{AB}^{AB}(AB) - \sum_{A}^{AB}(A) - \sum_{B}^{AB}(B) \tag{3.50}$$

Practically, to evaluate the energy of monomer A in the dimer basis, one places all the basis functions of monomer B on the atomic centers of monomer B while neglecting the electrons and the nuclear charges of monomer B. The atoms of B are referred to as "ghost atoms" in such a computation.

Chapter 4

Ab initio calculations of the lowest electronic states in the CuNO system

4.1 Introduction

Computational studies to characterize the NO binding mode in CuNO have been carried out in the past. But to get an insight into homogeneous catalysis and the chemical reaction dynamics, accurate prediction of the nature of the bond, as well as of the global potential energy surfaces (PES) is necessary in the gas phase [10, 11]. Metal mono-nitrosyls are difficult to study and only limited reports are available. For CuNO, the theoretical studies have not yet been able to unambiguously assign the ground state. Coupled cluster calculations with single and double excitations (CCSD) give a triplet ground state of CuNO, whereas perturbative inclusion of triple excitations (CCSD(T)) gives a singlet ground state of the A′ symmetry species [12], with an end-on bent structure and an estimated dissociation energy of 18.8 kcal/mol (≈ 30 mE_{h} or 6582 $hc\,\mathrm{cm}^{-1}$ per molecule; E_{h} is the hartree, h is the Planck constant and c is the speed of light in vacuum). Also in [12], the lowest triplet state, of the A″ symmetry species, is predicted to contain two stable isomers with CuON connectivity and facile isomerization. The CuNO^{+} cation was treated at the DFT and CCSD(T) level of theory in [13], where it was found that also the cationic system has an end-on bent minimum energy structure of the ^{2}A′ type, and

a dissociation energy into Cu^+ and NO of 22 kcal/mol (at the CCSD(T) level; 30 kcal/-mol with DFT), while configuration interaction calculations yield a linear structure [14]. To date, the enthalpies for both reactions $CuNO = Cu + NO$ and $CuNO^+ = Cu^+ + NO$ are still unknown experimentally.

In calculations using the density functional theory (DFT), pure density functionals assign a singlet ground state [7, 15], while hybrid functionals favor a triplet state as the lowest electronic energy state [7, 16] (see also the review [17]). The difficulty in making a clear assignment can be related to the small energy gap between the triplet and singlet states. However, spin-orbit coupling is reported to be weak [16]. The combined theoretical and experimental investigation of the infrared spectrum of CuNO in the matrix isolation studies [7] have also not enable the unambiguous assignment of the ground state symmetry species.

It is important to note that the aforementioned theoretical methods are essentially based on a single reference configuration, while it is not at all clear, whether the CuNO molecule has a single reference wave function at all. Since both Cu and NO are radical species, the wave function will eventually have a multi-reference character latest upon dissociation of CuNO. Clarifying this question is essential, last but not least, for the determination of global potential energy surfaces.

In the present study, a systematic investigation of calculation settings and technical aspects related to an accurate prediction of the electronic wave function for the ground and excited states is carried out at the multi-configurational self-consistent-field (MCSCF) and multi-reference configuration interaction (MRCI) levels of theory, albeit restricted to single and double excitations. For the analysis, we focus first on three linear structures of the CuNO system, so as to enable direct comparison and confirm convergence of C_{2v} and C_s energy values. This investigation aims at establishing adequate settings of MRCI calculations that give energy values to within 1 mE_h ($\sim 220\ hc\,cm^{-1}$) accuracy, which is sufficient to enable the calculation of a physically sound, global potential energy surface for the electronic ground state of the CuNO system.

Calculations at bent structures finally allow us to elucidate the symmetry species of the ground state and binding energies. We compare results from MRCI calculations with new coupled cluster calculations at the CCSD(T) level, as well as with coupled cluster calculations including triple excitations explicitly (CCSDT), with the aim of

clarifying the accuracy of the predicted dissociation energy and equilibrium structure of this system. We discuss to what extent the treatment of electronic correlation can be improved also in view of a potential multi-reference character of the wave function. The dissociation energy of CuNO is defined as the energy difference between the dissociated Cu and NO fragments, where the nitrogen and oxygen atoms are separated by 115 pm (see [18]), and the CuNO complex at its equilibrium geometry, the energy reference state is that of dissociated Cu + NO. Thus, for any bound structure of CuNO, the energy has a negative value.

4.2   Methods

The calculations on the ground and excited electronic states were performed using the MCSCF method followed by the internally contracted MRCI method of Werner and Knowles [27, 28, 29, 30] as implemented in the MOLPRO [48] suite of programs. The orbitals used to set up the CI expansion were obtained by state averaged MCSCF calculations using $\mathbf{C}_s$ and $\mathbf{C}_{2v}$ symmetry for the linear structures, with equal weights for all the participating states. Here the number of roots to be state averaged at the MCSCF calculations were varied. Spin-orbit energies were calculated as eigenvalues of the matrix representation of the full Breit-Pauli operator in the set of singlet and triplet MRCI states.

In the calculations, we use the augmented correlation-consistent polarized n-tuple ζ-basis sets ("aug-cc-pVnZ", but abbreviated here "AVnZ", where n=D(2),T(3),Q(4),5) of Dunning and co-workers [49, 50], for N and O, and of Balabanov and Peterson [51] for convergent basis sets for transition metals. We found, however, that the AVTZ basis is largely sufficient for the purposes and aims of this work. The use of a quintuple-ζ basis was not possible within the large multiple states calculations carried out at the MRCI level. Specifically, the AVTZ basis contains for both nitrogen and oxygen a regular set of 10 s, 5 p, 2 d and one f primitive functions, which were contracted to 4 s, 3 p, 2 d and one f function; for Cu 20 s, 16 p, 8 d, 2 f and one g primitive functions were contracted to 7 s, 6 p, 4 d, 2 f and one g function; for each angular momentum function present in the regular set one additional diffuse function was added. We also considered a reduced basis set obtained from the AVTZ basis by omission of the g function of Cu and f functions in N and O. This basis set, which we call RVTZ in this paper, yields relative energies

that agree with relative energies obtained with the AVTZ basis to within the expected accuracy of 1 mE_h. We should point out here that technical problems of the calculations are primarily related to the choice of the active space and the number of roots, and less with the size of the basis. Finally, we also used the Bauschlicher ANO (BANO) basis implemented in MOLPRO, which is comparable to the basis set from [13]. The BANO basis has more primitive f and g functions for Cu than the AVTZ basis.

For the calculations of the ground state, we also used the coupled cluster method. We report results at the CCSD(T) as well as at CCSDT level of theory (coupled cluster with single and double excitation and perturbative triple, respectively, with full triple excitation). These results are obtained with the MOLPRO program suite, in particular the methods denoted CCSD-T and RCCSD-T in [52] were used. The CCSDT calculations used the currently available extension of the MOLPRO program to include the MRCC code by M. Kállay [53].

In order to estimate relativistic corrections, we performed CCSD(T) calculations with the Douglas-Kroll-Hess hamiltonian [54, 55] in the vicinity of the equilibrium, as well as for the isolated fragments Cu and NO. In this case, the AVTZ-DK basis was used for copper; for nitrogen and oxygen, the corresponding VTZ-DK bases were used, to which the diffuse s and p functions from the augmented non-contracted bases were added, i.e. s (with the exponent 0.0576) and p (0.0491) for nitrogen, as well as s (0.07376) and p (0.05974) for oxygen. All contracted DK bases were used as implemented in the 2009.1 version of MOLPRO.

4.3   Results

The ground state of the copper atom is ^{2}S ([Ar]s^{1}d^{10}) and the first excited state is ^{2}D ([Ar]s^{2}d^9). NO has a Π ground state with a calculated bond length of 115 pm at the AVTZ basis and the MRCI level of theory, which agrees with the experimentally estimated value (115.1 pm [18]).

A transition metal atom like Cu can bind to NO in different ways [7, 12, and references cited therein]. As NO is an open shell with a singly occupied π^* orbital in the ground state configuration, and the Cu atom has a single electron in a 4s orbital in its lowest state, the Cu-NO interaction can be expected to result in a bent ground state. The

three dimensional configuration space may be spanned by the coordinates r_{NO}, r_{Cu} and θ_{Cu} shown in Figure 4.1, where r_{Cu} is the distance of the copper atom from the point at the center of the NO distance.
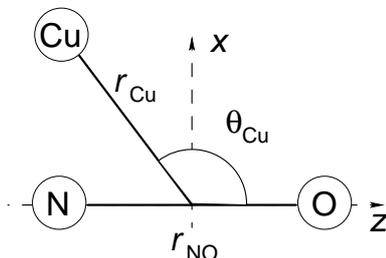
FIGURE 4.1: General coordinates for the {Cu, N, O} system, supposed in the xz-plane; r_{Cu} is the distance of the copper atom from the point bisecting r_{NO} ; $0 \leq r_{NO} < \infty$, $0 \leq r_{Cu} < \infty$, $0° \leq \theta_{Cu} \leq 180°$.

However, because we aim at establishing appropriate CAS spaces and orbitals, we consider first to investigate the linear structures LS1, LS2 and LS3. Specifically, the coordinates are $r_{Cu} = 257$ pm for both LS1 and LS2, while $r_{Cu} = 0$ pm for LS3; $r_{NO} = 115$ pm for both LS1 and LS2, and $r_{NO} = 360$ pm for LS3; $\theta_{Cu} = 180°$ for LS1 and $0°$ for LS2.

In LS1 we understand a Cu interaction with NO via the nitrogen atom, in LS2 as a Cu interaction with NO essentially through the oxygen atom, while in LS3, the interaction is shared among both N and O atoms Figure 4.2.
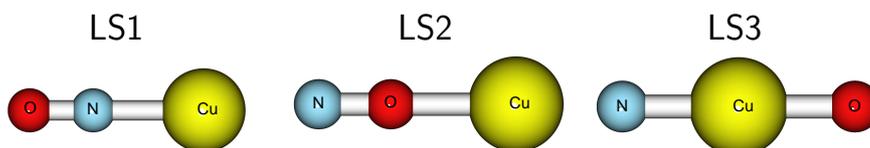
FIGURE 4.2: Three representative linear arrangements of the system composed of N, O and Cu.

Atomic distances defining specific structures used in the calculations of Table 4.2 are:

	$d(NO)$/pm	$d(CuN)$/pm	$d(CuO)$/pm
LS1	115.0	199.5	314.5
LS2	115.0	314.5	199.5
LS3	360.0	180.0	180.0

TABLE 4.1: The three representative linear structures LS1, LS2 and LS3

4.3.1 MCSCF calculations

Table 4.2 shows the singlet MCSCF energies of the linear structures LS1, LS2 and LS3 of the neutral {N,O,Cu} system. All results are obtained from state averaged MCSCF calculations with the AVTZ basis and a $(18,12)$ CAS which includes the d electrons from Cu in the active space. More details about the CAS will be given below. For a given structure, the MCSCF energy obtained at $\mathbf{C}_{2v}$ and $\mathbf{C}_s$ symmetry are compared.

In the table, under $\mathbf{C}_{2v}$, the symbol 2442 means that 12 roots are calculated $(2 \times {}^1A_1, 4 \times {}^1B_1, 4 \times {}^1B_2, 2 \times {}^1A_2)$, and under $\mathbf{C}_s$ the corresponding $(6 \times {}^1A', 6 \times {}^1A'')$ are also given. Calculations are considered converged if the energy of the $\mathbf{C}_{2v}$ and $\mathbf{C}_s$ structure are within 1 mE_h accuracy. Also the Π state degeneracy for the B_1, and B_2 representations is verified for physically valid convergence.

		LS1		LS2		LS3	
		$\mathbf{C}_{2v}$	$\mathbf{C}_s$	$\mathbf{C}_{2v}$	$\mathbf{C}_s$	$\mathbf{C}_{2v}$	$\mathbf{C}_s$
roots		2442	66	2442	66	2442	66
${}^1A_1$	${}^1A'$	-258.9	-258.9	-288.2	-288.3	-247.7	-247.7
		-241.5	-241.4	-279.6	-279.6	-222.6	-222.7
${}^1B_1$		-265.1	-265.1	-290.0	-290.0	-233.5	-233.5
		-242.2	-242.3	-280.4	-280.4	-192.8	-192.8
		-241.7	-241.7	-280.2	-280.2	-186.4	-186.4
		-226.5	-226.5	-214.5	-214.5	-183.2	-183.2
${}^1B_2$	${}^1A''$	-265.1	-265.1	-290.0	-290.0	-233.5	-233.5
		-242.2	-242.3	-280.4	-280.4	-192.8	-192.8
		-241.7	-241.7	-280.2	-280.2	-186.4	-186.4
		-226.5	-226.5	-214.5	-214.5	-183.3	-183.3
${}^1A_2$		-241.4	-241.5	-279.6	-279.6	-222.7	-222.7
		-241.2	-241.2	-279.4	-279.4	-222.0	-222.0

TABLE 4.2: Singlet MCSCF energies E of the linear structures LS1, LS2 and LS3. All results using the AVTZ basis and a $(18,12)$ CAS. Values reported are $-(1768\ E_h + E)/mE_h$.

4.3.1.1 MCSCF pitfalls

In this study, we carefully chose the number of states computed in each symmetry to overcome convergence failures at the MCSCF level. Test calculations with only the lowest roots gives bad convergence and Π degeneracy in $\mathbf{C}_s$ is broken, the energy values differ by 100 mE_h between $\mathbf{C}_s$ and $\mathbf{C}_{2v}$. Some of these are shown in Table 4.3

It is necessary to calculate higher roots at the MCSCF level. The choice of the number of roots calculated per irreducible representation has a dramatic effect in the convergence of the *ab initio* calculation. An unbalanced number of roots leads to broken symmetries as can be clearly seen from the table. For instance, when $2 \times {}^1A_1$, $2 \times {}^1B_1$, $2 \times {}^1B_2$ roots are considered in $\mathbf{C}_{2v}$, energies differ significantly from those obtained with $4 \times {}^1A'$, $2 \times {}^1A''$ roots under $\mathbf{C}_s$ for the LS3 structure.

	$\mathbf{C}_{2v}$	$\mathbf{C}_s$	$\mathbf{C}_{2v}$	$\mathbf{C}_s$	$\mathbf{C}_{2v}$	$\mathbf{C}_{2v}$	$\mathbf{C}_s$	$\mathbf{C}_{2v}$	$\mathbf{C}_s$
LS1	1110	21	1111	22	2220	2211	42	2222	44
${}^1A_1$	-302	-220	-251	-254	-302	-303	-302	-303	-303
	-	-	-	-	-287	-286	-287	-287	-287
${}^1B_1$	-302	-254	-279	-272	-300	-297	-300	-300	-300
	-	-	-	-	-288	-288	-288	-287	-287
${}^1B_2$	-302	-254	-279	-274	-300	-303	-300	-300	-300
	-	-	-	-	-288	-	-288	-287	-287
${}^1A_2$	-	-	-269	-238	-	-290	-	-287	-287
	-	-	-	-	-	-	-	-287	-287
LS2									
${}^1A_1$	-301	-299	-200	-	-301	-301	-301	-301	-301
	-	-	-	-295	-293	-293	-294	-294	-294
${}^1B_1$	-305	-296	-219	-303	-304	-301	-304	-303	-303
	-	-	-	-	-294	-295	-293	-293	-293
${}^1B_2$	-306	-297	-219	-303	-304	-306	-304	-303	-303
	-	-	-	-	-294	-	-	-293	-293
${}^1A_2$	-	-	-212	-295	-	-296	-294	-294	-294
	-	-	-	-	-	-	-	-293	-293
LS3									
${}^1A_1$	-246	-246	ERR	-247	-247	-247	ERR	-247	-245
	-	-	-	-	-222	-223	-	-223	-221
${}^1B_1$	-236	-236	-	-236	-234	-235	-	-234	-233
	-	-	-	-	-195	-193	-	-195	-194
${}^1B_2$	-236	-236	-	-235	-234	-235	-	-234	-232
	-	-	-	-	-195	-	-	-195	-194
${}^1A_2$	-	-	-	-224	-	-223	-	-223	-221
	-	-	-	-	-	-	-	-222	-220

TABLE 4.3: Singlet MCSCF energies E of the linear structures LS1, LS2 and LS3. All results using the AVTZ basis and a $(18, 12)$ CAS. Values reported are $-(1768\,E_h + E)/\mathrm{m}E_h$.

Also, severe root-flipping problems occur when we fail to include all states of an electronic multiplet in the MCSCF calculations, leading to erratic prediction of the order of the states by the variational algorithm because states with higher energy may alternate

during calculation with states of slightly lower energy, leading to slow or failing convergence. (ERR shown for LS3 in Table 4.3 So it is always prudent to include states in a balanced way in order to minimize errors due to root-flipping between close lying states.

A calculation in $\mathbf{C}_s$ corresponding to $6 \times {}^1\mathrm{A}'$ and $6 \times {}^1\mathrm{A}''$ roots is very physical and comes out naturally from the symmetries of asymptotic states of CuNO. This can be easily understood from the multiplication rules of representations. The six states of Cu corresponding to ^{2}S and ^{2}D split into $3 \times {}^2\mathrm{A}_1$, $1 \times {}^2\mathrm{B}_1$, $1 \times {}^2\mathrm{B}_2$, $1 \times {}^2\mathrm{A}_2$; NO has a Π ground state and splits into $1 \times {}^2\mathrm{B}_1$, $1 \times {}^2\mathrm{B}_2$ under $\mathbf{C}_{2\mathrm{v}}$. Therefore at the Cu + NO asymptote we would obtain $2 \times {}^1\mathrm{A}_1$, $4 \times {}^1\mathrm{B}_1$, $4 \times {}^1\mathrm{B}_2$, $2 \times {}^1\mathrm{A}_2$ under $\mathbf{C}_{2\mathrm{v}}$ or $6 \times {}^1\mathrm{A}'$, $6 \times {}^1\mathrm{A}''$ under $\mathbf{C}_\mathrm{s}$, and similarly for the corresponding triplet states. The energies agree within our accuracy criteria when we follow this as shown in Table 4.2, rather than just opting to calculate an increasing number of roots. However, we should point out that this method of checking the correct assymptotic states is possible as this is a triatomic system, and will be increasingly difficult with the system size.

After getting the number of roots needed correct if we include 3d electrons of Cu in the active space, in the next section, we give the details of optimising the active space in the MCSCF.

4.3.2 Active Space

The choice of the active space was systematically increased for clean convergence. The valence complete active space is composed of 22 electrons in 14 orbitals, a $(22, 14)$ CAS in short notation, with occupation scheme $19 \times \mathrm{A}' + 6 \times \mathrm{A}''$ in $\mathbf{C}_\mathrm{s}$ or $14 \times \mathrm{A}_1 + 5 \times \mathrm{B}_1 + 5 \times \mathrm{B}_2 + 1 \times \mathrm{A}_2$ in $\mathbf{C}_{2\mathrm{v}}$. The nature of these orbitals is reproduced in Table 4.4, where the energy ordered natural orbitals obtained from the state averaged MCSCF calculations are given at the dissociation asymptote Cu + NO. The symbols refer to the most important atomic orbitals participating at the construction of the given orbital. These orbitals maintain a high degree of localization on the individual fragments also at close distances between them. In the table we indicate in bold face characters the major admixtures from frontier orbitals that occur at a bent structure (BS) of the CuNO molecule, which will be discussed below.

		$^1A'$		$^1A''$	
closed	1.1	Cu 1s	1.2	Cu $2p_y$	
	2.1	Cu 2s	2.2	Cu $3p_y$	
	3.1	Cu $2p_x$			
	4.1	Cu $2p_z$			
	5.1	O 1s			
	6.1	N 1s			
	7.1	Cu 3s			
	8.1	Cu $3p_z$			
	9.1	Cu $3p_x$			
active	10.1	NO σ	3.2	NO π_y	
	11.1	NO σ	4.2	Cu d_{xy}	
	12.1	NO σ^*	5.2	Cu d_{yz}	
	13.1	NO π_x	6.2	NO π_y^*	
	14.1	Cu d_{z^2}			
	15.1	Cu $d_{x^2-y^2}$			
	16.1	Cu d_{xz}			
	17.1	(**NO π_x^*+**) Cu 4s			
	18.1	(**Cu 4s -**) NO π_x^*			
virtual	19.1	Cu 4p			

TABLE 4.4: MCSCF-orbitals at the asymptote of CuNO

Energy ordered MCSCF orbitals in Cs symmetry for CuNO at $r_{Cu} = 450$ pm. The z axis is chosen as the NO binding axis and the molecule plane is the xz-plane (see Figure 4.1). In the MRCI calculations these are natural orbitals and attributions correspond to the leading contributions from fragment orbitals, which vary little when fragments approach (bold face characters indicate the most important admixtures occurring at the BS structure - see also text and Table 4.5). In the coupled cluster calculations, orbitals are from Hartree-Fock calculations, which are delocalized on both fragments, and the attribution does not hold.

In the MCSCF calculations we found that, on top of considering all d orbitals, we also needed to include all d electrons in the active space in order to obtain physically sound results. Orbital rotations within the set of closed and active orbitals were observed at several instances.

In the $(18, 12)$ CAS used in Table 4.2 we close orbitals 10.1 and 11.1, where we essentially neglect the correlation of electrons pertaining to the NO moiety.

4.3.2.1 Dissociation of CuNO

The dissociation of CuNO along $\theta_{Cu} = 180°$ and $\theta_{Cu} = 0°$ would result in Cu + NO. We remember that at the asymptote, the MCSCF energies obtained should be exactly the same,(within our accuracy limits of 1 mE_h) both θ_{Cu} angles. This is obvious as Cu is

now far away from the NO moiety and the absolute energy does not depend anymore on the angle. Obtaining the correct asymptote along a θ_{Cu} ray of dissociation is a physical and stringent test of our choice of roots and depends importantly on the active space used in the MCSCF calculations. In Figure 4.3 we show the dissociation of CuNO singlet using the $(18, 12)$ CAS along the linear rays, starting from the MCSCF wave function at the LS1 geometry and dissociating outward along $\theta_{Cu} = 180°$ and from MCSCF at LS2 and dissociating outward along $\theta_{Cu} = 0°$. Here a state averaged total of 12 roots $(2 \times A_1 + 4 \times B_1 + 4 \times B_2 + 2 \times A_2)$ in $\mathbf{C}_{2v}$ are used. Only A$'$ symmetry $(= A_1 \oplus B_1)$ are shown here.
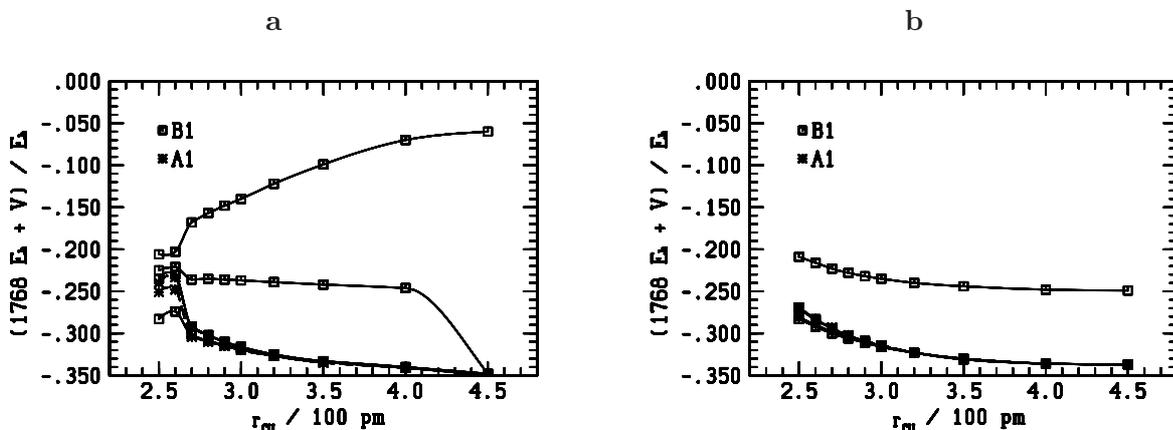
FIGURE 4.3: $(18, 12)$ CAS -potential energy functions $V(r_{Cu})$ for the lowest linear singlet states of A$'$ symmetry $(= A_1 \oplus B_1)$ at $r_{NO} = 115$ pm, $\theta_{Cu} = 180°$ (panel **(a)**, Cu-N-O configuration) and $\theta_{Cu} = 0°$ (panel **(b)**, N-O-Cu configuration). Lines are cubic spline interpolations and give MCSCF electronic energies E as numerical function $1768 + E/E_h$ of the copper distance r_{Cu}.

This graph clearly illustrates many things that can and will go wrong in a multi-reference calculation. Even obtaining exactly same energies at $\mathbf{C}_{2v}$ and $\mathbf{C}_s$ for LS1 and LS2 structures, the asymptotes obtained can be widely different.

We can clearly see the artificial, unphysical behaviour of LS1 like PES. That is of course a problem. But even more troubling is the energy mismatch of 13 mE_h at the asymptote between the $\theta_{Cu} = 180°$ and $\theta_{Cu} = 0°$. This is a clear indication that in the MCSCF calculations at least the asymptote is not converged. Some of these issues can be resolved to an extent by increasing the p-space configurations used in MCSCF calculations, but this does not solve everything. On careful study of orbitals at the MCSCF level, we find that, at the asymptote, the highest active ^{1}A$'$ orbital 19.1 corresponding to $\mathbf{C}_s$ turns out

to be a 4p of copper instead of the expected NO σ^* orbital.(c.f Table 4.4). This leads to an unphysical lowering of energies in the state averaged calculations. This problem is not possible to solve easily. We can do it point by point carefully with different strategies, but that is not optimum for finding a global PES. A general solution is proposed in the following section.

We mention here that problems like this do not go away with increasing the basis set used in the calculations. In fact AVTZ is a very good basis for our calculations, we even show later it is possible to get good results even with a reduced basis. Errors come purely from the active space used in the calculations.

It should also be pointed out that these problems could not be solved by performing a MRCI calculation on top of the MCSCF states.

We also see that the states at the asymptote are inverted with $E_{\mathrm{Cu}}(^2S) > E_{\mathrm{Cu}}(^2D)$ which is at variance to known spectroscopic states of Cu atom. We come back to it later.

4.3.2.2   MCSCF PES at Linearity

The $(22, 13)$ complete active space thus consists of 13 orbitals, $6 \times {}^1\mathrm{A}_1$, $3 \times {}^1\mathrm{B}_1$, $3 \times {}^1\mathrm{B}_2$, $1 \times {}^1\mathrm{A}_2$ with 22 electrons and gives rise to 645, 581, 581, and 559 configuration state functions for ${}^1\mathrm{A}_1$, ${}^1\mathrm{B}_1$, ${}^1\mathrm{B}_2$ and ${}^1\mathrm{A}_2$, respectively. In $(22, 13)$ CAS, we have removed the orbital 19.1 from the active space.(it is marked as virtual in Table 4.4) It is possible, with some additional effort, to have orbital 19.1 converged to be the NO σ^* orbital within the sensibly larger $(22, 14)$ CAS. However, this calculation is difficult and expensive, while the effect on the energies is negligible compared to a $(22, 13)$ CAS calculation, where orbital 19.1 has been omitted.

Figure 4.4 gives the singlet MCSCF states for the dissociation into Cu and NO where $\theta_{\mathrm{Cu}} = 180°$ and $\theta_{\mathrm{Cu}} = 0°$. Here we use a $(22, 13)$ CAS and the AVTZ basis.

We can clearly see the marked difference in this graph compared to Figure 4.3. The asymptote at $\theta_{\mathrm{Cu}} = 180°$ and $\theta_{\mathrm{Cu}} = 0°$ are identical as expected. This shows that great care must be taken during the calculation. Also at geometries where Cu is close to NO, one has to take care to find the right MCSCF orbitals.
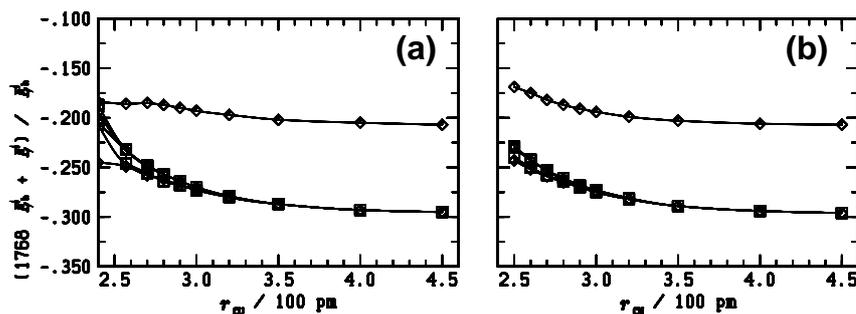
FIGURE 4.4: $(22, 13)$ CAS - potential energy functions $V(r_{Cu})$ for the lowest linear singlet states of A$'$ symmetry $(= A_1 \oplus B_1)$ at $r_{NO} = 115$ pm, $\theta_{Cu} = 180°$ (panel **(a)**, Cu-N-O configuration) and $\theta_{Cu} = 0°$ (panel **(b)**, N-O-Cu configuration). Lines are cubic spline interpolations and give MCSCF electronic energies E as numerical function $1768 + E/E_h$ of the copper distance r_{Cu} .

Legend:

— □ — A_1

— ◇ — B_1

We find that using converged MCSCF orbitals from the asymptote as a starting point for calculations at other geometries gives reliable results. However, the MCSCF calculations provide ^{2}S as the excited state and a degenerate ^{2}D as the ground state for the Cu product with an energy difference of more than 90 mE_h (~ 19700 $hc\,\mathrm{cm}^{-1}$). Experimentally the ^{2}D level lies above the ^{2}S level by about 11200 cm^{-1} [58]. This unphysical inversion of the states at the MCSCF level of calculation is also obtained for the Cu atom alone if we include the 3d orbitals in the active space[63]. This problem can only be solved at the MRCI level of calculations using natural orbitals following from the MCSCF calculation, as discussed in the following.

4.3.3 MRCI calculations

In the remainder we report MRCI relative energies calculated with respect to energies of the following reference structure at the asymptote: $r_{NO} = 115$ pm and $r_{Cu} = 450$ pm ($\theta_{Cu} = 130°$, the potential becomes roughly an invariant of the angle here).

4.3.3.1 Linear structures

In order to be able to carry out the MRCI calculations in an efficient way, we froze the closed orbitals used in the preceding MCSCF calculations with the MOLPRO "core"

card, i.e. we froze 22 electrons in 11 core orbitals; singly and doubly excited configu-rations were included in the MRCI from 13 active orbitals, thereby correlating 22 elec-trons, i.e. in a $(22, 13)$ CAS. The total number of contracted configurations is 7690805 in $\mathbf{C}_s$ symmetry, per irreducible representation, and corresponds to about 422241365 non-contracted configurations in MRCI. The next contribution to the correlation energy may result from correlating the Cu (3)p shell which contains six additional electrons. It was not possible to correlate this shell in the MRCI calculation as it demands much higher computational effort. We checked for the effect of including orbital 19.1 within a $(22, 14)$ CAS and found it to be negligible also at the MRCI level.

Figure 4.5 shows the singlet and triplet A_1 and B_1 MRCI states for the dissociation into Cu + NO at $\theta_{Cu} = 180°$ and $\theta_{Cu} = 0°$ ($(22, 13)$ CAS, AVTZ basis).
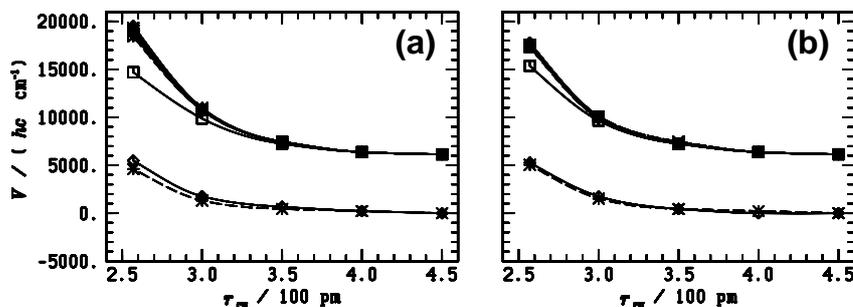
FIGURE 4.5: MRCI potential energy functions $V(r_{Cu})$ for the lowest singlet and triplet states of A′ symmetry and $\theta_{Cu} = 0°$ (panel **(b)**). Configurations are as in Figure 4.4, but here lines, which are cubic spline interpolations, give wave numbers of relative electronic energies $E - E_{ref}$, where $E_{ref} = E(r_{Cu} \to \infty)$, as functions of the copper distance r_{Cu}. The MRCI energies were obtained from a $(22, 13)$ CAS and 12 state averaged MCSCF configuration states with the AVTZ basis. The multi-reference space includes 2 A_1 and 4 B_1 roots as explained in the text. For both the singlet and triplet symmetries, the lowest A″ state, which is not shown in the figure, coincides with the lowest A′ state to within the accuracy of the present work $(1 \, mE_h)$.

Legend:

— □ —   singlet A_1

— ◇ —   singlet B_1

-- × --   triplet A_1

-- ∗ --   triplet B_1

Here also, for both $\theta_{Cu} = 180°$ and $\theta_{Cu} = 0°$, we obtain the same asymptotes. More importantly, the MRCI calculations have flipped the states into the correct order and provide a non degenerate ^{1}A′ component as the ground state and a five fold degenerate ^{1}A′ component of the excited state with an energy difference of over 6500 $hc \, cm^{-1}$, at

the asymptote. This energy difference is still about half the experimental value of the excitation energy $E(^2\mathrm{D}) - E(^2\mathrm{S})$ in copper [58].

It is important to note that, technically, all reference configurations used to define the lowest MCSCF states of each individual spatial symmetry species, that is $2 \times \mathrm{A}_1$ and $4 \times \mathrm{B}_1$ in Figure 4.4, are needed to correctly describe the CI vectors of the states shown in Figure 4.5. Also, asking for a single root in MRCI calculations, fails as there is a root flipping from the MCSCF for example at the asymptote, where the $E_{\mathrm{Cu}}{}^2\mathrm{S}$ is the sixth and highest root. And this changes at different geometries, thereby forcing us to use all six MCSCF roots as reference for the MRCI in each symmetry species, A′ and A″ . Even after correctly identifying roots, we found significant energy differences if we use a single root MRCI calculation or if we use the more accurate 6 root calculations.

The potential energy surface is still repulsive at the linear structures. Also, the $^3\mathrm{A}'$ MRCI states are slightly lower in energy compared to the singlet states. The lowest singlet and triplet states have degenerate B_1 and B_2 branches and compose a Π level. Spin-orbit coupling among these states might thus be significant, which will be addressed below.

We also considered to use a $(18, 11)$ CAS in which we also remove the 19.1 orbital from the active space compared to the $(18, 12)$ CAS. This gave results which are comparable in accuracy to our $(22, 13)$ CAS. In Table 4.5 we compare MRCI energies obtained at the selected linear geometries with the $(22, 13)$ and $(18, 11)$ CAS, as well as the AVTZ and RVTZ bases. In addition to results at linear structures, Table 4.5 contains also MRCI results for a bent structure, that were obtained with several basis sets. We address these results later.

We see that, within the $(22, 13)$ CAS, the error of using the RVTZ instead of the AVTZ basis is not larger than 400 $hc\,\mathrm{cm}^{-1}$. Within the RVTZ basis, the error of using the $(18, 11)$ instead of the $(22, 13)$ CAS is about 350 $hc\,\mathrm{cm}^{-1}$, for the end-on geometries LS1 and LS2, while it is largest for LS3 (almost 2000 $hc\,\mathrm{cm}^{-1}$). Since the overall energy at the LS3 structure is much higher anyway, the increased inaccuracy of our energy calculations in this region of the molecular geometries is less relevant. The states at the LS1 and LS2 geometries compose a Π level, while at LS3 electrons are in a Σ state, which can be anticipated from inspection of Table 4.2.

	$E_{\text{ref}}/E_{\text{h}}$	$(E - E_{\text{ref}})/hc\,\text{cm}^{-1}$			
	ref	LS1	LS2	LS3	BS
MRCI-22-13-AVDZ	-1768.8719	-	-	-	-2107
MRCI-22-13-AVTZ	-1769.0078	5662	5443	19316	-2224
MRCI-22-13-AVQZ	-1769.0602	-	-	-	-2250
MRCI-22-13-BANO	-1769.0206	-	-	-	-2197
MRCI-22-13-RVTZ	-1768.9547	5774	5552	18906	-2036
MRCI-18-11-RVTZ	-1768.8150	5500	5895	17160	-1983
MRCIQ-22-13-AVTZ	-1769.1240	-	-	-	-1768
MRCIQ*-22-13-AVTZ	-1769.1467	-	-	-	-
MRCI-18-11-ECP[a]	-326.0360	-	-	-	-3072.6

[a] for Cu the ECP basis as defined in section was used, where [Ne] is the core; for N and O we used the RVTZ basis. Also $r_{\text{Cu}} = 250$ pm, which is close to BS with $r_{\text{Cu}} = 260$ pm

TABLE 4.5: Singlet energies E of specific geometries calculated at several levels of theory and with basis sets defined in the text; "ref" is the asymptotic reference molecular structure, which is defined by $r_{\text{Cu}} = 450$ pm, $rno = 115$ pm and $\theta_{\text{Cu}} = 130°$ for the MRCI energies; for the coupled cluster results, the reference energy is the sum of the Cu and NO energies calculated separately - the acronyms indicate the number of correlated electrons and the basis used (see text); LSi $(i = 1, \ldots, 3)$ are linear structures defined in the text, BS is the bent "end-on" structure defined by $r_{\text{Cu}} = 260$ pm, $r_{\text{NO}} = 115$ pm and $\theta_{\text{Cu}} = 130°$.

4.3.3.2 Spin-orbit calculations

Spin-orbit coupling may be important when singlet and triplet Π-levels are close in energy. We checked this issue with point-wise calculations. Table 4.6 gives the eigenvalues obtained from the diagonalization of the rank 48 matrix Hamiltonian of the Breit-Pauli involving the first twelve singlet and triplet MRCI levels calculated with the $(22, 13)$ CAS and the RVTZ basis. Only the lowest levels of Π symmetry at the linear structures LS1 and LS2 are reported in this table. The separation of the uncoupled singlet and triplet levels is roughly 1000 $hc\,\text{cm}^{-1}$ at the LS1 structure, and 200 $hc\,\text{cm}^{-1}$ at the LS2 structure. The maximum shift in energy induced by spin-orbit coupling is around 300 $hc\,\text{cm}^{-1}$ for both geometries.

4.3.3.3 Bent structures

We return to the discussion of Table 4.5, where we also compare results at a bent structure (BS), defined by $r_{\text{Cu}} = 260$ pm, $r_{\text{NO}} = 115$ pm and $\theta_{\text{Cu}} = 130°$. Here, relative energies with respect to the asymptote are negative, the molecule is stable. The BS

| | $\tilde{\nu}/\mathrm{cm}^{-1}$ | |
	LS1	LS2
B_2	1367.79	541.15
B_1	1367.73	541.15
A_1	358.06	154.11
A_2	356.16	154.11
B_2	158.04	63.69
B_1	155.70	63.67
A_2	20.74	0.56
A_1	0.00	0.00

TABLE 4.6: Wave numbers of spin-orbit energies at the LS1 and LS2 geometries calculated using a $(22, 13)$ CAS with the RVTZ basis (see text). The lowest 8 states pertaining to the singlet and triplet Π level manifold are reported.

structure is indeed quite close to the equilibrium structure of the CuNO complex, as will be shown below.

In order to discuss the effect of the basis set on the energy of bound states, we first compare in Table 4.5 the energies obtained with the AVDZ, AVTZ and AVQZ bases. While absolute energies decrease strongly, the variation of the relative energies at the BS structure falls within the 1 mE_{h} (220 $hc\,\mathrm{cm}^{-1}$) tolerance interval adopted in this work. We expect thus the basis set error on the dissociation energy of CuNO obtained with the AVTZ basis to be of the order of the variation from the AVTZ to AVQZ result, i.e. less than 50 $hc\,\mathrm{cm}^{-1}$. Using the BANO basis leads to a decrease of the absolute energy by about 14 mE_{h} for all 6 states at the asymptote. Relative energies are however very similar to those obtained with the AVTZ basis. This agreement allows us to be confident about the choice of the valence-ζ type basis in the calculations.

Using the RVTZ instead of the AVTZ basis decreases the absolute value of the relative energy at the BS structure from 2217 to 2041 $hc\,\mathrm{cm}^{-1}$. This difference is almost constant in the low energy domain of the potential, whereas the reduction of the active space from $(22, 13)$ to $(18, 11)$ leads to an insignificant additional decrease from 2041 to 1975 $hc\,\mathrm{cm}^{-1}$, here.

In concluding the discussion of the MRCI energies in Table 4.5, we estimate that the expected precision of a potential energy surface (PES) obtained at this level of theory, i.e. from a $(18, 11)$ CAS and the RVTZ basis should be at least 200 to 400 $hc\,\mathrm{cm}^{-1}$ in the lower energy domain and that it increases by a factor 5 to 10 for energies of

10 000 $hc\,cm^{-1}$ and higher, above the minimum. The choice of the $(18, 11)$ CAS with the RVTZ basis seems appropriate to develop a global PES within these uncertainties.

Figure 4.6 shows the potential functions of singlet and triplet MRCI states for the dissociation into Cu + NO along bent structures where $r_{NO} = 115$ pm and $\theta_{Cu} = 130°$. These energies were obtained with the $(22, 13)$ CAS and the RVTZ basis. One of the $6\times^1A'$ states is a bound state, while the $6\times^3A'$, $6\times^1A''$ and $6\times^3A''$ states are essentially repulsive, along this section. The BS structure described above is close to the bottom of the potential well of the lowest $^1A'$ state.
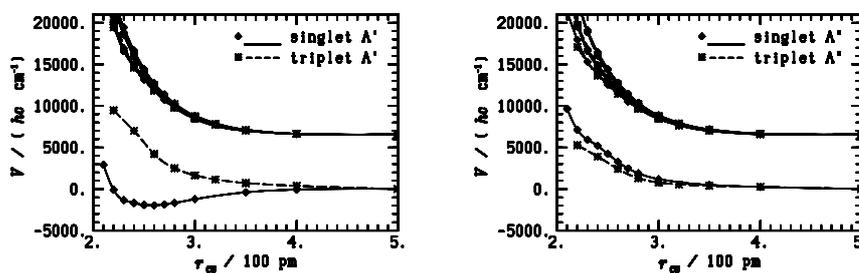
FIGURE 4.6: MRCI potential energy functions $V(r_{Cu})$ for the lowest singlet and triplet states of A' (panel (**a**)) and A'' (panel (**b**)) symmetry at the fixed values $\theta_{Cu} = 130°$ and $r_{NO} = 115$ pm. Energies were obtained from a (22,13) CAS with the RVTZ basis. The BS structure defined in the text and mentioned in Table 4.5 is located at the minimum of the lowest A' potential energy function in panel (a). The angle of $130°$ is close to the equilibrium value for θ_{Cu} from [12].

Legend:

— ◇ —   singlet

– – ∗ – –   triplet

We recall that, technically, all reference configurations pertaining to the lowest six MC-SCF states of each individual spatial symmetry species are needed to correctly describe the CI vectors in Figure 4.6, in particular that of the bound ground state. The ground state wave function has contributions from a large number of configurations. The most important configurations, which compose 82 % of the wave function at the BS structure, are given in Table 4.7.

The leading configuration is denoted Φ_1 here, and has singly occupied orbitals 17.1 and 18.1 from Table 4.4; 17.1 is the Cu 4s and in-plane NO π_x^* bonding orbital, denoted simply "s+π_x^*" here, for brevity, orbital 18.1 is the corresponding anti-bonding orbital - we checked this attribution by inspection of the orbitals.

I	Φ_I	C_I^2
0	$\ldots(\pi_y)^2(d_{xy})^2(d_{yz})^2(d_{xz})^2(s+\pi_x^*)^2(s-\pi_x^*)^0(\pi_y^*)^0$	0.19
1	$\ldots(\pi_y)^2(d_{xy})^2(d_{yz})^2(d_{xz})^2(s+\pi_x^*)^1(s-\pi_x^*)^1(\pi_y^*)^0$	0.53
2	$\ldots(\pi_y)^2(d_{xy})^2(d_{yz})^1(d_{xz})^2(s+\pi_x^*)^2(s-\pi_x^*)^0(\pi_y^*)^1$	0.03
3	$\ldots(\pi_y)^2(d_{xy})^2(d_{yz})^2(d_{xz})^1(s+\pi_x^*)^2(s-\pi_x^*)^1(\pi_y^*)^0$	0.06
4	$\ldots(\pi_y)^0(d_{xy})^2(d_{yz})^2(d_{xz})^2(s+\pi_x^*)^1(s-\pi_x^*)^1(\pi_y^*)^2$	0.01
sum		0.82

TABLE 4.7: Leading configurations of the ground state wave function $\Psi = \sum_I C_I \Phi_I$ at the BS structure - see Table 4.5; only the higher-most occupied orbitals are shown and symbols are defined as in Table **??** - "S+π_x^*" denotes the Cu 4s and in-plane NO pi$_x^*$ bonding orbital, "S-π_x^*" is the corresponding anti-bonding orbital; data are from the (22,13) CAS AVTZ calculation.

This configuration correlates with the expected ground state configuration of the dissociated Cu + NO system. The second most important configuration is denoted Φ_0 and it corresponds to the lowest closed shell configuration. See Table 4.4 for the explanation of the remaining symbols. Similar decompositions of the CI vector were obtained and discussed for the NiCO and FeCO compounds in [64]. Following [13], the stability of the CuNO$^+$ cation is essentially due to the formation of a one electron bond, where the single occupied orbital has 12%Cu and 88% N (almost entirely 2p). That orbital is related to orbital 17.1 from the present work. Quite astonishingly, the additional electron of the neutral compound CuNO preferably occupies the anti-bonding orbital, rather than the bonding orbital. Consequently, the cation could be expected to be more strongly bound than the neutral molecule.

Configurations Φ_2 and Φ_3 may be assigned to the "d-to-π" back-donation mechanism of the bonding, while configuration Φ_4 is an internal NO double excitation. Note that Φ_1 to Φ_3 are single excitations from configuration Φ_0. Thus, in a single reference SD-CI calculation, they would contribute negligibly to the correlation energy. In addition, configuration Φ_4 can be obtained from Φ_0 via a triple excitation, only, and a SD-CI calculation would not be capable to recover correlation stemming from the internal excitation of the NO fragment. This demonstrates clearly the multi-reference character of the wave function close to the CuNO equilibrium structure.

4.3.3.4 CAS effects

The potential energy functions for the lowest $^1A'$ and $^3A''$ MRCI-$(22, 13)$ states are repeated in Figure 4.7, where they are compared to results from the aforementioned calculations based on $(18, 11)$ and $(6, 5)$ CAS. With the $(18, 11)$ CAS, we close the orbitals 10.1 and 11.1 whereby we neglect the correlation of electrons pertaining to the NO moiety. Here, a similar potential energy function is obtained. The $(18, 11)$ CAS is therefore a very good alternative for calculating global PES as it allows for a more economic determination of the potential energy surface with a similar data quality.

In the $(6, 5)$ CAS, we keep only the 4s Cu orbital active. As is clearly shown in the figure, the form of the potential function obtained from an MRCI calculation based on the CAS $(6, 5)$, where all the d orbitals of Cu are frozen, is very different. It should also be noted here that there are several orbital rotations necessary with a series of MCSCF calculations before we get the physically correct $(6, 5)$ CAS at the MCSCF. These orbitals are then used for subsequent MRCI calculations. Despite yielding a similarly deep potential well, this rather limited calculation gives a much longer, non physical equilibrium value of 300 pm for r_{Cu}. Here, since the d orbitals are not included in the active space, we calculate a single root per symmetry in the MCSCF and MRCI calculations and we do obtain the asymptotic ^2S states for Cu in the MCSCF as well as in the MRCI calculations. This comparison shows the necessity of correlating the Cu d electrons to obtain a more accurate description of the potential energy surface of the system.

Some of the d electrons could possibly be excluded from the active space. As indicated in Table 4.7, some of the CAS orbitals have invariant occupancies in the leading configurations. However, we cannot be sure that this picture holds in the overall space of molecular geometries. With the aim of obtaining a global PES, we thus prefer to consider a CAS containing all Cu d electrons.

4.3.3.5 Critical assessment of the MRCI energies

The present MRCI calculations confirm the order of singlet and triplet states from previous results [12]. The relative triplet-singlet energies around the BS structure are larger than $5\,000\ hc\,\mathrm{cm}^{-1}$, spin-orbit coupling is not found to be important here. Furthermore,
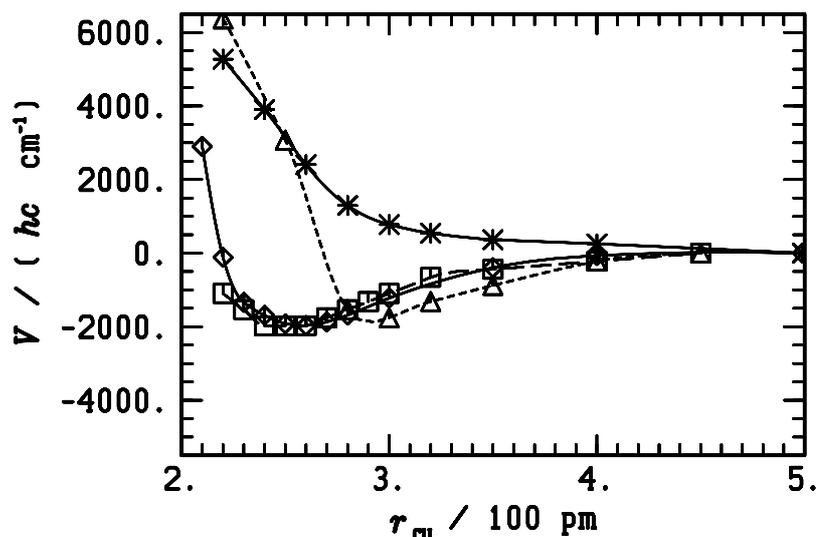
FIGURE 4.7: Potential energy functions $V(r_{\mathrm{Cu}})$ for the lowest singlet and triplet states at the fixed values $\theta_{\mathrm{Cu}} = 130°$ and $r_{\mathrm{NO}} = 115$ pm. See also Figure 4.6. Legend: multi-reference CI energies - all energies shown here were obtained with the RVTZ basis;

———— ◇ ———— $^1A'$, (22,13) CAS, $E_{\mathrm{ref}} = -1768.955\ E_{\mathrm{h}}$ (see Table 4.5)

———— * ———— $^3A''$, (22,13) CAS, E_{ref} as for $^1A'$

— —□— — $^1A'$, (18,11) CAS, $E_{\mathrm{ref}} = -1768.815\ E_{\mathrm{h}}$ (see Table 4.5)

· · · △ · · · $^1A'$, (6,5) CAS, $E_{\mathrm{ref}} = -1768.295\ E_{\mathrm{h}}$

they do not indicate that bound triplet states exist, contrary to what is suggested in [12], where a stable $^3A''$ state is predicted to lie about $2\,500\ hc\,\mathrm{cm}^{-1}$ ($11\ \mathrm{m}E_{\mathrm{h}}$) higher than the $^1A'$ state, at quite a similar geometry.

They are also in qualitative agreement with results obtained at the DFT level of theory, when pure functionals are used [7, 15]. They are in strong contrast to results obtained from the use of hybrid functionals [16]. While the latter were confirmed there by CAS MP2 calculations, which state that a triplet A'' state is lowest in energy at a bent geometry, we emphasize here that MRCI calculations involving at least 6 reference configurations of each spatial symmetry species are necessary to correctly calculate the ground state of the system, and that severe root flipping may occur. Perturbation theory is therefore likely to fail.

In [12], a dissociation energy of more than $6500\ hc\,\mathrm{cm}^{-1}$ has been estimated for CuNO. This is roughly three times larger than the energy required to dissociate CuNO from the

BS structure.

We also carried out the spin-orbit calculations at specific geometries. In Table 4.8 we report the spin-orbit correction to the BS geometry. As can be seen there, the effect of spin-orbit coupling near the equilibrium is small.

	$\tilde{\nu}/\text{cm}^{-1}$
	BS
A″	6181.03
A′	6180.57
A″	6180.36
A″	5235.80
A′	4388.55
A′	4387.54
A″	4387.40
A′	0.00

TABLE 4.8: Wave numbers of spin-orbit energies at the BS geometry calculated using a $(22, 13)$ CAS with the RVTZ basis. The lowest 8 states pertaining to the singlet and triplet A′ and A″ level manifold are reported.

In Table 4.5, we also report an energy obtained from MRCI calculation using an ECP basis for Cu, and RVTZ basis for N and O. The $(18, 11)$ CAS was used as the active space. The characteristics of the interaction between Cu and NO remains the same with the ECP basis following our method of calculating 6 roots. But more importantly, we find that it gives a significantly increased relative energy compared to the calculation with RVTZ basis in Table 4.5 with the same active space.

It should also be noted that the potential function has a minimum at a slightly different geometry while we are using the ECP basis. The deeper minimum obtained from the ECP calculations is likely related to the relativistic effects included in the core potential. But otherwise the form of the potential function remains the same for both singlet and triplet states. Therefore we still do not find a minimum in the ^{3}A″, as reported in coupled cluster calculations [12]. Our results show that we should wherever possible use the ECP results for a global PES.

A more careful investigation of the MRCI results is nevertheless needed. Surely, size inconsistency is a drawback. Benchmark calculations of several systems showed [29] that the internally contracted MRCI method, as it is used here, is superior to other methods that are expected to respect more closely size consistency, such as the average

coupled pair approximation [65]. In that work, it was also shown that the best calculated values for dissociation energies underestimated their experimentally estimated values by an amount of the order of 1000 $hc\,\mathrm{cm}^{-1}$, which could be related to the lack of correlation arising from the neglect of higher lever excitations. In our calculations, we may consider the multi reference formula of the Davidson correction to estimate the effect of quadruple excitations. The CuNO system is particularly difficult to treat, however, because of the ambiguities related to the definition of the reference wave function. We also have to bear in mind the complete root flipping of states at the MRCI level of calculation in oour system. In the 2010 version of MOLPRO, the Davidson correction is calculated with respect to a rotated reference wave function, which has maximal overlap with the MRCI wave function. The results are in Table 4.5.

We first note that the absolute value of the relative energy at the BS structure decreases from 2224 to 1768 $hc\,\mathrm{cm}^{-1}$ when the Davidson correction is applied. Secondly, the Davidson corrected energy of the super-molecule at $r_{\mathrm{Cu}}/\mathrm{pm}$ is still 23 mE_{h} higher than the sum of the Davidson corrected energies of the fragments (acronym "MRCIQ*" in Table 4.5). The potential is already flat at this geometry. Therefore we can conclude that the Davidson correction fails to recover full size consistency. The fragments' MRCIQ energies are -1639.4278 and -129.7189 E_{h} respectively for Cu and NO moities, including Davidson correction. The CCSD(T) fragments' energy on the other hand are -1639.4377 and -129.7254 E_{h} . We can see that the difference between the CCSD(T) and the MRCIQ is almost 10 mE_{h} for the Cu atom and about 6 mE_{h} for the NO. The difference on the NO molecule can be reduced to 0.6 mE_{h} , when the full valence CAS is used for this molecule. Reducing the difference on the Cu probably needs a very important increase of the active space. We managed to reduce the difference between the CCSD(T) and the MRCIQ energy of Cu to 9 mE_{h} using a $(11, 10)$ CAS on Cu i.e including the 5s orbital, and calculations become prohibitively expensive beyond that. The failure of the Davidson correction in recovering size consistency can thus be related to a rather poor description of correlation by the singles and doubles MRCI method on the Cu alone.

We do conclude that our MRCI data suffer indeed from an important lack of correlation arising from the neglect of excitations higher than double. Such excitations are inherently accounted for at the coupled cluster level of theory and in the next section we show the coupled cluster results. This can also be strongly seen in the trend in Figure 4.7

where the increase in correlation with active space in the calculations does lead to a deeper potential well and to shorter bond lengths.

4.3.4   Coupled Cluster calculations

In the remainder we report CCSD(T) and CCSDT dissociation energies. Since coupled cluster results are inherently size-consistent at all truncation orders, reference energies are obtained as the sum of separate Cu and NO fragment energies, with $r_{NO} = 115$ pm. But it should be remembered that, only calculations involving RHF wave functions of closed shell molecules which also dissociate into separate into closed shell fragments are fully size consistent. Here CuNO can be treated in a closed shell RHF calculation, but the fragments are calculated with ROHF, which might have an effective size consistency error, when we sum over these fragments.

The reference configuration for all coupled cluster calculations is obtained point-wise from a Hartree-Fock calculation, where 17 orbitals of A$'$ and 5 orbitals of A$''$ symmetry species are doubly occupied, similarly to configuration Φ_0 in Table 4.7. Here, the doubly occupied orbitals remain delocalized on both Cu and NO fragments, when the distance between them is augmented. Thus, the single reference configuration is not able to describe the dissociation into the two open shell fragments properly. Nevertheless, close to equilibrium, calculations might be reasonable.

We refer to Table 4.9, where we show CCSD(T) energies from several calculations, in which we vary the basis set or the number of electrons that are correlated. Results indicated by the acronym "CCSD(T)-22" include full valence correlation. From the variation of the binding energy between AVTZ and AVQZ we estimate that the basis set error on the dissociation energy of CuNO obtained with the AVTZ basis is on the order of 50 $hc\,\mathrm{cm}^{-1}$, similar to what was found with the MRCI calculations. Similarly, the RVTZ binding energy at the BS structure is roughly 200 $hc\,\mathrm{cm}^{-1}$ weaker than the AVTZ value.

For energies reported under "CCSD(T)-18", the NO σ electrons in orbitals 10.1 and 11.1 are frozen. Here, the absolute value of the RVTZ binding energy decreases by about 200 $hc\,\mathrm{cm}^{-1}$, compared to the CCSD(T)-22-RVTZ value; the decrease is almost a factor of 3 larger than that obtained in the corresponding MRCI calculations. When

	$E_{\mathrm{ref}}/E_{\mathrm{h}}$	$(E - E_{\mathrm{ref}})/hc\,\mathrm{cm}^{-1}$
	ref	BS
CCSD(T)-22-AVDZ	-1768.9988	-3081
CCSD(T)-22-AVTZ	-1769.1631	-3215
CCSD(T)-22-AVQZ	-1769.2250	-3242
CCSD(T)-22-RVTZ	-1769.0996	-2974
CCSD(T)-18-RVTZ	-1768.9225	-2626
CCSDT-18-RVTZ	-1768.9216	-2465
CCSD(T)-22-AVTZ-DK [a]	-1783.4014	-3446
BCCSD(T)-18-RVTZ[b]	-1768.9218	-2580

[a] for Cu the aug-cc-pVTZ-DK basis was used; for N and O we used the VTZ-DK bases and added diffuse s and p functions with exponents 0.0576 and 0.0491, respectively, for nitrogen, and exponents 0.07376 and 0.05974, respectively, for the s and p functions of oxygen.
[b] Brückner coupled cluster theory

TABLE 4.9: Singlet energies E of specific geometries calculated at several levels of theory and with basis sets defined in the text; "ref" is the asymptotic reference molecular structure, which is defined by the sum of the Cu and NO energies calculated separately - the acronyms indicate the number of correlated electrons and the basis used BS is the bent "end-on" structure defined by $r_{\mathrm{Cu}} = 260$ pm, $r_{\mathrm{NO}} = 115$ pm and $\theta_{\mathrm{Cu}} = 130°$.

18 electrons are correlated in CuNO, care is taken for the calculation of the reference energy of separate Cu and NO fragments to put the four NO σ-orbital electrons into the core space, so that seven electrons in the NO fragment are correlated, whereas in Cu the eleven valence electrons are correlated.

When all valence electrons are correlated, the binding at the BS structure obtained from the CCSD(T) calculations with the AVTZ basis is about 1000 $hc\,\mathrm{cm}^{-1}$ stronger than in the corresponding MRCI calculation. The difference reduces to 900 $hc\,\mathrm{cm}^{-1}$ for the calculations with the RVTZ basis, and to 800 $hc\,\mathrm{cm}^{-1}$ when 18 electrons are correlated. These differences are in line with the aforementioned estimations from benchmark calculations [29] and seem to underline, at a first sight, the superiority of the coupled cluster calculations.

4.3.4.1 To multi-reference or not?

We should note that the T1-diagnostic is roughly 0.07 for the calculation with 22, and 0.09 with 18 correlated electrons. This is not unexpected, given the number of singly excited configurations contributing to the CI vector in Table 4.7. Coherently with [66], this value is an additional indicator of the multi-reference character of the wave function

at the BS structure. Yet, a single reference coupled cluster calculation based on a sufficiently large basis and an adequate inclusion of higher excitations could in principle recover much of the missing correlation [67]. Multi-reference coupled cluster calculations can be used to indicate that the accuracy of the CCSDT calculations is within $1 \, \text{m}E_\text{h}$ [76, 78]. While the accuracy of CCSDT results based on restricted Hartree-Fock single-determinant references for simple bond breaking reactions such as in $F_2 = 2F$ is at least $5 \, \text{m}E_\text{h}$, when evaluated asymptotically in the super-molecular approach, calculations at this level of theory severely overestimate the correlation energy for the triple bond breaking reaction $N_2 = 2N$, where at least a CCSDTQ level of theory is needed to obtain a qualitatively correct behavior at dissociation (see [67] and references cited therein).

In order to investigate the T1 diagnostic further, multi-reference coupled cluster calculations should be carried out. In MOLPRO, such calculations can be performed with the MRCC code by M. Kállay [53], when the numbers of active particles (N_ap) and holes (N_ah) are chosen to be different from zero [79]. These calculations are difficult to converge and expensive. We obtain the following electronic energies at BS for 18 correlated electrons at the CCSDT level of theory and the AVDZ basis: $-1768.8568 \, E_\text{h}$ for $N_\text{ap} = N_\text{ah} = 1$ and $-1768.8569 \, E_\text{h}$ for $N_\text{ap} = N_\text{ah} = 2$, while the single determinant yields $-1768.8569 \, E_\text{h}$. Variances are thus in the sub-millihartree domain. With the same code one could obtain a single reference CCSDT result, when $N_\text{ap} = N_\text{ah} = 0$ with the RVTZ basis. Table 4.9 contains the CCSDT value from a calculation with 18 correlated electrons and the RVTZ basis. With the CCSDT calculation the binding at the BS structure is about $300 \, hc \, \text{cm}^{-1}$ weaker than with the CCSD(T) calculation, approaching thus the MRCI value. We should keep in mind that as we go towards CCSDT, CCSDTQ etc in coupled cluster, we are getting closer and closer to the full CI solution. The calculation with CCSDT can in some sense find configurations through connected triples that can be found in the multi-determinantal calculation, even though we start with a single reference wave function.

A larger portion of the potential energy surface is shown in Figure 4.8, where the evolutions of the CCSD(T) energies are given for different types of calculations as functions of r_Cu. We discuss first results obtained from the correlation of 18 electrons and the use of the RVTZ basis, in order to conclude the comparison with the CCSDT data. One clearly sees that the CCSD(T) calculations start to give unphysical results for r_Cu
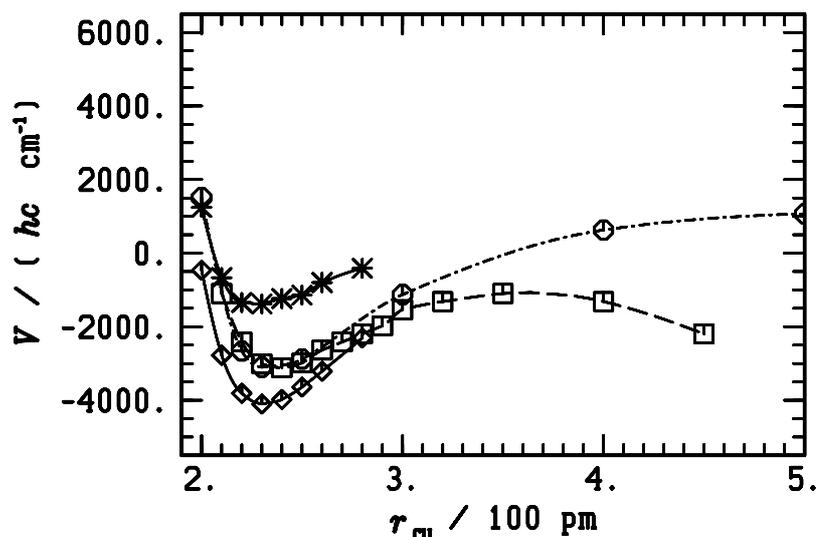
FIGURE 4.8: Potential energy functions $V(r_{\mathrm{Cu}})$ for the lowest singlet and triplet states at the fixed values $\theta_{\mathrm{Cu}} = 130°$ and $r_{\mathrm{NO}} = 115$ pm.
Legend:
Coupled cluster energies: - the acronyms indicate the number of correlated electrons and the basis used;

— —□— — $^1\mathrm{A}'$, CCSD(T)-18-RVTZ, $E_{\mathrm{ref}} = -1768.922\ E_{\mathrm{h}}$ (see Table 4.5)

— · — ◦ — · — $^1\mathrm{A}'$, CCSDT-18-RVTZ, $E_{\mathrm{ref}} = -1768.922\ E_{\mathrm{h}}$

——— ◇ ——— $^1\mathrm{A}'$, CCSD(T)-22-AVTZ, $E_{\mathrm{ref}} = -1769.163\ E_{\mathrm{h}}$ (see Table 4.5)

——— ∗ ——— $^3\mathrm{A}''$, CCSD(T)-22-AVTZ, E_{ref} as for $^1\mathrm{A}'$

exceeding 280 pm, which we relate to the perturbational treatment of triple excitations based on a Hartree-Fock reference function that does not have the appropriate physical behavior at dissociation. When triple excitations are fully taken into account in the CCSDT calculations, a physically sound asymptotic behavior of the potential function is obtained. However, the asymptotically constant CCSDT energy is roughly 1100 $hc\,\mathrm{cm}^{-1}$ (~ 5 mE_{h}) higher than the reference energy, which are related again to the inappropriate Hartree-Fock reference configuration used in these calculations. If the choice was made to use a reference function from an unrestricted Hartree-Fock calculation, the general behavior of the CCSDT potential function could probably be improved to yield the expected size consistent result. We refrain from using symmetry breaking methods, here.

The quite expensive CCSDT calculations allow nevertheless to corroborate the quality of the CCSD(T) data around the bottom of the potential well in Figure 4.8, where the

difference between the CCSDT and CCSD(T) values decreases and is even smaller than at the BS structure. We conclude that the remaining error of the CCSD(T) values should be within the ranges reported in previous work and discussed above, i.e. about 1 mE_h , for bound open shell systems. We also expect the minimum of the CCSD(T) PES to be closer to $r_{Cu} \approx 240$ pm, rather than 250 pm from the MRCI values. These results show a definite trend where the increase of correlation in the *ab initio* calculations leads to a deeper potential well and to shorter bond lengths.

Lines given by the acronyms "CCSD(T)-22" in Figure 4.8 are results from calculations where all electrons in the full valence space are correlated. Here, the AVTZ basis is used. We see that the minimum of the $^1A'$ state is further shifted to smaller values of r_{Cu} , and the depth of the potential well is further increased, when compared to the calculations where only 18 electrons are correlated. This result is at an interesting variance with the MRCI calculations: It seems that the NO σ-orbital electrons, while not directly participating at the formation of the bond, contribute considerably to its strength, when they are correlated via excitations to degrees higher than two. The difference between the coupled cluster and the MRCI energies increases to more than 2000 $hc\,\mathrm{cm}^{-1}$, when all valence electrons are correlated and geometries are relaxed.

So far, our calculations did not include relativistic corrections. Scalar relativistic effects have been shown in [51, 63] to be quite relevant for the correct description of excitation energies in the copper atom.

4.3.5 Relativistic corrections

Relativistic corrections are estimated here from CCSD(T) calculations using the Douglas-Kroll-Hess (DKH) hamiltonian to fourth order. While the corresponding bases implemented in MOLPRO were contracted with respect to order two DKH calculations on the atoms, we considered to go to order four and higher DKH calculations to verify the convergence behaviour. We found that energies are converged with order four.

In all DKH calculations correlation involves the full set of valence electrons. The reported values in Table 4.9 indicate the size of relativistic corrections to the ground state energy of the CuNO system. At the BS structure, the binding is strengthened by roughly 240 $hc\,\mathrm{cm}^{-1}$.

In   Figure 4.9 the potential energy functions from the non-relativistic coupled cluster calculations are repeated and compared to the DKH calculations. We conclude that the relativistic corrections lead to an additional shift of the minimum geometry toward smaller values of r_{Cu} , and that the binding is strengthened by additional 1000 $hc\,cm^{-1}$, roughly.

In contrast to the MRCI results but in agreement with [12], the present CCSD(T) calculations indicate that the triplet A″ state might be bound around $\theta_{Cu} = 130°$, although weaker than the singlet state. Results from the $^3A''$ are also shown in Figure 4.8. From the figure we estimate the difference to the singlet A′ state to be on the order of 2500 $hc\,cm^{-1}$. We also see that the energy of the $^3A''$ does not show significant increase in the binding with the inclusion of the relativistic effects. The minimal CCSD(T) energy in Figure 4.8 indicates that the dissociation energy of CuNO should be expected to be around 4000 $hc\,cm^{-1}$, which is about 60% of the value reported in [12]. We should note that, in that paper, relativistic effective core potentials have been used.
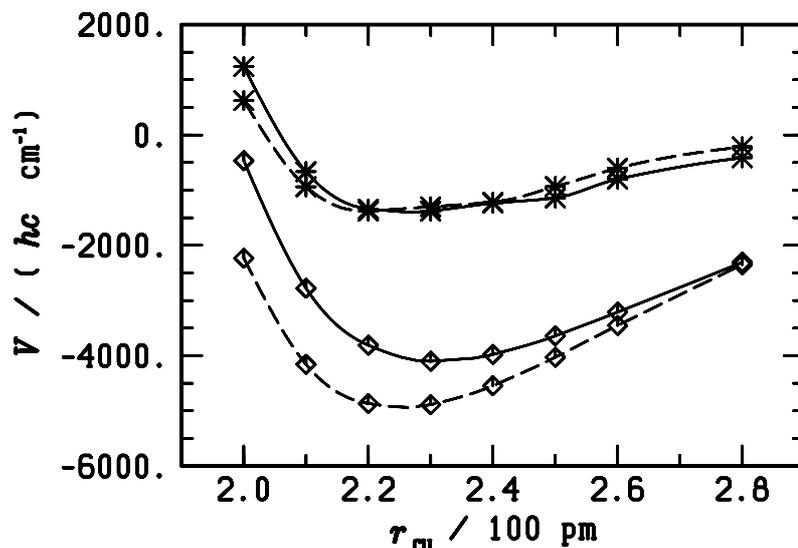
FIGURE 4.9: Potential energy functions $V(r_{Cu})$ from CCSD(T) calculations, including full valence shell correlation and AVTZ basis. The calculation with relativsistic effects lowers the energy slightly. (see text) Geometries as in Figure 4.8. Reference states are the separated Cu and NO fragments with r_{NO} =115 pm; reference energies from Table 4.9

In the next section, we determine the equilibrium structure and the corresponding energy of the CuNO system following the various levels of theory studied in this work.

4.3.6 Equilibrium structure and dissociation energy

The equilibrium geometry and the dissociation energy are obtained from the adjustment of a quadratic force field to a limited set of relative energy data restricted to the intervals $220 \leq r_{Cu}/pm \leq 270$, $113 \leq r_{NO}/pm \leq 118$, and $120° \leq \theta_{Cu} \leq 140°$, for the MRCI data. For the coupled cluster energies, the cube is shifted to $220 \leq r_{Cu}/pm \leq 240$ and $113 \leq r_{NO}/pm \leq 121$, in case of the $^1A'$ state, respectively to $220 \leq r_{Cu}/pm \leq 240$, $118 \leq r_{NO}/pm \leq 124$, and $130° \leq \theta_{Cu} \leq 150°$, in case of the $^3A''$ state. The relative energies are defined with respect to the reference energies given in Table 4.5. MRCI energies were calculated with the RVTZ basis and 18 correlated electrons; for the CCSD(T) energies, all valence electrons were correlated and the AVTZ basis was used. The non-linear adjustment on typically 50 data points was carried out following the Levenberg-Marquardt algorithm (see [82] for an extension of this algorithm), and yields satisfying residuals that do not exceed the desired 1 mE_h uncertainty. Results are reported in Table 4.10. Essentially, the dissociation energy is 2100 $hc\,cm^{-1}$ for the singlet A$'$ ground state at the MRCI level of theory, it increases to 4200 $hc\,cm^{-1}$ when the CCSD(T) method is used, and to 5100 $hc\,cm^{-1}$ when relativistic effects are additionally considered; the triplet A$''$ state is metastable with a calculated dissociation energy of roughly 2900 $hc\,cm^{-1}$, at the CCSD(T) level of theory, while it is repulsive from MRCI calculations.

			r_{Cu}/pm	r_{NO}/pm	θ_{Cu}/deg	$D_e/hc\,cm^{-1}$
MRCI	$^1A'$	RVTZ	253 ± 1	113 ± 1	129.7 ± 0.5	2124 ± 40
CCSD(T)	$^1A'$	AVTZ	234 ± 1	117 ± 1	130.7 ± 0.2	4189 ± 40
CCSD(T)	$^1A'$	AVTZDK	227 ± 1	117 ± 1	131.5 ± 0.1	5080 ± 20
CCSD(T)	$^3A''$	AVTZ	230 ± 1	121 ± 1	138.8 ± 1.0	2885 ± 90

TABLE 4.10: Ground state equilibrium geometries and equilibrium dissociation energy of
CuNO = Cu + NO (at r_{NO} =115 pm). "MRCI" refers here to the (18, 11) CAS MRCI calculations. In the CCSD(T) calculations all 22 valence electrons were correlated. Error bars are statistical uncertainties from the fit, on top of them systematic errors might apply (see text).

4.3.6.1 Error bars in the prediction of dissociation energy

To the statistical error bars indicated in the table we need to add systematic errors which we estimate as follows. First, the error of using the RVTZ basis set for the MRCI energies

should lead to an effective increase of the dissociation energy by about 300 $hc\,cm^{-1}$, because the AVTZ-RVTZ difference is between 200 and 250 $hc\,cm^{-1}$ (see Table 4.5), to which a remaining error of 50 $hc\,cm^{-1}$ for the AVTZ basis is added. The error for using the AVTZ basis in the CCSD(T) calculations is probably less than 100 $hc\,cm^{-1}$. In [12], the overall increase of the dissociation energy due to basis set incompleteness was estimated to be 4 kcal/mol (roughly 1400 $hc\,cm^{-1}$).

Secondly, the basis set superposition error (BSSE) is estimated here with the counterpoise correction and leads to a reduction of the dissociation energy by approximately 150 $hc\,cm^{-1}$ for the MRCI data with the RVTZ or AVTZ basis (the counterpoise correction is on the order of 400 $hc\,cm^{-1}$ when an aug-cc-VDZ basis is used); for the CCSD(T) calculations, the counterpoise correction is about 240, with the RVTZ or AVTZ basis, and 500 $hc\,cm^{-1}$, when the aug-cc-VDZ basis is used. The latter value corresponds roughly to 1/3 of the BSSE estimation of 4.4 kcal/mol in [12]. The present calculations with the RVTZ or AVTZ bases are clearly more accurate. Note that in [12] the energy from the BSSE estimation was added to the calculated dissociation energy of about 10 kcal/mol, while the counterpoise correction must be deduced from the raw calculated value of the dissociation energy. When this logical inconsistency is removed, the BSSE correction in that work almost compensates the energy of 4 kcal/mol added there to the calculated dissociation energy in order to account for the basis set incompleteness, such that the final dissociation energy of CuNO from [12] including all corrections should be about 9.6 kcal/mol (3360 $hc\,cm^{-1}$), which agrees rather well with the present value for the dissociation energy from the present non-relativistic CCSD(T) calculations with the AVTZ basis, when 18 electrons are correlated.

Finally, there is the error stemming from the method used. Here, we trust that the CCSD(T) calculations yield the more accurate results for the electronic energies at configurations close to the equilibrium, despite the inappropriate values from the T1-diagnostic. These calculations recover a quite large portion of correlation energy, since they are comparable with the CCSDT calculations. They carry an intrinsic error related to the use of a single reference wave function. Based on multi-reference coupled cluster calculations carried out at the CCSD level of theory, we make a rough estimation of this uncertainty to be smaller than 220 $hc\,cm^{-1}$, which is in line with error estimations for similar systems [76, 78].

Inclusion of triple and disconnected quadruple excitations in the coupled cluster calculations apparently helps to augment the correlation energy by about 50%, when compared to the present MRCI calculations, which are limited to single and double excitations. In absolute numbers, differences are larger than those from benchmark calculations [29], i.e. 2000 instead of 1000 $hc\,\mathrm{cm}^{-1}$. One could ry to add manually highly excited configurations in the hope of grasping the missing states that would help to improve the MRCI energy further, but this task is difficult to automatize and it is questionable, whether it would be useful for the derivation of a global PES.

Relativistic effects are visibly important for copper. We thus make a conclusive estimation of the dissociation energy of CuNO to be 4940 $hc\,\mathrm{cm}^{-1}$, from the present relativistic CCSD(T) calculations (5080 from Table 4.10, -240 from the counterpoise correction, +100 from basis set incompleteness; values in $hc\,\mathrm{cm}^{-1}$). This energy is about 2/3 the dissociation energy of the cation CuNO$^+$ reported in [13] (22 kcal/mol $\sim$ 7700 $hc\,\mathrm{cm}^{-1}$), and corroborates our estimation from the analysis of the CI vector in Table 4.7. Error bars are on the order of ± 400 $hc\,\mathrm{cm}^{-1}$ and include both statistical (from the fit) and other remaining potential systematic errors such as core electron effects, or the additional the uncertainty related to single-reference based coupled cluster calculations.

The CCSD(T) values for the geometric parameters in Table 4.10 yield an equilibrium CuN distance of 193 pm and an end-on Cu-N-O binding angle $\alpha = 118°$, which are both sligthly smaller than the values 207 pm and 119° from [12]. The NO distance obtained there (119 pm) is larger than the value obtained here, which in turn agrees quite well with the NO distance for CuNO$^+$ from [13]. The MRCI values for the geometric parameters probably suffer from a poorer description of electronic correlation. We expect the CCSD(T) relativistic equilibrium geometries from Table 4.10 to be quite realistic.

4.4   Conclusions on the *ab initio* calculations

In this study, we have investigated the electronic structure of the neutral triatomic system composed of N, O and Cu. We have successfully optimized settings to calculate *ab initio* the ground state at varied positions of the nuclei. Both coupled cluster and multireference configuration interaction (MRCI) methods have been used - the latter with

singly and doubly excited configurations, the former to up to perturbative (CCSD(T)) and full inclusion of triple excitations (CCSDT).

Focusing on linear structures at the first place provides a handle to actually compare energies obtained using $\mathbf{C}_{2v}$ symmetry to those obtained in $\mathbf{C}_s$ symmetry. It has been shown that 12 roots are necessary in the MCSCF calculation to get a clean convergence and comparable states of $\mathbf{C}_s$ or $\mathbf{C}_{2v}$ symmetry.

We also show that the active space in the MCSCF calculations should contain all 3d electrons of Cu to accurately describe the system.It is also shown that the MCSCF calculation alone gives asymptotically inverted roots and that in order to describe the ground state properly we have to use the computationally expensive MRCI calculations over 6 states per symmetry simultaneously. The MRCI calculations invariably lead us to obtain the PES for the 12 lowest states in CuNO, the 6 lowest states of each spatial symmetry. The largest active space used here for the MRCI calculations is a $(22, 13)$ CAS which is close to the full valence space of the system. With a smaller $(18, 11)$ CAS it is possible to obtain MRCI energy values that are semi-quantitatively correct.

With these settings, we definitely show that the ground state belongs to the $^1A'$ irreducible representation, with a minimum at a bent end-on-structure in the nuclear configuration Cu-N-O, in agreement with some of the previous work on this system [7, 12, 15], and in disagreement with a more recent work using DFT [16]. The dissociation energy from the $^1A'$ ground state equilibrium of CuNO into Cu an NO is estimated to be approximatively 2150 $hc\,\mathrm{cm}^{-1}$, from the MRCI calculations. Since the MCSCF reference states are inverted at the asymptote, the Davidson correction is difficult to be included.

We also show that single reference coupled cluster calculations that include to up to triple excitations yield more accurate results for the ground state in these regions of the nuclear position space. Non-relativistic coupled cluster calculations involving all 22 valence electrons yield a dissociation energy of (4200 ± 400) $hc\,\mathrm{cm}^{-1}$, where uncertainties include possible errors related to the multi-reference character of the wave function. When relativistic effects are included with the Douglas-Kroll-Hess hamiltonian, the dissociation energy increases to about (4940 ± 400) $hc\,\mathrm{cm}^{-1}$. This value corresponds to 59 kJ/mol ($\approx$ 14 kcal/mol), which is sligthly larger than the result from [12], if the basis size superposition error is correctly accounted for in that work.

The lowest triplet state belongs to the A″ irreducible representation. The CCSD(T) calculations confirm that this state has a metastable structure about 1200 to 2000 $hc\,\mathrm{cm}^{-1}$ above but displaced with respect to the singlet A′ state, roughly in agreement with findings in [12], while the MRCI calculations yield repulsive states.

With the present data we plan to develop a global PES to be used for quantum dynamical calculations of the CuNO system, with focus on the lowest electronic states of each spin and spatial symmetry. While the MRCI data should be very reliable to obtain an overall qualitatively correct shape of the PES, the ground state equilibrium structure, bound potential wells and the corresponding dissociation energies are more reliably described by the CCSD(T) and CCSDT results. In order to adjust an analytical representation of the PES to the energies calculated *ab initio*, both data sets can either be used simultaneously in a merging procedure [83, 84], or by appropriate scaling [85, 86].

Chapter 5

Theoretical study of low-lying electronic states of Diatomics CuO and CuN

5.1   Introduction

We are primarily interested in the understanding of the dissociation channels of CuNO system. With this purpose in mind we investigate the electronic states which could be produced by dissociation of CuNO, in its $^1A'$ as the ground state. Some computational studies aiming at characterizing the ground and the lowest electronic states of CuO and CuN have been reported in the literature [88, 89, 90, 91, 92, 93, 94, 96]. None of these give trustworthy potential energy functions in the complete range of inter-atomic distances, which are necessary for a detailed quantum dynamical study of the reactions between Cu, N and O.

Hence, we need to review the complete potential energy function of both CuN and CuO, which is definitely difficult and requires cautious convergence criteria . The potential energy surface of transition metal complexes are governed, in general, by multi-configurational wave functions as was explained in the case of CuNO in the previous chapter. Therefore, wave function calculations for the ground and excited states is carried out at the multi-configurational self-consistent-field (MCSCF) and multi-reference configuration interaction (MRCI) levels of theory, albeit restricted to single and double excitations. As in the previous chapter, this investigation aims at establishing adequate settings of MRCI calculations that give energy values to within $1 \, \mathrm{m}E_\mathrm{h}$ ($\sim 220 \, hc \, \mathrm{cm}^{-1}$) accuracy.

The ground state of the copper atom is ^{2}S and the first excited state is ^{2}D, O is ^{3}P and N is ^{4}S. We observe these states as such with the AVTZ basis and at the MRCI level of theory.

When one considers the probable dissociation channels, we see that

$$(^1\mathrm{A'})\mathrm{CuNO} \rightarrow (^3\mathrm{P})\mathrm{O} + (^3\mathrm{X})\mathrm{CuN} \tag{5.1}$$

or

$$(^1\mathrm{A'})\mathrm{CuNO} \rightarrow (^4\mathrm{S})\mathrm{N} + (^4\mathrm{X})\mathrm{CuO} \tag{5.2}$$

or

$$(^1\mathrm{A'})\mathrm{CuNO} \rightarrow (^1\mathrm{P})\mathrm{O} + (^1\mathrm{X})\mathrm{CuN} \tag{5.3}$$

or

$$(^1\mathrm{A'})\mathrm{CuNO} \rightarrow (^2\mathrm{D})\mathrm{N} + (^2\mathrm{X})\mathrm{CuO} \tag{5.4}$$
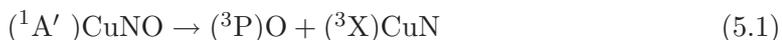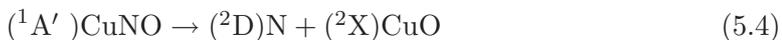
(^{1}X) CuN would not dissociate into (^{2}S) Cu and a (^{4}S) N, as the lowest energy channel; thus we can conclude that the singlet CuN must be an excited state. And henceforth, Eq. (5.3) is likely closed for conventional energies.

(^{4}X) CuO in Eq. (5.2) can further dissociate into (^{2}D) Cu and (^{3}P) O asymptotes, and is thus possibly the lowest state. From [92], we can say, however, that of the two channels given by Eq. (5.2) and Eq. (5.4), the doublet channel Eq. (5.2) will be the lowest energy.

5.2   Methods

The calculations on the ground and excited electronic states were performed using the MCSCF method followed by the internally contracted MRCI method of Werner and Knowles [27, 28, 29, 30] as implemented in the MOLPRO [48] suite of programs. The orbitals used to set up the CI expansion were obtained by state averaged MCSCF calculations using $\mathbf{C}_{2v}$ symmetry and with equal weights for all the participating states. Here the number of roots to be state averaged at the MCSCF calculations were varied. In the calculations, we use the augmented correlation-consistent polarized triple ζ-basis sets ("aug-cc-pVTZ", but abbreviated here "AVTZ") of Dunning and co-workers [49, 50], for N and O, and of Balabanov and Peterson [51] for convergent basis sets for transition metals. This was described in detail in the previous chapter on CuNO. For the coupled cluster calculations, we use the AVTZ-DK basis[51].

5.3   The lowest electronic states of CuO

The doublet and quartet electronic states of CuO are those corresponding to the channels, with (^2S) Cu + (^3P) O and with (^2D) Cu + (^3P) O. There are more than one bound state of Π symmetry.

5.3.1   MCSCF and MRCI

In this study, we carefully chose the number of states computed in each symmetry to overcome convergence failures at the MCSCF level. A state averaging procedure was used to optimize a common molecular orbital basis set for describing the states of interest in a given spin multiplicity. All results described here are obtained from state averaged MCSCF calculations with the AVTZ basis and aan active space consisting of 25 electrons in 14 orbitals, a $(25, 14)$ CAS. This essentially includes the 3s, 3p 3d, and 4s electrons from Cu and 2s, 2p electrons of O in the active space. For a given structure, the MCSCF energies are obtained at $\mathbf{C}_{2v}$ symmetry and doublet spin symmetry.

Under $\mathbf{C}_{2v}$, 54 roots were calculated ($17 \times {}^2A_1$, $13 \times {}^2B_1$, $13 \times {}^2B_2$, $11 \times {}^2A_2$). Calculations are considered converged if the energies reach 1 mE_h accuracy. Also the Π

state degeneracy for the B_1, and B_2 representations is verified for physically valid convergence. An unbalanced number of roots can lead to broken symmetries. Also, severe root-flipping problems occur when we fail to include all states of an electronic multiplet in the MCSCF calculations, leading to erratic prediction of the order of the states by the variational algorithm because states with higher energy may alternate during the calculation with states of slightly lower energy, leading to slow or failing convergence. The number of roots here correspond to the number of states that can be obtained by taking both the neutral and ionic product states producing a doublet state. This is easily obtained by examining the symmetry of the ground electronic states of individual fragments Cu and O. We reiterate that it is important to consider the ionic states also in the MCSCF calculations to obtain physically sound dissociation of the fragments.

We report MRCI relative energies calculated with respect to energies of a reference structure with the inter-atomic distance $r = 650$ pm. In order to be able to carry out the MRCI calculations in an efficient way, we froze the closed orbitals used in the preceding MCSCF calculations with the MOLPRO "core" card, i.e. we froze 12 electrons in 6 core orbitals; singly and doubly excited configurations were included in the MRCI from 14 active orbitals, thereby correlating 25 electrons, i.e. in a $(25, 14)$ CAS. The total number of contracted configurations is 4017821 in $\mathbf{C}_{2v}$ symmetry, per irreducible representation, and corresponds to about 88908448 non-contracted configurations in MRCI. The next contribution to the correlation energy may result from correlating the Cu (2)p shell which contains six additional electrons. It was not possible to correlate this shell in the MRCI calculation as it demands much higher computational effort.

5.3.2   Lowest doublet state

We derive an analytical potential energy function for the ground electronic state. The analytical form, is described in the V_{2b} potential in Chapter 6. This form is adjusted to adiabatic energy data calculated *ab initio* at the MRCI level of theory. The function is a generalization of the well known Morse potential. The fit is done following are an extension of the Levenberg-Marquardt algorithm using external conditions described previously by R. Marquardt.

The Figure 5.1 shows the potential energy function for the lowest electronic state of $^2B_1$ symmetry. The fit gives an equilibrium distance of 174 pm with a dissociation energy of

19920 $hc\,\mathrm{cm}^{-1}$ (≈ 2.47 eV) for the lowest bound electronic state. The $^2B_2$ energy points follow the exact same form.
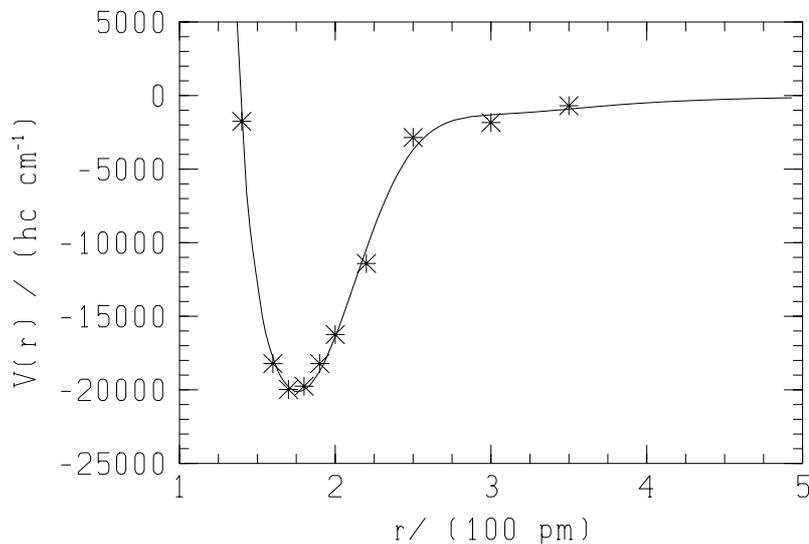
FIGURE 5.1: MRCI potential energy function $V(r_{\mathrm{Cu}})$ for the lowest $^2B_1$ state. Here lines, give wave numbers of relative electronic energies $E - E_{\mathrm{ref}}$, where $E_{\mathrm{ref}} = -1714.608$ E_{h} at $r = 650$ pm, as functions of the copper - oxygen distance r.

The $^2B_1$ minimum is close to the minimum reported earlier in the literature. In the literature, for CuO, the bond length R_{e} calculated with CCSD(T) differs from the experimental data by 0.037 $\mathring{A}$.[95]. The experimental values for the equilibrium bond length and fundamental vibrational transition are $R_{\mathrm{e}} = 1.724$ $\mathring{A}$, and $\omega_{\mathrm{e}} = 640.2\mathrm{cm}^{-1}$. The discrepancy in the CCSD(T) results for CuO, compared with the experimental data was attributed to the multi-configurational character or the incompleteness of the basis set [95, 96]. By increasing the basis set on the oxygen atom to aug-cc-pVQZ, the CCSD(T) results improved for CuO with $R_{\mathrm{e}} = 174.2$ pm , and $\omega_{\mathrm{e}} = 613\mathrm{cm}^{-1}$; a dissociation energy $D_0 \approx 2.97$ eV is also close to experimental values [95].

The present MRCI calculations perform well and gives $R_{\mathrm{e}} = 174$ pm and $\omega_{\mathrm{e}} = 643\mathrm{cm}^{-1}$ values. The value of ω_{e} corresponds to the vibrational fundamental on the analytical potential energy function and was obtained by a 1D hermite polynomial DVR of the vibrational Hamiltonian. The difference in the R_{e} from experiments may be due to further lack of dynamical correlation in the Cu atom in MRCI, which we have seen earlier for CuNO system.

Next we study the lowest electronic state of $^2A_2$ symmetry species in Figure 5.2.
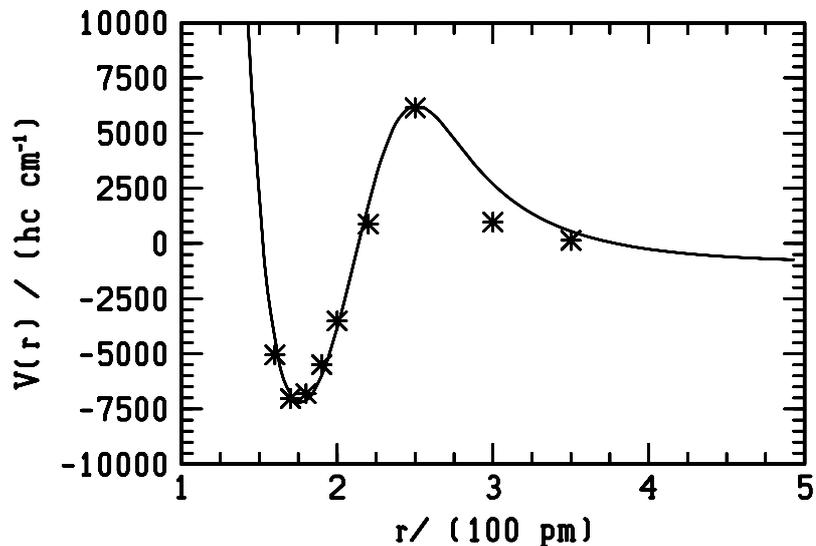
FIGURE 5.2: MRCI potential energy functions $V(r)$ for the lowest doublet states of $^2A_2$ symmetry species.Here lines, give wave numbers of relative electronic energies $E - E_{\text{ref}}$, where $E_{\text{ref}} = -1714.608 \; E_{\text{h}}$ at $r = 650$ pm pm, as functions of the copper - oxygen distance r.

This state has an equilibrium distance of 169 pm with a dissociation energy of 6508 $hc \, \text{cm}^{-1}$ for the lowest electronic state. We find that there is a barrier in the fit of the lowest electronic state of $^2A_2$ symmetry species. This is not seen in the potential function of $^2B_1$ symmetry. Such a barrier to dissociation has not been reported before for the CuO system. The question is whether the barrier is real or not. Since we are using many roots in MRCI calculation, we must be sure that this barrier is not an artefact from the method of calculating the electronic energies.

The calculations reported here with a reasonably big basis and a big active space at the MRCI level of theory still retain this significant barrier in the potential. Since this is a diatomic system, two potential functions do not cross if they are in the same symmetry species, which might lead to a barrier. This is well known as avoided crossing in the literature.

One way to check if the barrier is real is to investigate if there is a change in the configuration in the lowest electronic state of the $^2A_2$ symmetry species at the asymptote from that of equilibrium geometry. For this purpose, we follow the variation in the

permanent dipole moment along the lowest $^2A_2$ state as a function of the interatomic distance.

$^2B_1$ $^2A_2$
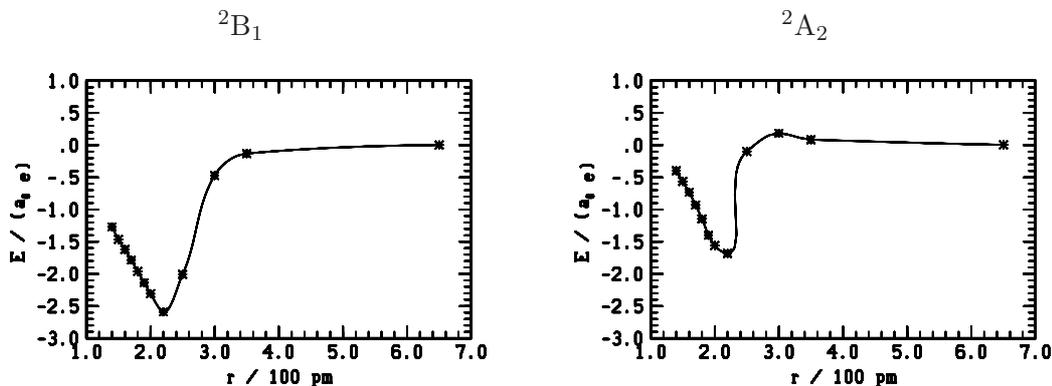
FIGURE 5.3: Spline interpolation of the permanent dipole moment for the lowest dou-
blet states of $^2B_1$ and $^2A_2$ symmetry species.

In Figure 5.3, we follow the interpolation of the values of dipole moments along the lowest electronic energy states of $^2B_1$ and $^2A_2$. Here, the dipole sign is defined along the z axis as follows: positive value corresponds to oxygen having a net fractional positive charge, and the negative value corresponds to copper having a net positive charge. At the asymptote, there is only a very small dipole in both $^2B_1$ (0.00335 a_0e) and $^2A_2$ (0.00526 a_0e) symmetry species. This is a reflection of the fact that at the asymptote, both Cu and O fragments are neutral. CuO is well known to be polarized $Cu^+ + O^-$ near the equilibrium and this reflects as a huge negative dipole moment near equilibrium geometries.

Here we see that, in the case of $^2B_1$ symmetry species, the permanent dipole moment starts from close to zero at the asymptote, and as the Cu and O approach towards the equilibrium geometry, the value of dipole moment monotonically becomes more negative. There is a fractional positive charge at Cu and a fractional negative charge in O. This increase in the dipole moment behaves as expected from the Cu and O interaction, with oxygen being the more electronegative species.

However, when we analyse the permanent dipole moment in the $^2A_2$ symmetry species, it shows a different trend. We find that the value of dipole moment actually increases from close to zero in the asymptote to (0.1845 a_0 e) at 300 pm (in the positive sign of dipole moment) as we move towards smaller internuclear distances. This means that,

remarkably, at these geometries, Cu is gaining electron density, and has a fractional negative charge at these geometries. And as Cu and O approach even more closer to equilibrium, the sign of the dipole moment inverts and becomes negative. As the system goes to geometries on the other side of barrier, the dipole becomes hugely negative as it reaches the equilibrium geometry. Therefore, we could infer that , in the MRCI calculations here, there is clear change in the configurations that make up the lowest state at the equilibrium geometries and at the asymptote. This change in configurations reflects as the barrier in the lowest electronic potential energy function.

We should mention that, the maximum negative value of the dipole moment does not exactly coincide with the R_e in both $^2B_1$ and $^2A_2$ symmetry species. The largest value of dipole is on a slighly higher internuclear distance. Finally, we point out that the barrier can vanish, or vary, or be much higher, if the number of appropriate roots is too small. The result shown in Figure 5.2 is fairly well converged with respect to the number of roots considered i.e the reference space for the MRCI calculation is complete.

5.3.3   Exited doublet states
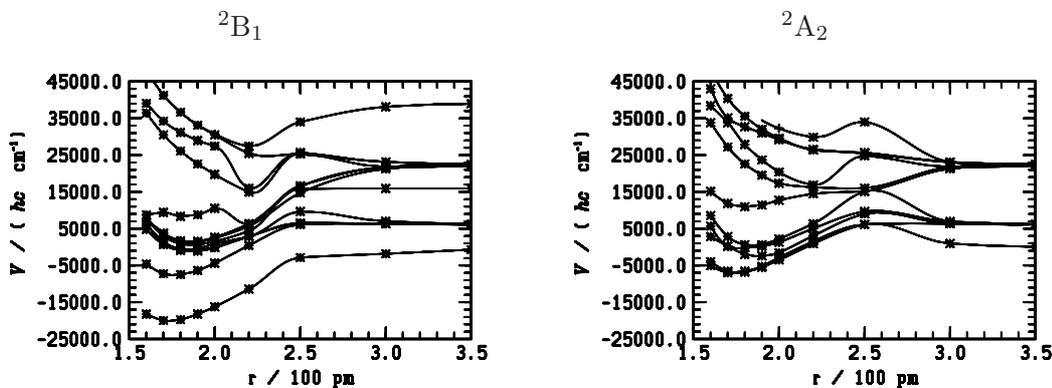
FIGURE 5.4: The lowest doublet states of $^2B_1$ and $^2A_2$ symmetry species. Energies were obtained from a (25,14) CAS with the AVTZ basis. The lines are cubic spline interpolations

In Figure 5.4, we plot the lowest adiabatic electronic energy states of $^2B_1$ and $^2A_2$ symmetry species. We note that for most of the adiabatic electronic states the potential energy functions are complicated by several avoided crossings between possible neutral or ionic states of CuO. We could follow the permanent dipole moment of each of these

states at different geometries. We find that, indeed, the electronic states change leading configurations several times between the asymptote and the equilibrium geometries. By following the dipole moment of the many electronic states here we could identify, the states that give rise to the neutral dissociation channel at the asymptote. The configurations that are ionic in nature are prominent and give a stable lowest electronic energy near the equilibrium. They should also be seen at higher energies at the asymptote. However, all $11 \times^2 A_2$ asymptotic states, shown in Figure 5.4 are neutral in nature and have a permanent dipole moment close to zero at the asymptote.

We need to calculate a significantly larger number of roots to completely see the asymptotes from the ionic channels, which are much higher in energy. This is at the moment beyond our computational capabilities. It was found that it becomes extremely difficult for the MRCI calculations to converge accurately with additional roots. Also we need more roots in the state averaged MCSCF. This also poses convergence issues.

Again, we should note that, all reference configurations used to define the lowest MCSCF states of each individual spatial symmetry species, that is $17 \times^2 A_1$, $13 \times^2 B_1$, $13 \times^2 B_2$ and $11 \times^2 A_2$ are needed to correctly describe the CI vectors of the states shown in Figure 5.4.

	T_e/cm^{-1}		Exp: T_e/cm^{-1}		T_e [a]$/\text{cm}^{-1}$		T_e [b]$/\text{cm}^{-1}$
$1\ ^2B_1$	0.0	X $^2\Pi$	0.0/277 [c]	X $^2\Pi$	0.0	X $^2\Pi$	0.0
$2\ ^2B_1$	12511	$2\ ^2\Pi$	15166 [c]	$2\ ^2\Pi$	15616	$\gamma\ ^2\Pi$	18581
$3\ ^2B_1$	19140	$3\ ^2\Pi$	18812 [d]	$3\ ^2\Pi$	18122	C $^2\Pi$	20259
$4\ ^2B_1$	19140	$4\ ^2\Pi$	21222 [e]	$4\ ^2\Pi$	20384		
$5\ ^2B_1$	20680	$5\ ^2\Pi$	21800 [e]	$5\ ^2\Pi$	23365		
$6\ ^2B_1$	21340	$6\ ^2\Pi$	25191 [e]	$6\ ^2\Pi$	24932		
$7\ ^2B_1$	21560						
$8\ ^2B_1$	28380						
$1\ ^2A_2$	12980	Y $^2\Sigma^+$	7865/7825 [g]/[h]	Y $^2\Sigma^+$	7600	Y $^2\Sigma^+$	5564
$2\ ^2A_2$	13420	$1\ ^2\Sigma^-$	16492 [e]	$1\ ^2\Sigma^-$	18020		
$3\ ^2A_2$	17600	$2\ ^2\Sigma^-$		$2\ ^2\Sigma^-$	15280	$\beta\ ^2\Delta$	21920
$4\ ^2A_2$	19800	$1\ ^2\Delta$	15317 [c]	$1\ ^2\Delta$	19017		
$5\ ^2A_2$	20680	$2\ ^2\Delta$	19473 [f]	$2\ ^2\Delta$	20877		
$6\ ^2A_2$	30020	$3\ ^2\Delta$	21104 [e]	$3\ ^2\Delta$			

[a] [92] [b] [94] [c] [100] [d] [98] [e] [99] [f] [101] [g] [102] [h] [106]

TABLE 5.1: The comparison of doublet states with those previously reported in the literature

In Table 5.1, we report the values of energies obtained from the MRCI calculations and compare them with those published earlier[92, 94]. We point out that the excited state energies reported here are of attractive states (that there is a minimum compared to the asymptote energy in that adiabatic electronic state). We generally obtain quite good agreement with the values reported by Peyerimhoff and Hippe [92]. The agreement with those reported in [94] is clear less good. The T_e values in this work give a lower energy for the excited states than reported in [92]. We do not calculate $^2A_1$ state therefore we cannot comment on the $Y^2\Sigma^+$ state.

Our calculations for the first two states of each symmetry species should be well converged with in the reference space considered. In [92], relativistic effects have been considered and the reference space was also specially expanded to consider excitations higher than double increasing hence the correlation energy of the result. Note that the present result for the second $^2A_2$ state at 13420cm^{-1} could be related to the $^2A_2$ component of the first $^2\Delta$ state in [92] at 15280cm^{-1} . We trust hence that the results are quite accurate, in particular to the ground states. We definitely doubt the results obtained from the CIPSI method discussed there.

5.3.4   Lowest quartet states

The quartet states of CuO are calculated at MRCI level of theory from the converged doublet MCSCF wave function as described previously. This provides a reliable handle to check the absolute energies of the lowest doublet and quartet states at the asymptote structure where they should be degenerate due to symmetry. The Figure 5.5 shows the potential energy function for the lowest electronic state of $^4B_1$ and $^4A_2$ symmetry.

In Figure 5.5, we see that the lowest electronic states in both $^4B_1$ and $^4A_2$ symmetry species show remarkably deep minima. The fit gives an equilibrium distance of 175 pm with a dissociation energy of 11193 $hc\,\text{cm}^{-1}$ for the lowest bound electronic state in the $^4B_1$ symmetry species, while the $^4A_2$ has an equilibrium distance of 171 pm with a dissociation energy of 11632 $hc\,\text{cm}^{-1}$ for its lowest bound electronic state. These deep minima are much lower than previously reported values. These states also seems to have a barrier in the potential energy functions.
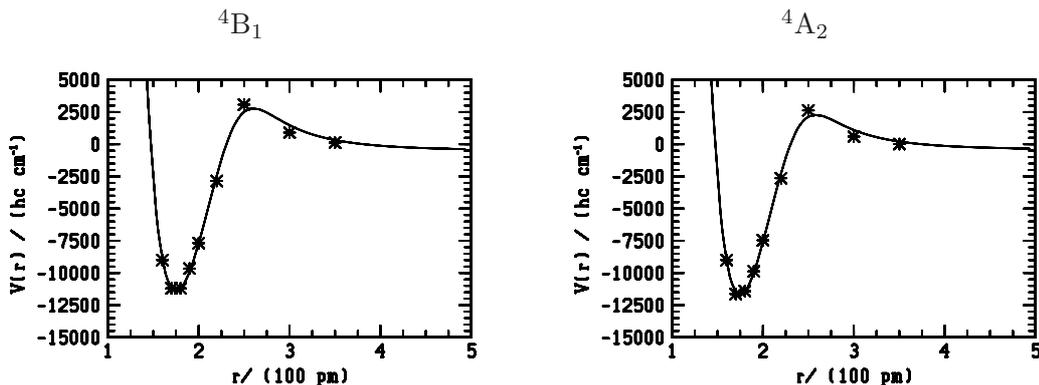
FIGURE 5.5: MRCI potential energy functions $V(r_{\mathrm{Cu}})$ for the lowest quartet states of $^4B_1$ and $^4A_2$ symmetry species. Here lines, give wave numbers of relative electronic energies $E - E_{\mathrm{ref}}$, where $E_{\mathrm{ref}} = -1714.608\, E_{\mathrm{h}}$ at $r = 650$ pm, as functions of the copper - oxygen distance r.

In [94], from CIPSI calculations, the $^4\Sigma^-$ and $^4\Pi$ potential functions have a maxima that occurs near 211.7 pm and 195.8 pm, respectively. The minima being at 171.4 pm and 159.8 pm. They then define the potential barrier as the energy difference between minimum and maximum, and obtain a value of 710 $hc\,\mathrm{cm}^{-1}$ for the $^4\Sigma^-$ state and 4180 $hc\,\mathrm{cm}^{-1}$ for $^4\Pi$ state. Following the authors of [94], these energy barriers are necessary for dissociating these states into (^2D) Cu + (^3P) O. Furthermore, the location of the maximum at a distance near the equilibrium bond length R_{e} of the $^2\Pi$ ground state and with a small energy above their (^2D) Cu + (^3P) O dissociation limit suggests that this might be a pre-dissociative state.

However, in the earlier work [92], the picture is different. Here, the authors obtained for the $^4\Sigma^-$ and $^4\Pi$ potential functions an equilibrium bond length of 171.9 pm and 173.6 pm respectively. Their potential functions are limited to internuclear distances of 200 pm. They do not mention or find a barrier. In the later publication [94], the extensive (and contrasting) data reported in [92] is neither discussed nor cited.

We can see that these values are quite different to the values of R_{e} reported here. For $^4\Pi$ state, our R_{e} is somewhat closer to the value in [92]. Also our ground state potential functions do not follow those given in [94] and the barriers we obtain are at larger internuclear distances for both $^4B_1$ and $^4A_2$ states.

Again, the question is whether the barrier we see in this work is real or perhaps an artifact of the calculations.

$^4\text{B}_1$ $^4\text{A}_2$
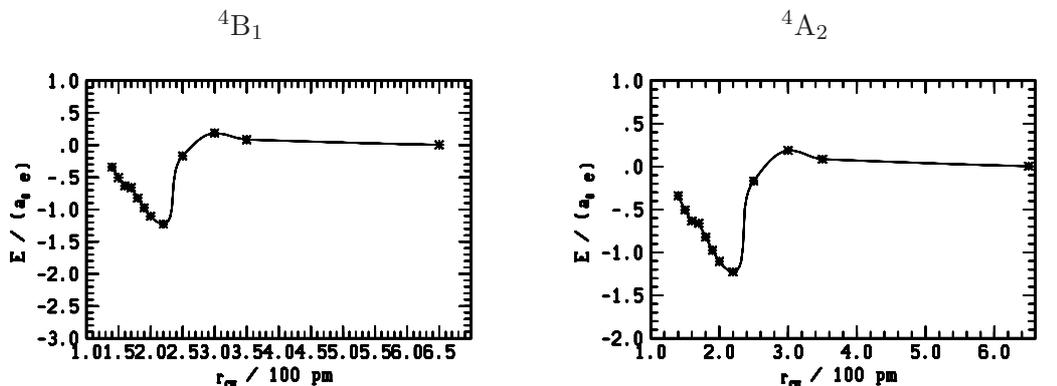
FIGURE 5.6: Spline interpolation of permanent dipole moment for the lowest doublet states of $^4\text{B}_1$ and $^4\text{A}_2$ symmetry species.

In Figure 5.6, we follow the same strategy we used before. When we analyse the permanent dipole moment in $^4\text{B}_1$ and $^4\text{A}_2$ symmetry species, it shows the trend. We again find that the value of dipole moment increases from the asymptote to the positive as we move towards equilibrium geometries and reach the barrier. Cu is gaining electron density, and has a fractional negative charge at these geometries. And as Cu and O approach more closer to equilibrium, the sign of the dipole moment inverts and becomes negative at close to the equilibrium geometries. Therefore, we may say that, in the present MRCI calculations, there is a possible change in the configurations that contributes most to the lowest state at the equilibrium geometries and at the asymptote and might be the reason for the barrier. However, we do recognise that at the moment, it is impossible to completely rule out the chance that barrier may modified if larger reference spaces are used.

5.3.5   Exited quartet states

Figure 5.7 shows the quartet $^4\text{B}_1$ and $^4\text{A}_2$ MRCI states close to equilibrium for the dissociation channel Cu + O at $(25, 14)$ CAS, AVTZ basis. Again, all reference configurations used to define the lowest MCSCF states of each individual spatial symmetry species, are used in the MRCI calcualtin of the quartet states also to correctly describe the CI vectors of the states.

$^4B_1$

$^4A_2$
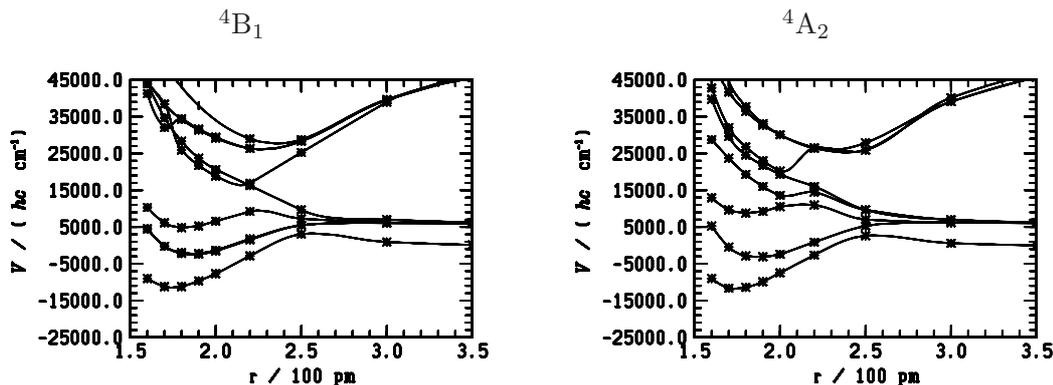
FIGURE 5.7:   MRCI potential energy functions $V(r)$ for the lowest quartet states of $^4B_1$ and $^4A_2$ symmetry species. Energies were obtained from a (25,14) CAS with the AVTZ basis. The lines are cubic spline interpolations.

	$T_e/$ cm^{-1}		T_e [a]/cm^{-1}		T_e [b]/cm^{-1}
1 $^4B_1$	8800	1 $^4\Pi$	13434	$^4\Pi$	15000
2 $^4B_1$	17600	2 $^4\Pi$	21884		
3 $^4B_1$	17380				
4 $^4B_1$	24860				
1 $^4A_2$	8360	1 $^4\Sigma^-$	10469	$^4\Sigma^-$	8823
2 $^4A_2$	16940				
3 $^4A_2$	28820	1 $^4\Delta$	21017		

[a][92][b][94]

TABLE 5.2:   The comparison of doublet states with those previously reported in the literature.$T_e = 0$ for lowest $^2\Pi state$.

In Table 5.2, we show the energies of the lowest quartet electronic states shown in Figure 5.7. The lowest electronic state we obtain for $^4B_1$ symmetry species is at 8800 hc cm^{-1} above the $^2B_1$ ground state. This value is lower than the previously reported values in [92, 94]. And we find at least three exited $^4B_1$ states within the energy range that have a potential well. These states have not been reported. The $^4A_2$ energies are also given in Table 5.2. The lowest electronic state of $^4A_2$ symmetry species is $8360hc$ cm^{-1} above the $^2B_1$ ground state. This value corroborates with the values given in [94] and is lower than that reported in [92].

5.3.6   Coupled cluster calculations

In this section we report the term values obtained from coupled cluster calculations performed using the Douglas-Kroll-Hess (DKH) hamiltonian to fourth order. The reference

configuration for all coupled cluster calculations is obtained point-wise from a Hartree-Fock calculation. Since coupled cluster results are inherently size-consistent, reference energies are obtained as the sum of separate Cu and O fragment energies.

$^2B_1$ $^2A_1$
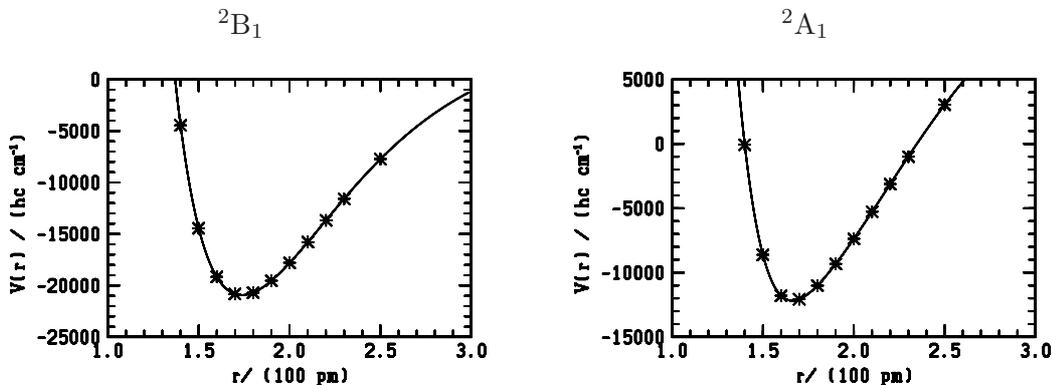
FIGURE 5.8: Coupled cluster potential energy functions $V(r)$ for the lowest doublet states of $^2B_1$ and $^2A_1$ symmetry species. Here lines, give wave numbers of relative electronic energies $E - E_{ref}$, where $E_{ref} = E(r \rightarrow \infty)$, as functions of the copper - oxygen distance r.

In Figure 5.8, we see that the lowest electronic states in both $^2B_1$ and $^2A_1$ symmetry species show deep minima. The equilibrium distance was found to be 171 pm with a dissociation energy of 20900 $hc\,cm^{-1}$ for the lowest bound electronic state in the $^4B_1$ symmetry species. This dissociation energy is $\approx 1000\ hc\,cm^{-1}$ more than those obtained from the MRCI calculation for the $^2B_1$ symmetry species. Also the equilibrium bond length shorten in the coupled cluster calculation. The increase in the dissociation energy can be attributed to the combined effect of recovering more dynamical correlation and the inclusion of scalar relativistic effects in the Coupled cluster calculations.

The lowest $^2\Sigma^+$ state has a dissociation energy of 12065 $hc\,cm^{-1}$ with an equilibrium bond length of 169 pm. The Te of this state is 8835 cm^{-1} which is slightly higher than the experimental values in [102] and [106]. However, the value we report agrees well with a previously reported coupled cluster value of $Te = 8065$cm^{-1} for this state by [103].

The $^4\Sigma^+$ state has a $T_e = 32824$ cm^{-1} from the lowest $^2\Pi$ state in coupled cluster calculation. The efforts to calculate the electronic states of other symmetry species in both doublet and quartet states of CuO did not converge at the coupled cluster level.
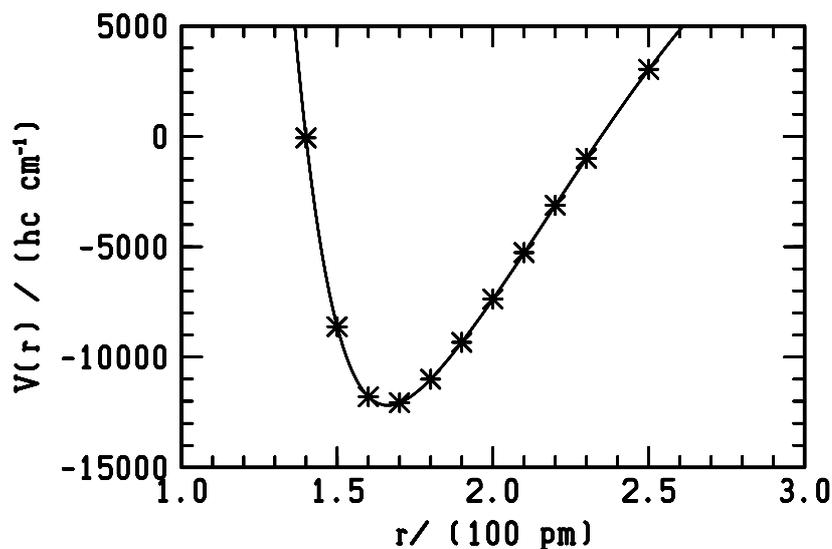
FIGURE 5.9: Coupled cluster potential energy functions $V(r)$ for the lowest quartet state of $^4A_1$ symmetry species. Here lines, give wave numbers of relative electronic energies $E - E_{\text{ref}}$, where $E_{\text{ref}} = E(r \to \infty)$, as functions of the copper - oxygen distance r.

5.4   The lowest electronic states of CuN

The lowest triplet state of the CuN molecule has been previously reported in [94, 95, 97].

5.4.1   MCSCF and MRCI

As described above, all results are obtained from state averaged MCSCF calculations with the AVTZ basis. The active space consists of 14 electrons in 9 orbitals i.e.a $(14, 9)$ CAS. This includes the 3d and 4s electrons from Cu and 2p electrons of N in the active space. For a given structure, the MCSCF energies are obtained at $\mathbf{C}_{2v}$ symmetry.

Under $\mathbf{C}_{2v}$, 72 state averaged roots were calculated ($18 \times$ $^3A_1$,$18 \times$ $^3B_1$, $18 \times$ $^3B_2$, $18 \times$ $^3A_2$). Similar convergence criteria have been followed as for the CuO system discussed above. The number of roots considered here correspond to the number of states that could be obtained by taking all the neutral and ionic configurations giving a singlet state by examining the symmetry of the ground states of individual fragments Cu and N.

We report MRCI relative energies calculated with respect to energies of a reference structure at the asymptote with an inter-atomic distance of 1000 pm.

As described above, we froze 22 electrons in 11 core orbitals; singly and doubly excited configurations were included in the MRCI from 9 active orbitals, thereby correlating 14 electrons. The total number of contracted configurations is 2682462 in $\mathbf{C}_{2\mathrm{v}}$ symmetry, per irreducible representation, and corresponds to about 18390104 non-contracted configurations in MRCI. The next contribution to the correlation energy may result from correlating the N 2s and Cu 3 s and (3)p shell which contains 10 additional electrons.

5.4.2 Lowest triplet state

The Figure 5.10 shows the potential energy function for the lowest electronic state of $^3\mathrm{A}_2$ symmetry. The fit gives an equilibrium distance of 179 pm. The dissociation energy D_e is 9904 $hc\,\mathrm{cm}^{-1}$ and ω_e is 616cm^{-1} . These values are close to values obtained at the CCSD(T) level in [95].
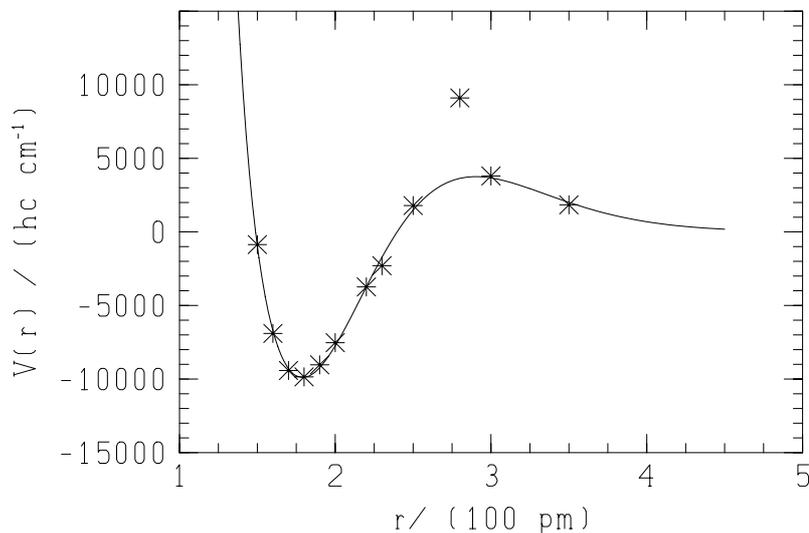
FIGURE 5.10: MRCI potential energy functions $V(r_\mathrm{Cu})$ for the lowest triplet states of $^3\mathrm{A}_2$ symmetry species. but here lines, give wave numbers of relative electronic energies $E - E_\mathrm{ref}$, where $E_\mathrm{ref} = -1693.783$ E_h at 1000 pm, as functions of the copper - nitrogen distance r.

The energy point at internuclear distance 280 pm seems to indicate a barrier. Here again we need to ask, whether this is a real barrier or not. We use the strategy of following the

change in permanent dipole moment to see signs of change in configuration. In contrast to CuO, here, the permanent dipole moment does not show any inversion in the direction of the dipole on moving towards equilibrium geometries. N is gaining electron density, and has a fractional negative charge as when approaching the equilibrium geometry. This leads us to two options: either the method of analysis of the permanent dipole moment is wrong or the MRCI values are not converged.

Indeed, on inspection at internuclear distance of 280 pm we find that the calculation is not converged at this geometry. The CI state tries to include a root that is not present in the underlying MCSCF reference space. The high energy at this geometry and the resulting barrier is hence artificial. Therefore we do not fit this energy point in our potential energy function. The analysis of changes in permanent dipole moment at different geometries thus helped in identifying correctly a wrongly converged calculation.

From the fit we still see that there is a small barrier at 300 pm. From our previous experience in CuO, we find that using a bigger active space was capable of removing artificial small barriers in the diatomic as we are including more correlation. It might be that the active space used here for the CuN is not large enough. An active space comparable to that of CuO would be a CAS $(24, 14)$ in CuN. But all our attempts of calculations with this bigger active space did not converge correctly. So we cannot say more about the smaller barrier in CuN with our current level of understanding.

5.4.3   Excited triplet states

Figure 5.11 shows the triplet $^3A_2$ MRCI states close to equilibrium for the dissociation channel Cu + N with the $(14, 9)$ CAS and the AVTZ basis.The figure shows the lowest 12 electronic states.

The MRCI calculations have the states into the correct order and again it is important to note that, technically, all reference configurations used to define the lowest MCSCF states of each individual spatial symmetry species, that is $18 \times {}^2A_2$ are needed to correctly describe the CI vectors of the states shown in Figure 5.11.

In Table 5.3, the T_e values some lowest $^3A_2$ states are given, the potentials of which can be seen in Figure 5.11. Our first excited $^3A_2$ state lies above some of the excited states reported in [94] as the first excited state of the CuN system. We do not calculate these
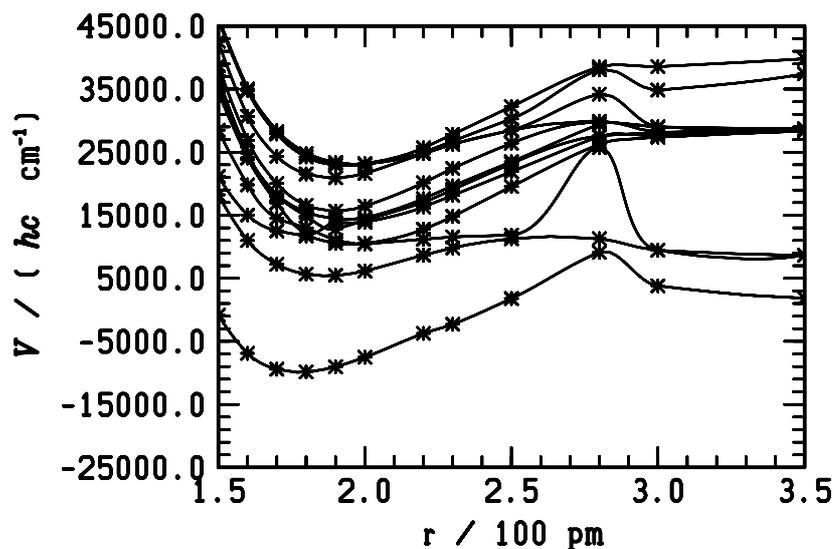
FIGURE 5.11: MRCI potential energy functions $V(r_{Cu})$ for the lowest triplet states of $^3A_2$ symmetry species. Energies were obtained from a $(14, 9)$ CAS with the AVTZ basis.

	$T_e/$ cm^{-1}		$T_e{}^b/$cm^{-1}	
$1\ ^3A_2$	0.0	$^3\Sigma^-$	0.0	
$2\ ^3A_2$	15308	$^5\Sigma^-$	9395	
$3\ ^3A_2$	20303	$^1\Sigma^+$	12291	^{b}[94]
$4\ ^3A_2$	21901	$^1\Delta$	11710	
$5\ ^3A_2$	22628	$^3\Pi$	12162	
$6\ ^3A_2$	24273	$^1\Pi$	20243	

TABLE 5.3: The comparison of some CuN excited states with those previously reported in the literature

states in our work as we know that this might not be a dissociation channel of CuNO, which we are primarily interested in understanding.

We also tried coupled cluster calculations for CuN system. However, convergence was not achieved.

5.5   Conclusions on *ab initio* calculations on CuO and CuN

In this study, we have investigated the lowest electronic states of the neutral diatomic systems CuN and CuO.

We have successfully optimized settings to calculate *ab initio* the ground state and the excited state potential energy functions, which show several avoided crossings. All methods were used as implemented in the MOLPRO program suite [48] The MRCI results allow to identify the multi-reference character of the electronic ground state wave function.

The potential energy function of the CuO doublet and quartet states show bound ground states with deep minima. Converged CuO needed large active spaces of 25 electrons in 14 orbitals. The MCSCF calculations are state averaged over $17, 13, 13, 11$ roots for $^2A_1$, $^2B_1$, $^2B_2$, $^2A_2$ symmetry species, respectively. Subsequent MRCI calculations over all the MCSCF references.

We derive an analytical function for the diatomic potential which is a modified Morse potential. The fit gives an equilibrium distance of 174 pm with a dissociation energy of 19920 $hc\,\mathrm{cm}^{-1}$ for the lowest bounded electronic state in the $^2\Pi$ symmetry species. In contrast to this, the $^2\Sigma^-$ state has an equilibrium distance of 169 pm with a dissociation energy of 6508 $hc\,\mathrm{cm}^{-1}$.

In the lowest electronic state of the $^2A_2$ symmetry species, we find a barrier to the dissociation. We use the method of following the change in permanent dipole moment in this state to get an insight into the nature of the barrier. This analysis shows a change in the direction of the dipole moment before and after the barrier as the internuclear distance approaches the equilibrium distance. This indicates that, there is a change in the major electronic configuration that is responsible for the stable ground state near equilibrium when compared with that of the asymptote. At the asymptote, these are predominantly neutral and near the equilibrium the major configurations are ionic in nature.

We report the spectroscopic values for the lowest electronic states in both $^4B_1$ and $^4A_2$ symmetry species showing much deeper minima than previously reported. The fit gives an equilibrium distance of 175 pm with a dissociation energy of 11193 $hc\,\mathrm{cm}^{-1}$ for the lowest electronic state in the $^4B_1$ symmetry species, while the $^4A_2$ has an equilibrium distance of 171 pm with a dissociation energy of 11632 $hc\,\mathrm{cm}^{-1}$ for its lowest electronic state. Also, we find a barrier in the lowest electronic potential energy functions of both $^4B_1$ and $^4A_2$ symmetry species. Previously, in [94], a barrier in both $^4B_1$ and $^4A_2$ symmetry species were reported, at shorter internuclear distances. We analysed the

barrier with respect to permanent dipole moment changes. To our best estimation, the barrier seems indeed real.

Again in CuO, we report on many excited states of both doublet and quartet symmetry which are non repulsive and the electronic term values of these states. We compare our results with previous reports. Generally, the values reported here are at lower energies.

We report on the lowest electronic states of CuN which are previously not available in the literature. For the MCSCF calculation we optimised the parameters, under $\mathbf{C}_{2v}$, for the 72 state averaged roots calculated ($18 \times {}^3A_1$, $18 \times {}^3B_1$, $18 \times {}^3B_2$, $18 \times {}^3A_2$). These were followed by MRCI calculations on 18 roots from the ${}^3A_2$ symmetry species. The analytical fit on the *ab initio* MRCI data gives an equilibrium distance of 179 pm for the lowest bound electronic state in the ${}^3A_2$ symmetry. The dissociation energy De is 9904 $hc\,\mathrm{cm}^{-1}$ and ω_e is 616 cm^{-1} . The values compare well with previous values from CCSD(T) calculations.

A high barrier in the lowest ${}^3A_2$ potential was found to be artificial.

Therfore, we see from our investigations we can say that,

$$E\left(({}^2D)N + ({}^2\Pi)CuO\right) - E\left(({}^4S)N + ({}^4\Pi)CuO\right) \tag{5.5}$$

$= 19200 - 8800 = 10400\ \mathrm{cm}^{-1}$. This means that, the analytical potential energy surface we use for the lowest singlet CuNO to use for dynamics, we use under the criterion that this is accessible with the Spin-Orbit coupling in the system.

The lowest electronic states of both CuO and CuN are indeed rich and complicated with several avoided crossings. We have reached convergence and found the spectroscopic parameters from this study which can now be used in the analytical fit of the lowest singlet electronic state of the CuNO system.

Chapter 6

Analytical Representation of a Potential Energy Surface

6.1   Introduction

A dynamical study of molecular collision requires a detailed knowledge of the interaction potential as an input. In dynamical calculations, the potential energy surface (PES) should be known in some convenient analytical or numerically interpolated form, which is capable of generating the potential and its derivatives accurately and efficiently at any arbitrary geometry. Research into analytical PES for reactive systems began by adopting some rather complicated functional form where the multitude of parameters are chosen to obtain agreement with *ab initio* energy calculations at selected reference configurations or with energies inferred from experimental data. A famous derived one is the LEPS (Lenard-Eyring-Polanyi) potential surface for H+H_2. However, the construction of such analytical functional form has proved to be difficult as the number of atoms or coordinates increases.

Significant advances have been made over many years in the accurate *ab initio* evaluation of the energy of molecules. Various analytical functions and numerical interpolations depending on a certain number of independent variables have been used for fitting the analytical function to the energy points obtained *ab initio* thereby obtain the analytical representation of the potential energy surfaces.

Further information about the form of the potential energy surface may be obtained from evaluating derivatives of the energy with respect to the nuclear coordinates; derivatives up to second order may be obtained at reasonable computational cost at various levels of *ab initio* theory. A major challenge to date is the development of realistic *global* representations of the potential energy surfaces which can be reasonably well used for both spectroscopic and dynamics studies. This problem has been studied in the scientific literature, it continues to grow in importance as experiments provide increasingly more sophisticated probes of molecules and reactions involving three or more atoms, and as *ab initio* methods become increasingly capable of determining accurate energies for these molecules and reactions.

6.2   Why global analytical PES?

One reason for developing analytical representations of the potential energy surfaces from *ab initio* calculations is that these calculations are sufficiently time consuming that the explicit on-the-fly calculation of energies and energy gradients at every point needed in a dynamics study is rarely feasible. [80]. The potential surface in our consideration is expected to account for bond breaking or forming in gas-phase reactions. Our goal is to describe elastic and inelastic atom-diatom scattering dynamics. Polynomial expansion methods which are useful for representing local regions of potentials like describing vibrational motions close to equilibrium are not totally applicable in our case.

Useful analytical representations that have a global character are of the type of a Morse potential for diatomic systems. A polyatomic analytical representation may be composed of Morse potential-like pair potentials, but this may not be sufficient for the sake of the accuracy of the spectroscopic data. Further development is needed to represent well binding potentials globally.

Unfortunately, developing a global surface is not an easy task and requires *both* good *ab initio* data, flexible as well as robust functional forms. Added to the problem is that we would wish to keep the parameters to a minimum, and also to have a physically sound rationalization of the parameters used.

We have obtained enough data from our *ab initio* calculations to proceed to fit these with an analytical function. Wright and Gray [81] have presented a list of criteria that a successful representation of a potential surface must satisfy [80].

(1) It should accurately characterize the asymptotic reactant and product molecules (or more generally any fragment of the full system)

(2) It should have the correct symmetry properties of the system.

(3) It should represent the true potential accurately in interaction regions for which experimental or nonempirical theoretical data are available.

(4) It should behave in a physically reasonable manner in those parts of the interaction region for which no experimental or theoretical data are available.

(5) It should smoothly connect the asymptotic and interaction region in a physically reasonable way.

(6) The interpolating function and its derivatives should have as simple an algebraic form as possible consistent with the desired goodness of fit.

(7) It should require as small a number of data points as possible to achieve an accurate fit.

(8) It should converge to the true surface as more data become available.

(9) It should indicate where it is most meaningful to compute the data points.

(10) It should have a minimal amount of ad hoc or "patched up" character.

These criteria should be met with in a reasonable accuracy if one has to do dynamics calculations on the analytical potential. The accuracy of the PES improves with an increased number of *ab initio* data points. A number of rather different methods have been developed and are still in common use for representing surfaces including spline fitting methods, methods in which semi-empirical potential surfaces are either fitted or corrected in order to match data from *ab initio* calculations or experiment, empirical

fits based on many-body expansions, and global surfaces that are defined using information determined along a reaction path. A new global analytical representation of the electronic potential energy surface might use one or more of these.

6.3   Analytical representation

Our strategy is to first derive analytical forms that give a correct representation of the topography of the lowest adiabatic PES. In a second step, parameters might be adjusted to *ab initio* data, to improve quantitatively the PES. Marquardt et al. have derived such forms [85, 87] of the potentials which are a) *global*, allowing for a representation of a potential energy hypersurface that is analytical in the complete configuration space, including all possible reaction channels in a given energy range. b) *flexible* as PES representations are obtained from an adjustment of parameters to data from electronic structure calculations, and the accuracy of the representation is related to the accuracy of the *ab initio* calculations in the first place. c) *compact* which means flexible enough, but with few parameters d) *robust* which implies small variations of parameter values should lead to small qualitative variations of a robust PES representation. Robust analytical forms are also important to ensure a physically correct behavior in regions of configuration space that are not well-sampled by data from electronic structure calculations.

In the same spirit, we aim at the derivation of a global analytical model potential for a triatomic system, ABC. For the determination of model parameters, we consider an adjustment procedure, fitting the model potential to a sufficiently large set of high level *ab initio* energy points on the potential surface the quality of the *ab initio* calculations being at least comparable to multi-reference configuration interaction (MRCI) methods, for large displacements from equilibrium, in order to account for changes of the character of the electronic wave function during a chemical reaction.

Throughout this chapter, we consider only the potential surface belonging to the lowest electronic state of CuNO which is of singlet A$'$ symmetry species.

The total potential energy surface for the CuNO system (or any triatomic) can be given as a sum:

$$V = \sum_{i=1}^{3} V_{2bi} + V_{3b} \tag{6.1}$$

where V_{2b} are the two-body terms. V_{3b}, the three-body term, is a bending potential. It will be a function of the bond angles, to a large extent, and will have a somewhat weaker dependence on the bond lengths. Thus all terms will contribute to the stretching potential of CuNO close to equilibrium. The present representation is built up of global forms.

6.3.1 Two-body term

$$V_{2b} = V_e(Y - 2(\cos\omega))Y + V_0 + (V_I - V_0)\exp^{-\left(\frac{r_6}{r}\right)^6} \tag{6.2}$$

where

$$Y = e^{-A(r-r_e)} \tag{6.3}$$

$$A = A_s\left(1 - b_s \arctan\left(\left(\frac{r_s}{r_i}\right)^2 - 2\left(\frac{r_s}{r_i}\right)\right)\right) \tag{6.4}$$

This is a modified Morse potential to describe the bond-stretching potential functions. This allows for a more flexible description of the anharmonicity of the stretching potential. In Eq. (6.2) whenever $0° < \omega < 90°$, there will be a well defined potential and the parameter r_e can be interpreted as equilibrium bond length of the 'diatomic' potential. V_I and A_s are asymptotic values of V, A respectively.

The $\exp^{-\left(\frac{r_6}{r}\right)^6}$ factor "switches" the last energy term from V_0 at $r \approx r_e$ to V_I for $r \to \infty$. If $b_s = 0$, then the anharmonicity term A is constant and the potential function reduces to conventional Morse potential (with $V_I = V_0$). Otherwise it is a function of r, which may vanish or even become negative giving rise to additional local maxima.

6.3.2 Three-body term

The three body term is essentially a bending potential. In contrast to bond-stretching potentials, there is no simple, compact analytical form that can be used to describe the

anharmonicity of bending potentials. The three body term here can be seen as a product of a function depending on θ and two damping terms y_1 and y_2

$$V_{3b} = V_b y_1 y_2 (y_1 y_2 - 2z) \tag{6.5}$$

$$y_i = e^{-a_r(r_i - r_{ei})} \tag{6.6}$$

$$z = -z_1 z_2 z_3 \tag{6.7}$$

$$z_i = b_i - e^{-a_i(\cos\theta - \cos\theta_e)(1 + c_i(\cos\theta - \cos\theta_e))} \tag{6.8}$$

Here, $r_1 = r_{\mathrm{Cu}}, r_2 = r_{\mathrm{NO}}$

We impose the following conditions on V_{3b}. V_{3b} will get a value $-V_b$ in the global minimum, which is at the equilibrium angle θ_e; and $V_{3b} \to 0$ when r_1 and r_2 goes to infinity. $z = 1$ can be obtained when $\cos\theta - \cos\theta_e = 0$. We can change the variable $\cos\theta - \cos\theta_e = x$, then

$$z(x = 0) = 1 \qquad \Leftrightarrow \qquad b_3 = \frac{-1}{(b_1 - 1)(b_2 - 1)} + 1 \tag{6.9}$$

$$\frac{\mathrm{d}z}{\mathrm{d}x}(x = 0) = 0 \Leftrightarrow a_3 = \frac{(b_1 - 1)a_2 + (b_2 - 1)a_1}{((b_1 - 1)(b_2 - 1))^2} \tag{6.10}$$

6.3.3   Switching functions

One requirement made to global model potentials is that all dissociation channels need to be described in a correct way within the same analytical representation for single or multiple valued potential surfaces. This implies conditions both on the symmetry aspects of the representations and adequate variation of parameter values for the different dissociation channels.

In order to achieve this goal, we use the switching functions.

$$S_{\mathrm{p}}(r) = e^{-\left(\frac{R_{sw}}{R}\right)^6} \tag{6.11}$$

where R_{sw} is an adjustable parameter. These functions are smoothly varying $S_p(r) \to 1$ for $r \to \infty$ and

$S_p(r) \geq 0$ for $R_{sw} \gg r_e$.

Any parameter p is then considered as a smoothly varying function between its value p_0 attained in the bound ABC systems and its value p_i attained in a dissociation channel. For instance, a parameter V_e in the two-body potential term is related to the AB fragment will be called $VEAB - 0$, when this term is used to construct the potential of the ABC complex, and $VEAB - i$, when atom C is dissociated from the complex. Hence V_e will be effectively given by

$$V_e (r_{AC}, r_{BC}) = VEAB - 0 \left(1 - S_p(r_{AC})S_p(r_{BC})\right) + VEAB - i \left(S_p(r_{AC})S_p(r_{BC})\right) \quad (6.12)$$

The potentials in the V_{3b} are not switched. R_{sw} may be interpreted as the limiting value of the dissociating bond lengths for A-BC or AB-C or B-CA after which the analytical representation describes the potential basically with just the two-body terms. The functions introduced here have the advantage of being really logical switching functions. We may use different R_{sw} parameters for different bonds.

6.4 Global potential fit

The analytical forms described above were adjusted to the *ab initio* data calculated as described in Chapter 4 within a modified version of the Levenberg-Marquardt algorithm that allows us to consider further analytical relations between adjustable parameters during the fitting procedure by introduction of Lagrange multipliers. The fit procedure was such that we obtain systematically improved accuracy in the global fit while reducing the number of effectively adjusted parameters. We give below the results obtained from a fit of the analytical potential over 530 *ab intio* data points from the MRCI calculation (RVTZ basis, $(18, 11)$ CAS, non-relativistic). We fit 19 parameters. Here, the V_2b for NO was allowed to vary, specifically the AS, RE and BS parameters.

The representation from the present work describes the lowest adiabatic electronic state rather accurately. Given below are the parameters used in the global analytic representation and the fitted values. A total of 19 fitted parameters are there. Some parameters are fixed at reasonable values. Other parameters, such as those for the isolated diatomic molecules were fitted to separate energy data points described in chapter 5. Here are some definitions: The atoms here are defined in the indices ABC where A = Nitrogen, B= Oxygen, and C= Copper The parameter names contain hence atom indices AB, BC, AC. Here the definitions are given more clearly.

$$
\begin{aligned}
\text{VEAB-i} &= \text{Ve} \ / \ hc\,\text{cm}^{-1} \ \text{ for the isolated NO} \\
\text{VEAB-0} &= \text{Ve} \ / \ hc\,\text{cm}^{-1} \ \text{ for NO in CuNO} \\
\text{REAB-0} &= r_\text{e} \ / \ \mathring{A} \ \text{for NO in CuNO} \\
\text{REAB-i} &= r_\text{e} \ / \ \mathring{A} \ \text{for the isolated NO} \\
\text{R6AB-0} &= r_6 \ / \ \mathring{A} \ \text{for NO in CuNO} \\
\text{R6AB-i} &= r_6 \ / \ \mathring{A} \ \text{for the isolated NO} \\
\text{RSAB-0} &= r_\text{S} \ / \ \mathring{A} \ \text{for NO in CuNO} \\
\text{RSAB-i} &= r_\text{s} \ / \ \mathring{A} \ \text{for the isolated NO} \\
\text{OMAB-0} &= \omega \ \text{angle for NO in CuNO}
\end{aligned}
$$

TABLE 6.1: Definition of two body parameters. All these parameters have same counterparts with BC, and AC.

In Table 6.2, the fit values of the two-body parameters are listed.

The three body potential has the following parameters:

The A3B, B3B,and C3B are dimensionless parameters used in Eq. (6.8) satisfying the conditions Eq. (6.10). There parameters were either found by free adjustment or, where appropriate, the value 0.0 was set. A flag in the table indicates parameters was fixed (0) or floated (1) in the fit. The values for the three-body parameters are:

The analytical potential with the above fitted parameters for the lowest singlet A′ PES will henceforth be called as CuNO-SAsp-01.

6.5   Discussion of the fit quality of CuNO-SAsp-01

In this section, we show typical cuts of the potential. This gives an idea of the quality of the potential function and its general shape.

parameter	value	flag	parameter	value	flag	parameter	value	flag
VEAB-0	52289.60	0	VEAC-0	111849.6	1	VEBC-0	184.2142	1
ASAB-0	6.995740	1	ASAC-0	2.114468	1	ASBC-0	3.864210	1
REAB-0	1.123340	1	REAC-0	0.2831354	1	REBC-0	2.000000	0
OMAB-0	0.000000	0	OMAC-0	0.000000	0	OMBC-0	90.00000	0
BSAB-0	0.5344114	1	BSAC-0	0.000000	0	BSBC-0	0.000000	0
RSAB-0	3.457926	0	RSAC-0	3.000000	0	RSBC-0	3.000000	0
V0AB-0	52806.00	0	V0AC-0	0.000000	0	V0BC-0	0.000000	0
VIAB-0	52864.00	0	VIAC-0	0.000000	0	VIBC-0	0.000000	0
R6AB-0	3.000000	0	R6AC-0	3.000000	0	R6BC-0	3.000000	0
VEAB-i	52289.60	0	VEAC-i	52857.76	0	VEBC-i	14151.49	0
ASAB-i	3.248656	0	ASAC-i	0.8733449	0	ASBC-i	4.150190	0
REAB-i	1.154746	0	REAC-i	1.807099	0	REBC-i	1.742564	0
OMAB-i	0.000000	0	OMAC-i	0.000000	0	OMBC-i	0.000000	0
BSAB-i	0.1188810	0	BSAC-i	2.147600	0	BSBC-i	0.2945370	0
RSAB-i	3.457926	0	RSAC-i	0.9649600E-01	0	RSBC-i	5.457254	0
V0AB-i	52806.00	0	V0AC-i	43013.32	0	V0BC-i	993.5195	0
VIAB-i	52864.00	0	VIAC-i	0.000000	0	VIBC-i	-32.49560	0
R6AB-i	3.000000	0	R6AC-i	3.270614	0	R6BC-i	2.756670	0
RSWAB	3.000000	0	RSWAC	3.000000	0	RSWBC	3.000000	0

TABLE 6.2: Values of two body parameters from the fit

$$\text{VB} = V_b \ /hc\,\text{cm}^{-1}$$
$$\text{THETE} = \theta_e \ /\text{deg}$$
$$\text{RPE} = r_{\text{Cu}} \ /100 \ \text{pm at equilibrium}$$
$$\text{RQE} = r_{\text{NO}} \ /100 \ \text{pm at equilibrium}$$

TABLE 6.3: Definition of three-body parameters

Here the potential is shown with the MRCI data along two different rays along different θ angles of 130° and 0°. The x-axis is the r_{Cu} distance up to the asymptote. The potential reproduces the completely different dissociation behaviour at these angles. At $\theta_{\text{Cu}} = 130°$, there is a well and at the $\theta_{\text{Cu}} = 0°$, this is a completely repulsive potential in the ground electronic state.

Here the potential is shown with the MRCI data along two different rays along different r_{Cu} distances of 250 pm and 450 pm. The x-axis is the θ_{Cu} angle. The analytical potential correctly reproduces the minimum structure from the MRCI data. And at the asymptote, it does not matter where the Cu is; the potential has to essentially the same energy value; here we define asymptotic energy as 0.

parameter	value	flag
VB	196.0899	1
THETE	128.9022	1
A3B-1	4.402112	1
A3B-2	-1.518012	1
B3B-1	2.000132	1
B3B-2	1.999629	1
C3B-1	0.000000	0
C3B-2	1.567849	1
C3B-3	1.078323	1
D3B	0.1000000	0
ADPO	0.4729284	1
RPE	3.336835	1
RQE	1.150000	0
XH	0.2000000	0
GV0	530.960	1

TABLE 6.4: Values of three-body parameters from the fit
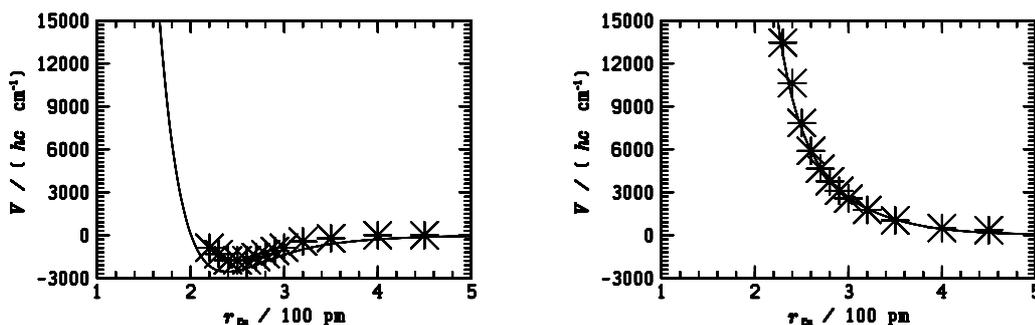
FIGURE 6.1: 1-D cuts of the analytical potential showing the variation with r_{Cu} distances with $\theta_{\text{Cu}} = 130°$ and $\theta_{\text{Cu}} = 0°$; $r_{\text{NO}} = 115$ pm. The crosses indicate the energy points calculated *ab initio* (non-relativistic MRCI, RVTZ basis and $(18, 11)$ CAS).

A 2-D cut of the potential is shown below, in the plane of the molecule (say the yz plane at fixed NO bond length.

The r_{NO} distance is 115 pm. The contours has the $V_{\text{min}} = -2000hc\,\text{cm}^{-1}$, $V_{\text{max}} = 7500hc\,\text{cm}^{-1}$, $\Delta V = 500hc\,\text{cm}^{-1}$. The root mean square is large (1774), but analytical representation grasps the general behaviour of the energy points correctly, hence one is satisfied. Global fits hardly do better.

Figure 6.4 shows a 2D cut of the SAsp-01 PES along the $r_{(\text{CuN})}$ and $r_{(\text{NO})}$ distances. (Here, it is not the r_{Cu} coordinate that is being used) at a Cu-N-O angle of 120° (this is
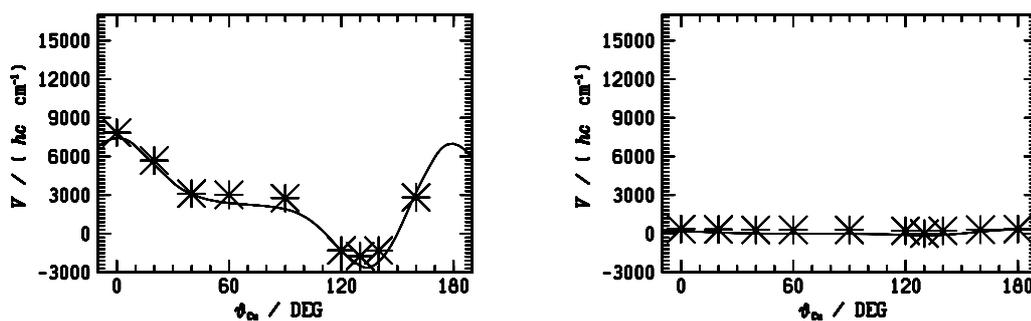
FIGURE 6.2: 1-D cuts of the analytical potential showing variation with θ_{Cu} angles with $r_{Cu} = 250$ pm and $r_{Cu} = 450; r_{NO} = 115$ pm. The crosses indicate the energy points calculated *ab initio* (non-relativistic MRCI, RVTZ basis and $(18, 11)$ CAS).
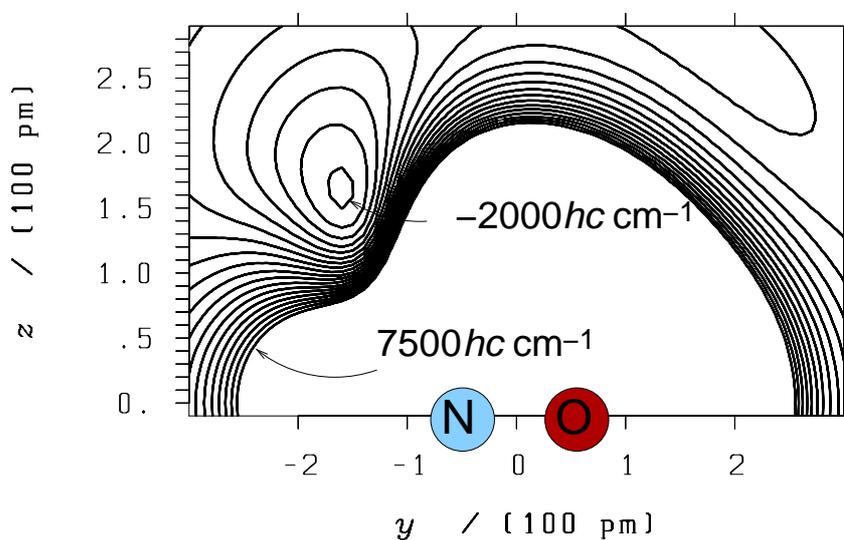
FIGURE 6.3: 2-D cut of the analytical potential showing variation with different r_{Cu} distances and θ_{Cu} angles with $r_{NO} = 115$ pm

close to the equilibrium angle). The plot shows the equilibrium geometry of the CuNO complex at small values of $r_{(CuN)}$ and $r_{(NO)}$, and the two dissociation channels CuNO $\rightarrow$ CuN + O (when $r_{(NO)} \rightarrow \infty$) and CuNO $r_{(CuN)} \rightarrow$ Cu + NO (reference energy, when $r_{(CuN)} \rightarrow \infty$). The estimation for the energy barrier is at ≈ 47750 cm^{-1} above the Cu + NO dissociation channel (the value of the outer contour line shown in the plot).
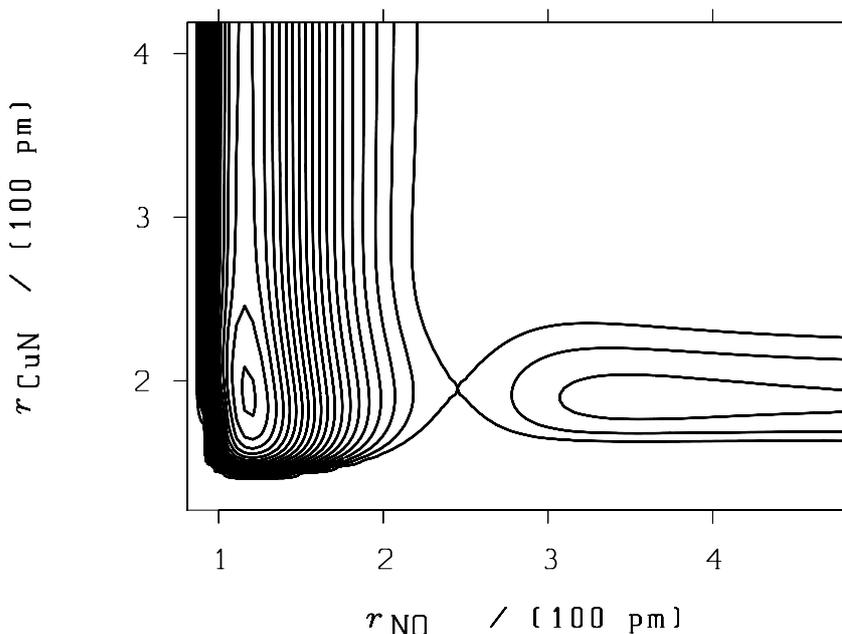
FIGURE 6.4: 2-D cut of the analytical potential showing variation along $r_{(CuN)}$ and $r_{(NO)}$ distances

6.6   Vibrational fundamentals from CuNO-SAsp-01

The analytical potential is used to obtain the vibrational fundamentals from a home made variational programme. This programme uses Jacobi coordinates and a 3D DVR of the Hamiltonian, which we address in the next chapter. The formula used in this programme were derived from [107] and the programme was successfully tested before on other well known triatomic molecular systems. The theoretical values of vibrational fundamentals can then be compared to experiment and ones we also calculate from a quadratic force field that was adjusted to a restricted data set around the equilibrium from the best CCSD(T) results including relativistic effects. This adjustment was performed similarly to the adjustment of the quadratic force field given in Table 4.10 From the analysis of the vibrational eigenfunctions, we assign clearly ν_1 to the NO stretching mode, ν_2 to the Cu-NO bending, and ν_3 to the Cu-NO stretching mode. This assignment is at variance with the [cite] where ν_2 was attributed to the Cu-NO stretching mode and ν_3 to the bending mode

We see that the results for the vibrational fundamentals from the MRCI potential are quite different to the experimental values. The values from the coupled cluster force

	Exp[a]	MRCI [b]	CCSD(T) [c]
ν_3 / cm^{-1}	278.23	159	254
ν_2 / cm^{-1}	452.60	503	412
ν_1 / cm^{-1}	1587.37	1542	1592

TABLE 6.5: Vibrational fundamentals from the CuNO-SAsp-01 compared with experimental values.
[a][8] [b] CuNO-SAsp-01; [c] anharmonic quadratic forcefield.

field are definitely much closer to experiment. The better agreement can be related to deeper potential well in the coupled cluster calculations including relativistic effects. One should note that the experiments were conducted in an argon matrix. It is difficult to judge about the relevance of the deviation from experiment in this case, since theory applies to the isolated molecule in the gas phase. We think that the shift is still too far from the potential fitted purely on the MRCI data.

Therefore an ideal PES should be the result of a merging of the coupled cluster data around equilibrium and the MRCI data at other geometries including dissociation. This should be done carefully, possibly including a proper scaling of the values, both energetic and geometric. As of now, we are developing a new analytical potential, with merged data, following the ideas presented elsewhere [83, 84, 85, 86]. Preliminary results show a definite improvement in the vibrational fundamentals of the global analytical representation.

As of now, the global analytical representation derived so far is good enough to do preliminary scattering dynamics calculations explained in the following chapters. From the analytical representation we could also find that the barrier to dissociation of NO with Cu is $\approx 47750 \ hc\,\mathrm{cm}^{-1}$. The D_e of NO alone is $52348 \ hc\,\mathrm{cm}^{-1}$ [82].

Chapter 7

Time-dependent wave packet study of Cu + NO scattering

7.1   Time dependent wave packet approach

The dynamical behavior of the state of an isolated quantum-mechanical system is described by the Schrödinger equation,

$$i\hbar\frac{\partial}{\partial t}\Psi(t) = \hat{H}\Psi(t) \qquad (7.1)$$

The main advantage of time-dependent wave packet calculation is such that the solution of the time-dependent Schrödinger equation is completely determined by specifying an initial wave packet and propagating it in time and thus providing an intuitive picture of the development of the dynamics. The integration over an infinitesimal time step $\mathrm{d}t$ yields an expression relating the wave function at time t to that for an infinitesimally later time $t+\mathrm{d}t$:

$$\Psi(t + \mathrm{dt}) = \Psi(\mathrm{t}) - \frac{\mathrm{i}}{\hbar}\hat{\mathrm{H}}\mathrm{dt}\Psi(\mathrm{t}) = \left(1 - \frac{\mathrm{i}}{\hbar}\hat{\mathrm{H}}\mathrm{dt}\right)\Psi(\mathrm{t}). \qquad (7.2)$$

The expression in parentheses is evidently an operator which propagates the wave function in time by an infinitesimally small amount $\mathrm{d}t$. If the Hamiltonian is time-independent, then successive infinitesimal propagations can be compounded to form an

operator that effects an arbitrary finite time difference

$$\hat{U}(t) = \lim_{N \to \infty} \left(1 - \frac{i}{\hbar} \hat{H} \frac{t}{N} \right)^N = \exp \left(-\frac{i\hat{H}t}{\hbar} \right). \tag{7.3}$$

The operator $\hat{U}$ is commonly referred to as the time-evolution operator (sometimes the term *propagator* is also used). When applied to an initial wave function, it traces out the dynamical evolution of that state in time

$$\Psi(t) = \hat{U}(t - t_0)\Psi(t_0). \tag{7.4}$$

Since $\hat{H}$ is hermitian, $\hat{U}$ is unitary, i.e. $\hat{U}^\dagger \hat{U} = \hat{U}\hat{U}^\dagger = 1$. This is important because it means time evolution conserves probability. Another property, which is easy to verify by inspection, is that $\hat{U}(-t) = \hat{U}^\dagger(t) = \hat{U}(t)$.

In principle, the time-evolution operator enables us to determine the exact wave function at any point in time from a given set of initial conditions. However, the form expressed in equation Eq. (7.3) is not immediately useful for numerical application. This can be accomplished by representing the operator in an orthonormal basis. Since, in practice, the number of components in the decomposition will be finite, the basis in question will not be complete, but even an incomplete basis should yield acceptable results for some class of "well-behaved" functions.

The eigenfunctions of $\hat{H}$ form a basis that is particularly easy to work with when calculating the propagator Let ϕ_n be an eigenfunction of the Hamiltonian with the eigenvalue E_n. Then ϕ_n will also be an eigenfunction of $\hat{U}$, propagating as

$$\phi_\mathrm{n}(t) = \hat{U}(t)\phi_\mathrm{n}(0) = \exp(-iE_n t/\hbar)\phi_\mathrm{n}(0) \tag{7.5}$$

The eigenfunctions of $\hat{H}$ correspond to stationary states, changing only by an overall phase under time evolution. The decomposition of the time dependent wave function for any time t in terms of this basis , also called state vector, is thus trivially related to the decomposition at $t = 0$. Finding the eigenfunctions of $\hat{H}$ for a general Hamiltonian is, of course, much harder, but can be done numerically. For a basis other than that of the eigenfunctions of $\hat{H}$, treating the exponential in equation Eq. (7.3) directly as a

series sum is generally impractical for numeric calculations, due to the computational costs of applying $\hat{H}^n$.

The successful development and application of various computational schemes in the past two decades, coupled with the development of fast digital computers, has significantly improved the numerical efficiency for practical applications of the time dependent methods to chemical dynamics problems.

7.2   Numerical implementation

By representing the wave functions as sums of products of basis functions, and then diagonalising a Hamiltonian matrix which couples the basis functions together, solutions can be found. The method of using orthogonal basis functions to represent a wave function is normally referred to as a finite basis representation (FBR). For strict variational behaviour the integration of the potential and basis functions must be exact. If the potential is very complicated analytic integration may not be possible and some kind of quadrature is employed. Finite basis methods have had much success in calculating energies in many different types of problems. However one limitation with the approach is that only the ground state and about the lowest 5 % of the eigenvalues obtained are well converged [117, 118].

By transforming the basis function so that the wave functions are now represented as amplitudes at points, one can approach the problems slightly differently. This method is known as the discrete variable representation method (DVR), and allows the truncation of the wave function in regions where it will have no magnitude because the potential is very high, and hence reduces the overall size of the problem. This therefore also allows for a better representation of high energy wave functions [119, 120]. The Discrete Variable Representation is a very general and is applied to one-dimensional problems or direct product basis functions in multidimensional problems. To state it simply, DVR is a localized (in coordinate space) but discrete representation. For any given finite basis set

$\psi_n(x)(n = 1, ..., N)$ one can define a unique DVR by diagonalizing the matrix

$$x_{\mathrm{mn}} = \langle \phi_{\mathrm{m}} | \hat{x} | \phi_{\mathrm{n}} \rangle \tag{7.6}$$

which generates N eigenvalues x_{n} and and eigenfunctions

$$X_{\mathrm{n}} = \sum_{m} \phi_m C_{\mathrm{mn}} \tag{7.7}$$

such that $\hat{x} X_{\mathrm{n}} = x_{\mathrm{n}} X_{\mathrm{n}}$

Eq. (7.7) implies that in this N-dimensional vector space, the coordinate operator $\hat{x}$ is approximated by

$$\hat{x} \;=\; \sum_{n=1}^{N} X_{\mathrm{n}} \delta X - X_{\mathrm{n}} \tag{7.8}$$

With this prescription for the operator $\hat{x}$, X_{n} is also an eigenstate of any operator function $F(\hat{x})$

$$F(\hat{x}) X_{\mathrm{n}} = F(x_{\mathrm{n}}) X_{\mathrm{n}} \tag{7.9}$$

Since the DVR basis set $\{X_n | n = 1, 2, \ldots, N\}$ is related to the finite basis set $\{\phi_n(x) | n = 1, 2, \ldots, N\}$ through a unitary or orthogonal transformation, both basis sets are equivalent in this N-dimensional vector space. The DVR basis function are highly localized in coordinate space, i.e., $X_n(x)$ is highly peaked near $x = x_n$ Due to this particular local property of the DVR basis, the matrix element of any local operator in the DVR basis is approximately diagonal. This result applies to any local operator which is a function of coordinates only, and should be understood in the sense that the coordinate operator is approximated. As the size of the basis increases, the approximation becomes better and better. Since most potential energy operators are local functions of coordinates, they are diagonal in the DVR representation, and the integration over the coordinates to construct the potential matrix can be eliminated.

One drawback of the DVR method is that it is not strictly variational since the integration leading to matrix elements may not be exact. The truncation stage must also

be carefully performed since there may be need to introduce many basis functions, ie DVR points, then truncate the problem to a manageable size. This can increase the inaccuracy of the representation since some regions of the potential will be ignored in the truncation. The corresponding energies can then be unreliable and wrongly converged.

7.3 The multiconfiguration time-dependent Hartree (MCTDH) method

The Hiedelberg multiconfiguration time-dependent Hartree (MCTDH) is a computer program capable of treating multi-dimensional, non-adiabatic systems in which the vibrational modes and surfaces are strongly coupled [108, 110]. In standard propagation methods, in which the wave packet and Hamiltonian are represented in a time-independent product basis, the calculation rapidly becomes computationally impossible as the number of degrees of freedom (DOF) increases. The key ingredient of the MCTDH scheme is to use a multiconfigurational ansatz for the wave function, with each configuration being expressed as a Hartree product of time-dependent basis functions for each dimension, known as single single particle functions (SPF).

The MCTDH wave function ansatz to solve the time-dependent Schrödinger equation is written as

$$\Psi(Q_1,...,Q_f,t) = \sum_{j=1}^{n_1} ... \sum_{j_f=1}^{n_f} A_{j_1...j_f}(t) \prod_{k=1}^{f} \phi_{j_k}^k(Q_k,t) \qquad (7.10)$$

where $Q_1,...Q_f$ are typically the nuclear coordinates, f is the number of degrees of freedom and the $A_{j_1...j_f}$ denote the MCTDH expansion coefficients; the $\phi_{j_k}^k$ are the single particle functions, n_k for k can be considered $(j_1...j_k)$. For f degrees of freedom there are $n_1,...,n_k$ SPF and these SPF are represented by $N_1,...,N_f$ primitive basis functions or DVR grid points χ_e^k.

Setting $n_1 = ... = n_f = 1$ one arrives at the time dependent Hartree wave function (TDH). TDH is thus contained in MCTDH as a limiting case. As the numbers n_k are increased, the more accurate the propagation of the wave function becomes, and the MCTDH wave function monotonically converges towards the numerically exact one as

n_k approaches N_k, where N_k is the number of primitive basis functions along coordinate k. The computational labour, however, increases strongly with increasing values of n_k.

The equations of motion for the expansion coefficients A_j and SPF $\phi_{j_k}^k$ have been derived using the Dirac-Frankel variational principle. The resulting equations of motion are coupled non-linear differential equations for the coefficients and the SPFs. The efficiency of the MCTDH algorithm grows with increasing f. The use of the variational principle ensures that the SPF evolve so as to optimally describe the true wave packet; i.e., the time-dependent basis moves with the wave packet. This provides the efficiency of the method by keeping the basis optimally small at each time step.

The populations of the natural orbitals, which are defined as the eigenvalues of the density matrix operator in each degree of freedom , reflect the degree of convergence of the wave function with respect to the size of the time-dependent basis set. In particular, a small value of the lowest natural orbital population indicates that enough SPF have been used for the single particle to achieve convergence. We mention that the accuracy of a MCTDH calculation depends on both the size of the primitive and the SPF bases. The populations of the limiting primitive basis functions, e.g. the limiting grid points is used to check that enough primitive basis functions have been used for the calculation.

The MCTDH approach is now capable of providing fully converged integral cross-section for atom-diatom reactions, state-to-state reaction probabilities for total angular momentum $J = 0$ and higher and state-to-state integral cross-sections, as well as accurate cumulative reaction probabilities and thermal rate constants. We apply this method here to study the Cu+NO scattering.

7.4   Refitting the PES

To solve the equations of motion requires the evaluation of the $\langle \Phi_J | | H | \Phi_L \rangle$ matrix and the $\langle H \rangle$ mean-fields at each time step of the integration. These f and $(f-1)$ dimensional integrals is circumvented if the Hamiltonian is written as a sum of products of single-particle operators

$$\hat{H} = \sum_{r=1}^{s} C_r \prod_{k=1}^{f} \hat{h}_r^{(k)} \tag{7.11}$$

where $\hat{h}_r^{(k)}$ operates only on the kth coordinate and C_r is an expansion coefficient. Hence, both the kinetic and potential energy operators need to be expressed in the product structure. The kinetic energy operator (KEO) usually has the required form if appropriate coordinate are chosen, but this is not the case for the potential energy operator in the general case,and the potential energy expression as obtained from our analytical representation depend on all DOF.

The (POTFIT) program is available to fit the potential to the desired product form. This method is based on the approximation theorem of Schmidt which defines an efficient scheme to generate a product representation of a given multidimensional function [111]. When the PES may be given on a product grid

$$V^{app}(q_1, ..., q_f) = \sum_{j_1=1}^{m_1} ... \sum_{j_f=1}^{m_f} C_{j_1,...,j_f} V_{j_1}^{(1)}(q_1)....V_{j_f}^{(f)}(q_f) \tag{7.12}$$

As we use DVRs we need to know the potential only at the grid points. Let $(q_i)^{(k)}$ denote the position of the ith grid point of the kth grid. Then we define

$$V_{i_1,...,i_f} = V\left(q_{i_1}^{(1)}, ..., q_{i_f}^{(f)}\right) \tag{7.13}$$

that is, $V_{i_1,...,i_f}$ denotes the value of the potential on the grid points. The approximate potential on the grid is given by

$$V_{i_1,...,i_f}^{app} = \sum_{j_1=1}^{m_1} ... \sum_{j_f=1}^{m_f} C_{j_1...j_f} V_{i_1 j_1}^{(1)} \ldots V_{i_f j_f}^{(f)} \tag{7.14}$$

where $V_{i_k j_k}^{(k)} = V_{j_k}^{(k)}(q_{i_k})^{(k)}$

and the single particle potentials (SPP) are assumed to be orthogonal on the grid. If the expansion orders and the number of grid points are equal, the approximated and the exact potential are identical. Not all regions of the PES are equally relevant for the dynamics. It is possible to define a relevant zone for the POTFIT procedure where the natural potentials are iteratively improved by a multidimensional iteration procedure. The potential fit accuracy is finally checked by the calculation of the root mean square error between V^app and V.

7.5 Convergence issues

	Natural potentials
r_{d}	contr
r_{v}	20
θ	30
	Relevent Region
V	¡80000 cm^{-1}
r_{d}	1000 pm
r_{v}	500 pm
RMS error on relevant grid points (meV)	2.03
RMS error on all grid points (meV)	4.36

TABLE 7.1: POTFIT parameters. "contr" indicates that the contraction technique is used.

In Table 7.2, the values of the converged POTFIT calculation are given. The RMS error on relevant region of grid points of the potential which will be used for scattering calculations, is good. We used sin DVR grids with 174 points for the collision coordinate R, which extends from 5 pm to 1000 pm for primitive basis. For our diatomic r coordinate, a Harmonic Oscillator grid with 24 functions centered around 1.155, which is the equilibrium NO distance, was used. For the angles, the primitive were Legendre DVR with 60 grid points. The number of SPF used for the R, r and θ DOF are 22, 9 and 22 respectively.

7.6 The Hamiltonian operator

An exact treatment of atom-diatom scattering requires three coordinates, one must choose not only internal coordinates, to describe the shape of the molecule, but also define a molecule-fixed axis system (that rotates with the molecule). Geometrically defined internal coordinates have the advantage that each point in configuration space is described by single valued set of coordinates. Of the $3N$ coordinates required to specify the configuration of the N nuclei of a non linear N-atom molecule, $3N - 6$ coordinates describe its shape [109]. Because basis functions are usually chosen as functions of the coordinates in terms of which the kinetic energy operator is written, choosing coordinates influences the quality of the basis functions. It is advantageous to choose coordinates to minimize coupling and therefore facilitate choosing good basis functions.

Using the Jacobi coordinates (R, r, θ) in the body-fixed (rotating) frame, the nuclear Hamiltonian operator for a triatomic molecule is expressed as:[107]

$$H(R, r, \theta) = T_R + T_r + T_\theta + V(R, r, \theta) + \frac{J(J+1) - 2K^2}{2\mu_R R^2} - \frac{C_{J,K}^+}{2\mu_R R^2}\hat{j}^+ - \frac{C_{J,K}^-}{2\mu_R R^2}\hat{j}^- \quad (7.15)$$

where

$$
\begin{aligned}
T_R &= \frac{-1}{2\mu_R}\frac{\partial^2}{\partial R^2} \qquad\qquad (7.16)\\
T_r &= \frac{-1}{2\mu_r}\frac{\partial^2}{\partial r^2}\\
T_\theta &= \left(\frac{1}{2\mu_R R^2} + \frac{1}{2\mu_r r^2}\right)\hat{j}^2\\
\hat{j}^2 &= \frac{-1}{\sin\theta}\frac{\partial}{\partial\theta}\sin\theta\frac{\partial}{\partial\theta} - \frac{K^2}{\sin\theta}\\
\hat{j}^\pm &= \pm\frac{\partial}{\partial\theta} - K\cot\theta\\
C_{J,K}^\pm &= \sqrt{J(J+1) - K(K\pm 1)}
\end{aligned}
$$

μ_R is the reduced mass of Cu-NO ;μ_r is the reduced mass of NO; V is the electronic potential energy, J the total angular momentum quantum number and K is the projection of the total angular momentum quantum number on to the body fixed z axis. K is also called the helicity angular momentum quantum number. The total angular momentum and its projection on the body fixed axis may be expressed in terms of the three Euler angles, (α, β, γ), which define the orientation of the body-fixed axes (x, y, z) with respect to the space-fixed (non-rotating) axes (X, Y, Z). J is a conserved quantity, hence its representation in those coordinates is trivial when rigid rotor eigen functions are used. Similarly, we obtain K knowing that $|K| \leq J$. Note that $\hat{j}^\pm$ acts as a differential operator on θ but as a shift operator on K. Ignoring the last two terms in the equation Eq. (7.15) of the triatomic system gives rise to the centrifugal sudden (CS) approximation. For $J > 0$, care must be taken while using the CS approximation in situations where coriolis coupling becomes important. In the calculations reported here, we always use the exact Hamiltonian.

7.7   Preparation of the Initial Wave packet

The initial wave packet is prepared as direct products. We use a Gaussian function along coordinate R,

$$\psi(R) = \frac{1}{\sqrt{2\pi d}} \exp^{-\left(\frac{R-R_0}{2d}\right)^2} \exp^{(ip_0(R-R_0))}. \tag{7.17}$$

with R_0, p_0 and d denoting its centre in coordinate space, centre in momentum space and the width, respectively.

For angular coordinates, associated Legendre functions are our appropriate choice.

$$\tilde{P}_l^m(\cos\theta) = \sqrt{\frac{2l+1}{2}\frac{(l-m)!}{(l+m)!}} P_l^m(\cos\theta) \tag{7.18}$$

with $0 \leq m \leq l$. The parameter m denotes the magnetic quantum number and is treated as a fixed parameter. P_l^m is the standard associated lengendre function and $\tilde{P}_l^m$ is the normalized form of it.

For the diatomic vibrational coordinate r, we use eigenfunctions of the 1D Hamiltonian with diatom potential as our initial SPFs.

At the end of the grid in the r_{Cu}, the wave packet is absorbed by a complex absorbing potential (CAP). Also, to compute the reaction attributes, the matrix elements of the flux operator (see below) are evaluated by matrix elements of a second CAP positioned at the dividing surface.

R_0	600 pm	center of initial Gaussian wave packet along r_{d}
p_0	$-9.0\frac{\hbar}{a_0}$	initial momentum
d	1.32 pm	Width parameter of Gaussian wave packet
$mass_r d$	20.3143 atomic mass unit	reduced atom-diatom mass
$mass_r v$	7.4667 atomic mass unit	reduced diatom mass
x_i/x_f (Sin DVR)	5 / 1000 pm	Translational coordinate Grid
ΔR	0.183 pm	Grid spacing
T_{prop}	1200 fs	propagation time
ΔT	1.0 fs	interval at which wave packet is written to file
η_R	3×10^{-4}	CAP strength parameter
R_c	900 pm	Starting point of CAP

TABLE 7.2: Numerical parameters of the MCTDH calculation if not otherwise stated.

7.8 Flux analysis

The conservation relation corresponding to the time-dependent Schrödinger equation 7.1 can be written as a continuity relation

$$\frac{\partial \rho}{\partial t} + \nabla \cdot J = 0 \tag{7.19}$$

where the divergence operator is defined appropriately. Here the density is given by $\rho = |\Psi(t)|^2$ and the current density component k is defined by the equation

$$J_k = -\frac{i}{2\hbar} \left[\Psi^* \partial k \Psi - \Psi \partial k \Psi^* \right] \tag{7.20}$$

$$J_k = -\frac{i}{2} \left[\Psi^* \partial k \Psi - \Psi \partial k \Psi^* \right] \tag{7.21}$$

in atomic units. Here ∂k is a short-cut notation for the derivative with respect to coordinate k

For any stationary wave function, Ψ, ρ is independent of time, so $\nabla \cdot J = 0$. This means that the flux of particles across any fixed hypersurface is constant. If the Hamiltonian $\hat{H}$ can be expressed as the sum of a kinetic energy operator for the coordinate s and a reduced Hamiltonian for the remaining N-1 degrees of freedom

$$\hat{H} = \frac{\hat{p}_s^2}{2} m_s + \hat{H}_s \tag{7.22}$$

where $\hat{H}_s$ is the reduced Hamiltonian, then we can evaluate the flux at a fixed surface at $s = s_0$ by integrating over the remaining $N - 1$ coordinates in 7.21

$$\Phi_{s_0} = \langle \psi | \, |\hat{F}| \, |\psi \rangle \tag{7.23}$$

where the flux operator $\hat{F}$ is defined

$$\hat{F} = -\frac{i}{\hbar} \left[\Theta(s - s_0) \frac{\hat{p}_s^2}{m_s} - \frac{\hat{p}_s^2}{m_s} \Theta(s - s_0) \right] \tag{7.24}$$

$$= -\frac{i}{2m_s\hbar} \left[\frac{\partial}{\partial s} \delta(s - s_0) + \delta(s - s_0) \frac{\partial}{\partial s} \right] \tag{7.25}$$

where Θ is Heaviside function

$$\Theta(x) = 0, x < 0 \tag{7.26}$$

$$\Theta(x) = 0, x \geq 0 \tag{7.27}$$

In atomic units Eq. (7.25) reads

$$\hat{F} = -\frac{i}{2m_\mathrm{s}} \left[\frac{\partial}{\partial s} \delta\left(s - s_0\right) + \delta\left(s - s_0\right) \frac{\partial}{\partial s} \right] \tag{7.28}$$

Note that,

$$\langle \Psi | | \frac{\partial}{\partial s} \delta\left(s - s_0\right) | | \Psi \rangle = - \langle \Psi^* | | \delta\left(s - s_0\right) \frac{\partial}{\partial s} | | \Psi^* \rangle \tag{7.29}$$

so that

$$\Phi_{\mathrm{s}_0} = 2Re\left[\langle \Psi | | i \frac{\partial}{\partial s} \delta\left(s - s_0\right) | | \Psi \rangle \right] \tag{7.30}$$

We can evaluate the reactive flux at a fixed surface in the asymptotic region of the product.

$$\Delta P = \int_{-\infty}^{\infty} \Phi \mathrm{d}t \tag{7.31}$$

In MCTDH we can evaluate the flux through a particular channel by placing a complex absorbing potential (CAP) on the channel of interest and then measuring the amount of the wave packet that interacts with the CAP [115]. CAP are usually used in wave packet dynamics to absorb parts of the wave packet that reach the end of the grid and hence to prevent reflection of the wave packet. The introduction of a complex absorbing potential near the end of the grid is equivalent to simply multiplying the wave function by a decaying function of coordinate near the boundary at the end of each propagation step. The CAPs used in MCTDH take the form

$$-iW(Q) = -i\eta(Q - Q_c)^n \Theta(Q - Q_c) \tag{7.32}$$

Θ again is the Heaviside function, a step function, allowing to switch the CAP $Q > Q_c$; Q_c is the starting point for the CAP, η is the CAP strength and n an integer. For a scattering calculation, a CAP can be placed on the "scattering" channel to measure the

amount of wave packet that goes in and the amount of scattered wave packet that goes out of the channel. For reactions in which there is more than one exit channel, the flux may be calculated for individual channels.

The successful application of the MCTDH algorithm requires a proper estimation of all the numerical parameters to maintain the desired accuracy. A systematic investigation for the number of SPFs for each mode and grid parameters have been tried to get converged results. This is very much necessary for performing accurate calculations in this heavy triatomic system.

7.9   Sample scattering at E =149 meV and $J = 0$

The initial Gaussian is placed at $R = 6.0$ Å and has a width of $d = 0.25$ a_0. An example for the initial momentum for the wave packet is $p_0 = -9.0$ a_0. Here we also perform calculations with changing the initial momentum value and thereby different total energies considered. The CAP used to absorb the wave function is placed way beyond the analysis point starts for our scattering coordinate at $R = 17.0a_0$ to prevent reflection of the wave packet at the grid edges. The strengths and orders of the CAP is 0.0003 and 3 respectively.The quality of convergence has been verified by checking the maximum over time of populations of the least occupied natural orbitals which was close to 10^{-6} for a typical calculation when wave packet was inside the dividing surface.

In Figure 7.1 we show the quantum flux $\Phi(t)$, or the amount of probability density, through a dividing surface S placed at $r_{Cu} = 800$ pm.

$$\Phi(t) = \int_S j_{r_d}(t) \cdot \mathrm{d}S$$

where

$$j_{r_d}(t) = -\mathrm{i}\frac{\hbar}{2\,\mu_{r_d}} \left(\psi^*(t)\frac{\partial\psi(t)}{\partial r_d} - \psi(t)\frac{\partial\psi^*(t)}{\partial r_d} \right)$$

Then we show the incoming and outgoing flux along the Cu-NO dissociation channel with a total propagation time of 1200 fs. The total energy of 0.149 meV of the system is conserved. $J = 0$ is also conserved. The wave packet approaches from all direction

towards NO in an initial state $\ell = 0$. We calculate the reaction probability at time t

$$\Delta P(t) = \int\limits_{-\infty}^{t} \Phi(t)\, \mathrm{d}t$$

from the MCTDH flux.
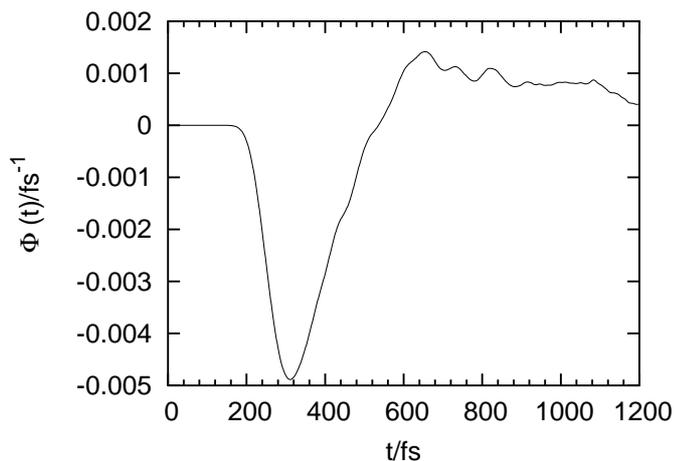
FIGURE 7.1: Flux at the dividing surface $r_{\mathrm{Cu}} = 800$ pm

The incoming wave packet moves through the dividing surface between 200 fs and 550 fs. The outgoing flux occurs between 550 fs and 1200 fs and shows clearly that this is a reactive scattering, at least during the first 12 ps.

$$\mathrm{Cu} + \mathrm{NO} \rightarrow \mathrm{CuNO}^* \tag{7.33}$$

In the absence of a collision partner, the intermediate species CuNO^* will eventually dissociate into Cu + NO so that $\Delta P(t \rightarrow \infty) \rightarrow 0$. At $t = 1.2$ ps $\Delta P \approx 0.007$ To understand more the nature of the dynamics, we show here the snapshots of the propagation at different times.

At time $t = 0$ fs, the wave packet which is centered around 600 pm in the R coordinate. And since the initial $\ell = 0$, the wave packet is completely delocalized over all θ angles. We can also see the spread of the wave packet here along R at the initial time. With the initial momentum in the negative direction, the wave packet propagates towards
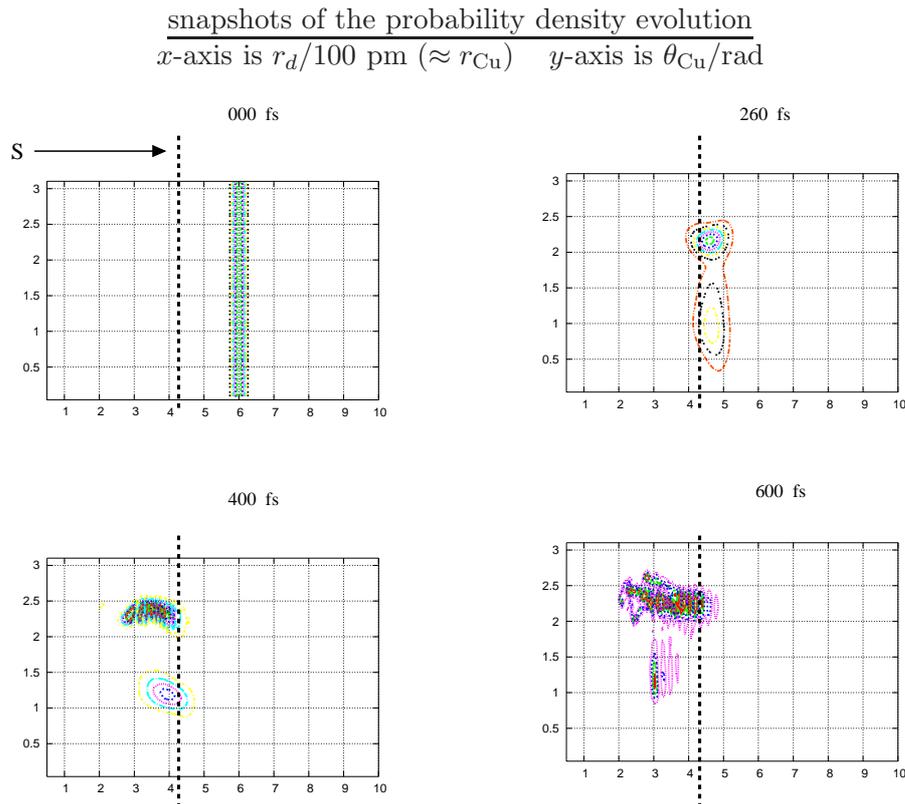
FIGURE 7.2: Snapshots of probability density evolution at four different times.see text for details

the dividing surface from the outside. By 100 fs of propagation, the wave packet starts to feel the potential and the completely delocalized nature of the wave packet along θ begins to change. By 260 fs, the wave packet is entering the dividing surface, and is beginning to concentrate along two θ angles which are roughly 126° and 60° radians. By 310 fs the wave packet splits into two parts and move simultaneously towards these two θ angles.

We can see strong interference effects along these two angles by 400 fs and now the wave packet is almost completely inside the dividing surface. For long propagation times the wave packet lingeringly starts to move out of the dividing surface around 600 fs. We can also clearly observe that the wave packet is now less concentrated along θ angles and slightly spreads over the other angles as it moves out of the dividing surface. The slow moving out continues even at 830 fs. The slow propagation causes the tail of the wave packet to begin to be absorbed by the CAP by around 1000 fs. We finish the propagation at 1200 fs.

The propagation clearly illustrates the inelastic nature of the scattering. Part of the initial kinetic energy in the R coordinate has been now lost to the bending vibration of the intermediately formed excited CuNO* system. We note that, in the long run, CuNO* $\rightarrow$ Cu + NO with excited rotational states of NO. the long run energy transfer at this energy is predominantly $T - R$. The NO $\nu = 1$ channel is not open at this energy. The strong $T - V$ energy transfer is evidenced by the interference effects. Also from the flux calculations, we can clearly see that there is net "reaction product" meaning, there is remaining population inside the dividing surface after the propagation.

7.10   Isotropic vs directional approach

The snapshots given above show that the wave packet approaches isotropically over all θ angles. This is a purely quantum way of approach. A propagation where the initial wave packet is along a particular θ angle and then starting the propagation along the R coordinate along the given θ ray gives a more intuitive picture of the scattering. Such a directional approach classically would require alignment of the NO molecules prior to the scattering, the initial state is then a linear superposition of many NO angular momentum states.

Now the wave packet will see the potential differently during the propagation. We show the flux obtained keeping the other parameters constant as the isotropic approach for comparison with such a directional approach. We chose an initial wave packet centred around $\theta \approx 130°$ for the propagation. The reason is that this θ is close to the minimum in the potential. And also we saw that the wave packet definitely concentrate along these angles while inside the dividing surface during our isotropic approach described earlier.

The dynamics is now different, the $\Delta P = 0.0052$ here, with about similar energies after the same time of propagation. At the initial $t = 0$ fs the wave packet is centered around θ but during propagation, the wave packet completely spreads among other angles also including even linear geometries.
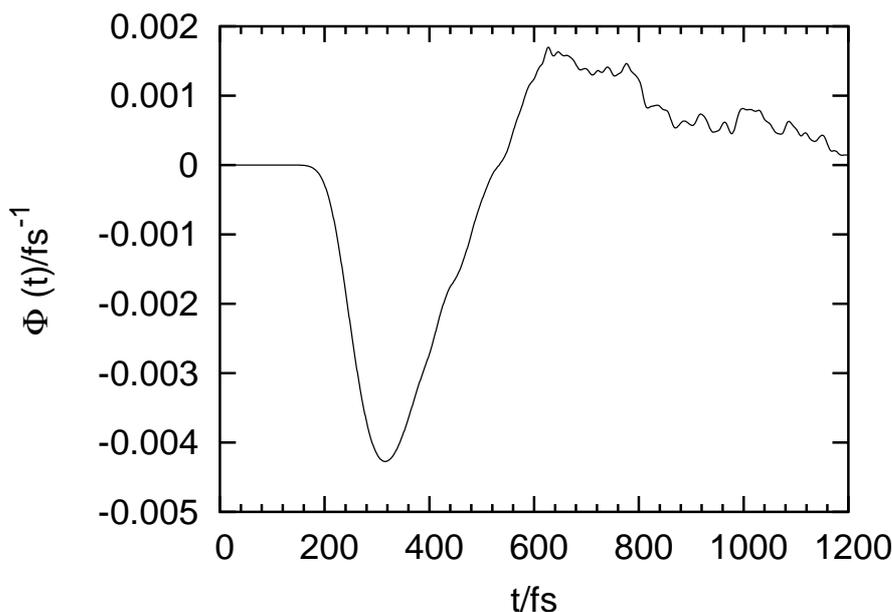
FIGURE 7.3: Flux at the dividing surface r_{Cu} =800 pm with initial wave packet
"aligned" along $\theta \approx 130°$

7.11   Dependence on Total Energy

The probabilities for generating metastable intermediate species CuNO* could be de-
pendent on the total initial energy (and width of the initial wave packet). Therefore
we are interested at the calculation of this "reaction probability" with different total
energies in the dynamics calculations. This can give us an indication of the energy re-
quired to get maximum products in this limited time span. The "reaction probability"
to form intermediate species CuNO* is defined by [eqn] where the final integration time
t is chosen such that the wave packet starts to become absorbed at the outer CAP.

Still at $J = 0$, the scattering dynamics along the isotropic approach with increasing
energy did not change ΔP value very much. Energies were varied by variation of the
initial momentum of the wave packet, the width of the wave packet being kept constant.

The Flux obtained at two different energies with the directional approach is shown here.

This clear difference in the ΔP values indicates that at higher energies we might obtain
less intermediate reaction products. A clearer picture can be obtained if we vary the
total energy of the scattering dynamics systematically.
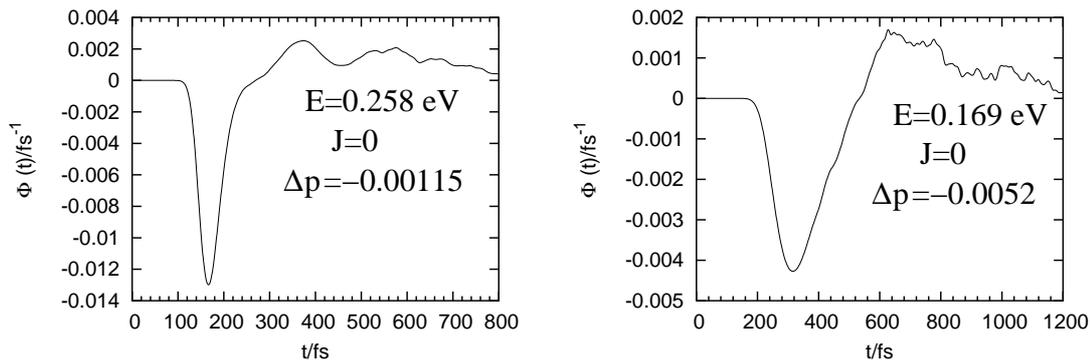
FIGURE 7.4: Flux at the dividing surface r_{Cu} =800 pm with initial wave packet along $\theta \approx 130°$ with different total energies

E /eV	ΔP
0.1453	-0.002136
0.1692	-0.005202
0.2114	-0.007820
0.2585	-0.001154
0.3510	-0.001328
0.3973	-0.002462

TABLE 7.3: The dependence of ΔP for different total energies

The Table 7.3 gives the ΔP with various initial energies. There is a clear dependence on the initial energies in particular and the dynamical behaviour of the system in general. We find that we get more reaction products at comparatively low energies. This also is in accordance with the physical picture we have that there is more probability for reactive scattering when the "reactants" are not moving too fast. We do see that there is more "products" at 211 meV and it again starts to increase around 397 meV. This is probably due to the fact that $\nu = 1$ of NO is ≈ 211 meV. And the 397 meV is close to the first overtone of NO.

t /fs	ΔP	integration grid	ΔP
800	-0.007850	20/20	-0.007850
795	-0.008002	19/20	-0.007443
790	-0.008153	18/20	-0.007064
780	-0.008437	17/20	-0.006683
775	-0.008577		
770	-0.008723		

TABLE 7.4: The variation of ΔP

We also carefully assessed the certainty in the ΔP value from the calculation. Since the ΔP is obtained by the integration of the flux over all the time steps (1 fs), we could check for fluctuations by changing the integration points in it and looking for possible fluctuations in the value ΔP. We find that the ΔP values obtained here are smooth and change only gradually with a small changes in the number of time steps considered for integration. In Table 7.4, the values of ΔP at different total integration times are shown from 770 fs to 800fs. The ΔP value slightly decreases along the increasing propagation time as the wave packet is moving out. It may be that at very much longer propagation time the ΔP value might reach zero as the intermediate CuNO* is long lived. We also show the ΔP values obtained by different integrations including all grid points (20/20), removing every 20th point (19/20) along propagation, removing every 20th and 19th points (18/20) ans so on. This also gives us an idea of the certainty of the ΔP value. The ΔP value decreases as more points are removed from the grid and they contribute the flux.

7.12 Dependence on J

Finally, we test also the dynamical behaviour of the system with the change in the total angular momentum J. This corresponds to a change in the impact factor of the scattering. As a start of this we can test with $J = 1$. Here we use the $KLEG$ DVR instead of LEG for the θ. We also use the isotropic approach explained above here (i.e $\ell = 0$ initially).
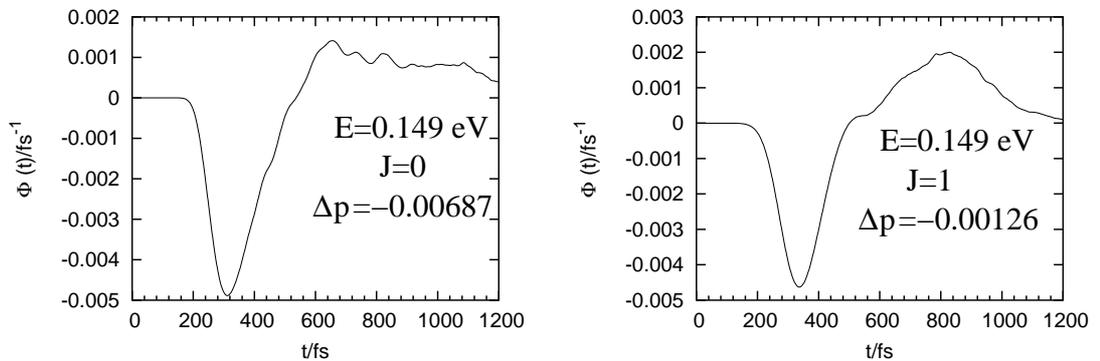
FIGURE 7.5: Flux at the dividing surface $r_{Cu} =800$ pm with with different $J = 0$ and $J = 1$ values

In Figure 7.5, the calculation with $J = 1$ shows inelastic scattering. But less intermediate reaction products are formed with $J = 1$. We can tentatively say that with increasing value of J, there will be less probability for formation of intermediate products in the scattering calculation.

One of the most fundamental and important tasks in chemical reaction dynamics is the accurate evaluation of thermal rate constants. As is known, the exact thermal rate constant for an elementary bimolecular reaction $(AB+C \rightarrow ABC)$ can be rigorously calculated by Boltzmann averaging the reactive flux over the initial states and the collision energy. One rigorous way to determine the rate constant is to solve the complete state-to-state reactive scattering Schrödinger equation to obtain the S-matrix as a function of total energy E and total angular momentum J, from which all the state-to-state scattering cross sections can be obtained. Boltzmann averaging these cross sections over initial quantum states, and summing over all final quantum state produces the rate constant. These preliminary calculations are a way towards this goal.

7.13   Conclusion from Cu + NO scattering dynamics

In summary, we have reported a full-dimensional wave packet propagation scheme as implemented in the MCTDH method to simulate Cu + NO collisions. In this work, that would take place on singlet A' ground state. For this, we used the global PES developed in this work.

The Hamiltonian operator consists of an exact form of the kinetic energy operator in Jacobi coordinates. It could be seen that the MCTDH approach is very efficient and powerful to calculate the state to state scattering calculations.

We have optimised the parameters for proper refitting of the analytical potential energy surface in the POTFIT and convergence criteria of the MCTDH propagation of the triatomic with the heavy element copper. The full-dimensional the quantum calculation for this system is time-consuming. This is difficult as a result of huge density of vibrational states which has now been fully achieved. The quality of convergence was checked by looking at the natural populations of the limiting SPF to with in $\leq 10^{(}-6)$ for all DOF. The number of SPF used for the propagation and the number of grid points in

the primitive basis of all degrees of freedom was increased systematically to provide an optimal convergence of MCTDH.

The results from the wave packet propagation calculations show inelastic/reactive scattering with CuNO at $J = 0$ and $J = 1$. There is formation of an intermediate excited metastable species CuNO* which lives for about $0.5 - 1$ ps. The probability of formation of this species, ΔP is obtained by integrating the flux through a dividing surface at all the time steps.

We find that there is an important $T - R$ or $T - V$ transfer in the system during the dynamics which is evidenced by the interference patterns in the snapshots of the probability density evolution. These patterns indicate the formation of excited CuNO* bending states during the collision which under rotationally excited NO scattering products after the CuNO* intermediate has had time to dissociate.

Again, we investigate the dependence of dynamics on the approach of initial wave packet through an isotropic (initial $\ell = 0$) and a directional way by placing a gaussian wave packet along r_d coordinate centered around $130°$ keeping $J = 0$. Depending on the approach of wave packet, the scattering dynamics is found to be very different. We also show the clear dependence of ΔP with different total energies in the directional approach. Higher energy scattering showed less "products", at least in the range of energies studied here. In comparison, a calculation with isotropic approach with a change in total energy did not show much different ΔP. However, we mention here that, we did not perform calculations with the same wide range of energies as in the directional approach.Preliminary results for the dependence of dynamics with different J value, which corresponds to a change in the impact factor is shown. Here the reaction probability decreases for $J = 1$ for the same total energy and unchanged remaining parameters.

We now have the ability to perform converged full dimensional quantum dynamical scattering calculations at even higher J values which will give us the detailed information about the fundamental kinetics including the rate constant of the atom-diatom scattering of the Cu + NO system.

Chapter 8

Conclusions

In this thesis, we have investigated the interaction of NO with the transition metal Cu. We have successfully optimized settings to calculate *ab initio* the ground state at varied positions of the nuclei. We developed an analytical global representation of the potential energy surface for this system and used that surface to perform successfully converged quantum dynamical scattering calculation of Cu + NO

8.1 CuNO

Both coupled cluster and multi-reference configuration interaction (MRCI) methods have been used - the latter with singly and doubly excited configurations, the former to up to perturbative (CCSD(T)) and full inclusion of triple excitations (CCSDT). All methods were used as implemented in the MOLPRO program suite [48] (see, in particular [27, 28, 29], for the internally contracted singles and doubles MRCI (MR-SDCI), [52], for the CCSD-T and RCCSD-T methods and [53, 79], for the CCSDT method).

The MRCI method preceded by an MCSCF calculation of configuration is the method of choice to determine a qualitativly global potential energy surface. The MRCI results allow to identify the multi-configurational, multi-reference character of the electronic ground state wave function even in regions close to the equilibrium structure. This character is due to both the dense level structure of the transition metal atom and the open shell character of the separated fragments NO and Cu. Focusing on linear structures at the first place provides a handle to actually compare energies obtained

using $\mathbf{C}_{2v}$ symmetry to those obtained in $\mathbf{C}_s$ symmetry. It has been shown that 12 roots are necessary in the MCSCF calculation to get a clean convergence and comparable states of $\mathbf{C}_s$ or $\mathbf{C}_{2v}$ symmetry.

The active space in the MCSCF calculations should contain all 3d electrons of Cu to accurately describe the system. The largest active space used here for the MRCI calculations is a $(22, 13)$ CAS which is close to the full valence space of the system. With a smaller $(18, 11)$ CAS it is possible to obtain MRCI energy values that are semi-quantitatively correct. These energy points carry a quite large method dependent, systematic error. Nevertheless, they are highly valuable for the development of a global, physically sound PES.

It is also shown that the MCSCF calculation alone gives asymptotically inverted roots and that in order to describe the ground state properly we have to use the computationally expensive MRCI calculations over 6 states per symmetry simultaneously. The MRCI calculations invariably lead us to obtain the PES for the 12 lowest states in CuNO, the 6 lowest states of each spatial symmetry.

With these settings, we definitely show that the ground state belongs to the $^1A'$ irreducible representation, with a minimum at a bent end-on-structure in the nuclear configuration Cu-N-O, in agreement with some of the previous work on this system [7, 12, 15], and in disagreement with a more recent work using DFT [16].

The dissociation energy from the $^1A'$ ground state equilibrium of CuNO into Cu an NO is estimated to be approximatively 2150 $hc\,\mathrm{cm}^{-1}$, from the MRCI calculations. Since the MCSCF reference states are inverted at the asymptote, the Davidson correction could not be reasonably included,but attampts are made.

A major result of this thesis is single reference coupled cluster calculations that include to up to triple excitations yield more accurate results for the ground state in those regions of the nuclear position space that are close to the minimum of the potential well despite the fact that the wave function has an important multiference character. In fact, the present CCSD(T) and CCSDT calculations are shown to recover much of the correlation energy that would otherwise be missing in a single reference approach limited to single and double excitations.

Dissociation energy: Non-relativistic coupled cluster calculations involving all 22 valence electrons yield a dissociation energy of (4200 ± 400) $hc\,\mathrm{cm}^{-1}$, where uncertainties include possible errors related to the multi-reference character of the wave function. When relativistic effects are included with the Douglas-Kroll-Hess hamiltonian, the dissociation energy increases to about (5000 ± 400) $hc\,\mathrm{cm}^{-1}$.

The lowest triplet state belongs to the A'' irreducible representation. The CCSD(T) calculations confirm that this state has a metastable structure about 1200 to 2000 $hc\,\mathrm{cm}^{-1}$ above but displaced with respect to the singlet A' state, roughly in agreement with findings in [12], while the MRCI calculations yield repulsive states. The latter lack important correlation from higher than double excitations, which are clearly important for the binding of the NO and Cu fragments. We should note, however, that the uncertainty of the triplet energies obtained from coupled cluster calculations is significantly larger than for the singlet state, given the difficulties related to the open shell character of the reference wave function, in addition to the stated multi-reference character of the wave function.

We speculate that, if a quasi-bound CuON structure exists in the $^3A''$ state, the isomerization between the two metastable structures postulated in [12] is very likely "facile". Clearly, the MRCI calculations yield fully repulsive triplet states.

8.2 Diatomics

We have obtained new, complete potential energy functions of the ground electronic states of CuO and CuN systems. In CuO, we find that we reqire very big active spaces for proper description of the potential. The lowest electronic state in the CuO is the $^2B_1$ state, with a dissociation energy obtained from a fit of an anharmonic potential at about 19920 $hc\,\mathrm{cm}^{-1}$.

We also report the barrier to dissociation in the lowest $^2A_2$ electronic state of which has not been observed before. By the careful analysis of the permanent dipole moments of the electronic states, we find that the barrier is from a change in the major confugrations from the asymptote to the equilibrium geometries. At the asymptote, the lowest

state is essentially neutral, but close to the equilibrium, the states with ionic contributions approach lower in energy and thus the configurations is finally inverted to become predominantly of ionic nature in the state.

Comparison of the term values for the lowest electronic states of CuO and CuN with those previously reported in literature shows agreement is quite good.

8.3 Analytical representations

Global potential energy hypersurfaces allow to understand the connected set of individually calculated *ab initio* potential points. The representation of potential surfaces through analytical functions are very helpful to describe the nuclear motion in polyatomic molecules. For polyatomic molecules, the derivation of compact global analytical representations of *ab initio* potential surfaces is a difficult task. We develop a novel analytical form of a potential in the form of a generalized Morse potential as sum of two-body and three-body terms. This representation enables us to gain a meaningful interpretation of the potential hypersurface. We can make a physically correct interpolation, and also the extrapolation of *ab initio* data points to asymptotic regions of configuration space.

Here we have derived a novel analytical representation of the ground adiabatic electronic surface of the CuNO system.

The representation, which is a sum of two body and three body terms is global and the potential behaves very well to capture the minima and all the way to the dissociation of the MRCI data.

The PES has only 19 adjustable parameters which also have a physical meaning. The potential has now provided a set of values at all geometries of the electronic ground state of the CuNO system which now enables us to do scattering dynamics of the system.

The representation with the determined set of parameter values is a highly valuable starting point to consider regions of potential where *ab initio* data might be difficult to obtain and indeed is an excellent way recognise and to to sort of some very poorly converged *ab inito* data even from high level calculations like MRCI.

However, it is also shown that to find accurate vibrational fundamentals comparing with experiments it might be necessary to merge, CCSD(T) and MRCI data and fit it with a new potential form starting from the current form.

The representations of the potentials obtained so far is trustworthy and describes globally the lowest electronic state of CuNO and its dissociation products. Parameter values have been determined, by fitting the model potential to a large set of *ab initio* energy points obtained from the MRCI calculations, so far.

8.4   Quantum Dynamics

The Hiedelberg multiconfigurational time dependent Hartree (MCTDH) program is applied to study the atom-diatom scattering of the Cu + NO collison. The molecule has three internal degrees of freedom to be considered. It has been successfully applied for propagating the wave packets, and flux calculations were performed to compute the reaction probabilities

The performance and reliability of the MCTDH results is examined for varied choices of the basis set representation in the MCTDH. We refit the analytical potential with the POTFIT algorithm to describe it in a product form which can be used efficiently in the MCTDH. Strict care was taken to converge all parameters for the dynamics by checking the natural populations in the SPF used for the caculation.

We find indeed that the scattering in CuNO is highly inelastic. Intermediate, excited meta stable reaction products $CuNO^*$ live for about 0.5 to 1 ps. The translational collison energy is very quickly redistributed into $CuNO^*$ bending vibrations (T-V transfer into the intermediate species), which eventually leads to rotationally hot NO products once the meta stable state has dissociated.

We also study the effect of the isotropic versus a directional approach in the dynamics of CuNO. Here we find that with a directional approach the scttaring gives more reaction products at lower total energies of scattering. The investigation of the scattering dynamics with a nonzero J value allows in the long run to calculate total scattering cross sections of the triatomic system. Our preliminary results on non zero J indicate that at higher J values there will be less intermediate reaction products.

The present study shows that an investigation of the quantam dynamics of a fairly complicated 3D system is feasible. The quantum calculations are in fact of good quality.

8.5   Perspective

A new merging of the MRCI and coupled cluster data to obtain a better potential energy surface is currently being performed and will be available soon. This new representation can reproduce the vibrational fundamentals in close agreement with experimental data and has a deeper minimum.

The new form of the potential will then be used to repeat the scattering calculations with MCTDH. We would begin by repeating the same calculations described here and see the change in the dynamics of the system. On the event of successful convergences, we will repeat the MCTDH for several J values, which is a way to calculate the rate constant of the Cu-NO scattering. Also, we need to calculate, with MCTDH, scattering matrix elements. We have dipole moments available from the MRCI data. We could calculate the spectra with a new dipole moment surface.

Again considering the potential reaction channels,

$$(^2\text{S})\text{Cu} + (^2\text{X})\text{NO} \rightarrow (^3\text{P})\text{O} + (^3\text{X})\text{CuN} \tag{8.1}$$

or

$$(^2\text{S})\text{Cu} + (^2\text{X})\text{NO} \rightarrow (^4\text{S})\text{N} + (^4\text{X})\text{CuO} \tag{8.2}$$

or

$$(^2\text{S})\text{Cu} + (^2\text{X})\text{NO} \rightarrow (^1\text{P})\text{O} + (^1\text{X})\text{CuN} \tag{8.3}$$

or

$$(^2\text{S})\text{Cu} + (^2\text{X})\text{NO} \rightarrow (^2\text{D})\text{N} + (^2\text{X})\text{CuO} \tag{8.4}$$
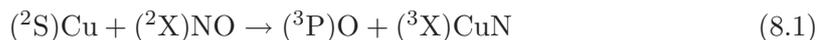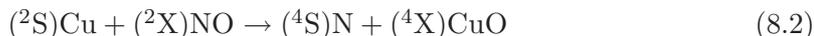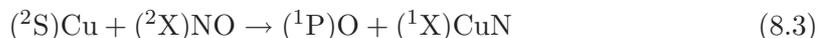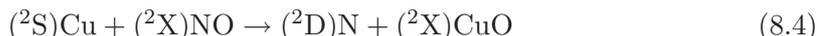
From the current work we some understanding of which channels would be feasible at different energy ranges. From the Te energy of Σ^- CuO at 8360 cm^{-1} . However ^{2}D N is 19224 cm^{-1} above the ^{4}S N. Therfore, the channel with $(^2\text{S})Cu + {}^2XNO \rightarrow (^4\text{S})N + (^4\text{X})CuO$ will be the lowest channel. In the future, we could investigate the

interaction of Cu with a NO dimer. This is a logical next step towards understanding,
NO reduction on Cu.

Bibliography

[1] G. B. Richter-Addo and P. Legzdins. *Metal Nitrosyls*. Oxford UniversityPress: New York, Oxford, 1992 edition, (1992).

[2] I. M. Wasser, S. de Vries, P. Moenne-Loccoz, I. Schroder, and K. D. Karlin, Chem. Rev., **102**, 1201 (2002).

[3] A. R. Ravishankara, J. S. Daniel, and R. W. Portmann, Science, **326**, 123 (2009).

[4] N. G. Rey and H. Arnolds, The Journal of Chemical Physics, **135**, 224708 (2011).

[5] J. A. Chiarelli and D. W. Ball, J. Phys. Chem., **98**, 12828 (1994).

[6] D. W. Ball and J. A. Chiarelli, J. Mol. Struct., **372**, 113 (1995).

[7] M. Zhou and L. Andrews, J. Phys. Chem. A, **104**, 2618 (2000).

[8] L. Krim, X. Wang, L. Manceron and L. Andrews, J. Phys. Chem. A, **109**, 10264 (2005).

[9] Sülzle, D. and Schwarz, H. and Moock, K. H. and Terlouw, J. K., Int. J. Mass Spec. and Ion. Proc., **108**, 269 (1991).

[10] Böhme, D. K. and Schwarz, H., Angew. Chem. Int. Ed., **44**, 2336 (2005).

[11] W. B. Tolman, Angew. Chem. Int. Ed., **49**, 1018 (2010).

[12] J. Hrusak, W. Koch, and H. Schwarz, J. Chem. Phys., **101**, 3898 (1994).

[13] J. L. C. Thomas, J. C. W. Bauschlicher, and M. B. Hall, J. Phys. Chem. A, **101**, 8530 (1997).

[14] A. T. Benjelloun, A. Daoudi, G. Berthier, and C. Rolando, J. Mol. Struct., **360**, 127 (1996).

[15] C. Blanchet, H. A. Duarte, and D. R. Salahub, J. Chem. Phys., **106**, 8778 (1997).

[16] E. L. Uzunova, J. Phys. Chem. A, **113**, 11266–11272 (2009).

[17] L. Andrews and A. Citra, Chem. Rev., **102**, 885–911 (2002).

[18] G. Herzberg. *Molecular Spectra and Molecular Structure I. Spectra of Diatomic Molecules.* Van Nostrand Reinhold Co., New York, reprint(1989) edition, (1945).

[19] M. Born and J .R. Oppenheimer, Ann. Phys.,**84**, 457 (1927)

[20] P. A. M. Dirac, Proc. R. Soc. London A., **123**, 714, (1929).

[21] D. R. Hartree, Proc. Camb. Phil. Soc., **24**, 329 (1928).

[22] V. A. Fock, Z. Phys.,**15**, 126 (1930).

[23] C. J. Slater, Phys. Rev.,**35**, 210 (1930).

[24] C. Roothaan, Rev. Mod. Phys., **23**, 69 (1951).

[25] G. Hall, Proc. R. Soc. London A, **205**, 541 (1951).

[26] H.-J. Werner and E.-A. Reinsch, J. Chem. Phys., **76**, 3144 (1982).

[27] H.-J. Werner and P. J. Knowles, J. Chem. Phys., **82**, 5053 (1985).

[28] H.-J. Werner and P. J. Knowles, J. Chem. Phys., **89**, 5803 (1988).

[29] P. J. Werner, H. J. Knowles, Theoretica Chimica Acta, **78**, 175 (1990).

[30] P. J. Knowles and H.-J. Werner, Chem. Phys. Lett., **145**, 514 (1988).

[31] S. R. Langhoff and E. R. Davidson, Int. J. Quantum Chem., **8**, 61 (1974).

[32] D. Figgen, G. Rauhut, M. Dolg, and H. Stoll, Chem. Phys., **311**, 227 (2005).

[33] Anna I Kirlov, Annu. Rev. Phys. Chem., **59**, 433 (2008).

[34] S. F. Boys, Proc. Roy. Soc. A., **200**, 542 (1950).

[35] S. F. Boys and F. Bernardi, Mol. Phys.,**19**, 553 (1970)

[55] G. Jansen and B. A. Hess, Phys. Rev., **39**, 6016 (1989).

[37] K. A. Peterson, D. E. Woon, and T. H. Dunning Jr., J. Chem. Phys., **100**, 7410 (1994).

[38] T. Helgaker, W. Klopper, H. Koch, and J. Noga, J. Chem. Phys., **106**, 9639 (1997).

[39] C. C. J. Roothaan, Rev. Mod. Phys., **23**, 69 (1951).

[40] C. Möller and M. S. Plesset, Phys. Rev., **46**, 618 (1934).

[41] J. Olsen, B. O. Roos, P. Jørgensen, and H. Jørgen Aa. Jensen, J. Chem. Phys., **89**, 2185 (1988).

[42] G. D. P. III and R. J. Bartlett, J. Chem. Phys., **76**, 1910–1918 (1982).

[43] R. Ditchfield, W. J. Hehre, and J. A. Pople, J. Chem. Phys., **54**, 724 (1971).

[44] R. Krishnan, J. S. Binkley, R. Seeger, and J. A. Pople, J. Chem. Phys., **72**, 650 (1980).

[45] T. H. Dunning Jr, J. Chem. Phys., **90**, 1007 (1989).

[46] D. E. Woon and T. H. Dunning Jr, J.Chem. Phys., **98**, 1358 (1993).

[47] R. A. Kendall, T. H. Dunning Jr, and R. J. Harrison, J. Chem. Phys., **96**, 6796 (1992).

[48] R. D. Amos, A. Bernhardsson, A. Berning, P. Celani, D. L. Cooper, M. J. O. Deegan, A. J. Dobbyn, F. Eckert, C. Hampel, G. Hetzer, P. J. Knowles, T. Korona, R. Lindh, A. W. Lloyd, S. J. McNicholas, F. R. Manby, W. Meyer, M. E. Mura, A. Nicklass, P. Palmieri, R. Pitzer, G. Rauhut, M. Schütz, U. Schumann, H. Stoll, A. J. Stone, R. Tarroni, T. Thorsteinsson, and H.-J. Werner. Molpro, a package of ab initio programs designed by H.-J. Werner and P. J. Knowles, version 2009.1, (2009).

[49] T. H. Dunning, Jr., J. Chem. Phys., **90**, 1007 (1989).

[50] R. A. Kendall, T. H. Dunning Jr., and R. J. Harrison, J. Chem. Phys., **96**, 6797 (1992).

[51] N. B. Balabanov and K. A. Peterson, J. Chem. Phys., **123**, 064107 (2005).

[52] M. J. O. Deegan and P. J. Knowles, Chem. Phys. Lett., **227**, 321 (1994).

[53] M. Kállay and P. R. Surjan, J. Chem. Phys., **115**, 2945 (2001).

[54] M. Douglas and N. M. Kroll, Annals of Physics, **82**, 89 (1974).

[55] G. Jansen and B. A. Hess, Phys. Rev. A, **39**, 6016 (1989).

[56] A. Wolf, M. Reiher, B. A. Hess, J. Chem. Phys.,**117**, 9215 (2002).

[57] M. Reiher, A. Wolf, J. Chem. Phys., **121**, 2037-2047 (2004),

[58] C. E. Moore. *Selected tables of atomic spectra: A, atomic energy levels; B, multiplet tables: data derived from the analysis of optical spectra*, volume 3 of *Nat. Stand. Ref. Data Ser., Nat. Bur. Stand.* National Bureau of Standards, Washington, D.C., (1982).

[59] Attila Szabo and Neil S. Ostlund, Modern Quantum Chemistry: Introduction to Advanced Electronic Structure Theory, Reprint Edition, Dover publications, 1989.

[60] R. McWeeny: Methods of Molecular Quantum Mechanics, Academic Press, 1992

[61] T. Helgaker, P. Jorgensen, J. Olsen, T. Helgaker: Molecular electronic-structure theory. Wiley, New York, 2000. (ISBN 0-471-96755-6)

[62] P.J. Knowles, M. Schütz, H.-J. Werner, *Ab initio methods for electron correlation in molecules*, in: J. Grotendorst (Ed.), Modern Methods and Algorithms in Quantum Chemistry, NIC Series, vol. 3, John von Neumann Institute for Computing (NIC) 2000.

[63] N. B. Balabanov and K. A. Peterson, J. Chem. Phys., **125**, 074110 (2006).

[64] C. W. Bauschlicher, Jr., P. S. Bagus, C. J. Nelin, and B. O. Roos, J. Chem. Phys., **85**, 354–364 (1986).

[65] R. J. Gdanitz and R. Ahlrichs, Chem. Phys. Lett., **143**, 413 (1988).

[66] T. J. Lee and P. R. Taylor, Int. J. Quantum Chem., **23**, 199 (1989).

[67] R. J. Bartlett and M. Musial, Rev. Med. Phys., **79**, 291 (2007).

[68] P.-O. Löwdin, Phys. Rev., **97**, 1509–1520 (1955).

[69] P.-O. Löwdin, Phys. Rev., **97**, 1490–1508 (1955).

[70] P.-O. Löwdin, Phys. Rev., **97**, 1474–1489 (1955).

[71] C. D. Sherrill and H. F. S. III. The configuration interaction method: Advances in highly correlated approaches. volume 34 of *Advances in Quantum Chemistry*, pages 143 – 269. Academic Press, London, (1999).

[72] D. J. Dean and M. Hjorth-Jensen, Phys. Rev. C, **69**, 054320 (2004).

[73] C. C. J. Roothaan, Rev. Mod. Phys., **32**, 179–185 (1960).

[74] J. A. Pople and R. K. Nesbet, The Journal of Chemical Physics, **22**, 571–572 (1954).

[75] R. J. Bartlett, Ann. Rev. Phys. Chem., **32**, 359 (1981).

[76] M. Kállay and J. Gauss, J. Chem. Phys., **121**, 9257 (2004).

[77] M. Kállay and J. Gauss, J. Chem. Phys., **129**, 144101 (2008).

[78] M. Kállay, J. Gauss, and P. G. Szalay, J. Chem. Phys., **119**, 2991 (2003).

[79] M. Kállay, P. G. Szalay, and P. R. Surjan, J. Chem. Phys., **117**, 980 (2002).

[80] G. C. Schatz, Rev. Mod. Phys., **61**, 669 (1989).

[81] J. S. Wright, S. K. Grey., J. Chem. Phys., **69**, 67 (1978).

[82] R. Marquardt, J. Math. Chem., **50**, 577 (2012)

[83] R. Marquardt, K. Sagui, J. Zheng, W. Thiel, S. Yurchenko, D. Luckhaus, F. Mariotti, and M. Quack, (2012). In preparation.

[84] X. Zhang, S. Zou, L. B. Harding, and J. M. Bowman, J. Phys. Chem. A, **108**, 8980 (2004).

[85] R. Marquardt and M. Quack, J. Chem. Phys., **109**, 10628 (1998).

[86] R. Marquardt and M. Quack, J. Phys. Chem. A, **108**, 3166 (2004).

[87] R. Marquardt, K. Sagui, W. Klopper and M. Quack, J. Phys. Chem. B, **109**, 8439 (2005).

[88] H. Basch and R. Osman, Chem. Phys. Lett. **93**, 51 (1982).

[89] P. S. Bagus, C. J. Nelin, and C. W. Bauchlicher, J. Chem. Phys. **79**, 2975 (1983).

[90] P. V. Madhavan and M. D. Newton, J. Chem. Phys. **83**, 2337 (1985).

[91] S. R. Langhoff and C. W. Bauchlicher, Chem. Phys. Lett. **124**, 241 (1986).

[92] D. Hippe, S.D. Peyerimhoff, Mol. Phys. **76** 293 (1992).

[93] D. Hippe, S.D. Peyerimhoff, J. Chem. Phys. **96** 3503 (1992).

[94] A. Daoudi, A. Touimi Benjelloun, J. P. Flament, and G. Berthier, J. Molec. Spec.,
194, 8 (1999)

[95] L. F. A. Ferrao, O. Roberto-Neto, F. B. C. Machado **108**, 2512 (2008)

[96] G. L. Gutsev, L. Andrews, C. W. Bauschlicher, Theor. Chem. Acc., **109**, 298 (2003)

[97] Z. J. Wu, J. Mol. Struct: Theochem., **728**, 167 (2005)

[98] O. Appelblad, and A. Lagerqvist., Physica Scripta, **13**, 275 (1976)

[99] O. Appelblad, A. Lagerqvist, Y. Lefebvre, B. Pinchemel, and J. Schamps, Physica
Scripta, **18**, 125 (1978).

[100] O. Appelblad, A. Lagerqvist, I. Renhorn, and R. W. FieLd, Physica Scripta, **22**,
603 (1981).

[101] J. M. Delavel, F. David, , Y. Lefebvre, P. Bernage, P. Niay, and J. Schamps., J.
molec. Spectrosc., **101**, 358 (1983).

[102] Y. Lefebvre, B. Pinchemel, J. M Delavel, and J. Schamps., , Physica Scripta, **25**,
329 (1982).

[103] H. Xian, Z.X. Cao , X. Xu, X. Lu, and Q.E. Zhang., Chem. Phys. Lett.,**326**, 485
(2000)

[104] A.J. Merer, Annu. Rev. Phys. Chem., **40**, 407 (1989)

[105] M. L. Polak, M. K. Gilles, J. Ho, W. C. Lineberger, J. Phys. Chem., **95**, 3460
(1991).

[106] H. Wu, S. R. Desai, L. S. Wang, J. Phys. Chem. A., **101**, 2103 (1997).

[107] M. Mladenović, J. Chem. Phys, **112**, 1070 (2000).

[108] M. H. Beck, A. Jäckle, G. A. Worth, and H.-D. Meyer., Phys Rep **324**, 1 (2000).

[109] F. Gatti and C. Iung, Phys Rep **484**,1 (2009).

[110] Meyer, H.-D., Gatti, F. and Worth, G. A. (2009) Multidimensional Quantum
Dynamics: MCTDH Theory and Applications (eds H.-D. Meyer, F. Gatti and G.
A. Worth), Wiley-VCH Verlag GmbH & Co. KGaA, Weinheim, Germany.

[111] U. Manthe, H.-D. Meyer, and L. S. Cederbaum, J. Chem. Phys., **97**, 3199 (1992).

[112] H.-D. Meyer and G. A. Worth, Theo. Chem. Acc., **109**, 251 (2003).

[113] F. Richter, M. Hochlaf, P. Rosmus, F. Gatti, and H.-D. Meyer, J. Chem. Phys., **120**, 1306 (2004).

[114] A. Jäckle and H.-D. Meyer, J. Chem. Phys., **104**, 7974 (1996).

[115] A. Jäckle and H.-D. Meyer, J. Chem. Phys., **105**, 6778 (1996).

[116] D. Neuhauser, M. Baer, R. S. Judson, and D. J. Kouri, J. Chem. Phys., **93**, 312 (1990).

[117] J. Tennyson, Computer Phys. Reports., **4**, 1 (1986).

[118] S. Carter, N. C. Handy, Comput. Phys. Rep., **5**, 115 (1986).

[119] Z. Baćić, J. C. Light, Annu. Rev. Phys. Chem.,**40**, 469 (1989) .

[120] J. C. Light, T. Carrington Jr., Adv. Chem. Phys., **114**, 263 (2000).